CRANFIELD UNIVERSITY

SEIMON POWELL

NON-REFLECTING BOUNDARY CONDITIONS AND TENSILE INSTABILITY IN SMOOTH PARTICLE HYDRODYNAMICS

SCHOOL OF ENGINEERING

PhD THESIS

CRANFIELD UNIVERSITY

SCHOOL OF ENGINEERING

DEPARTMENT OF APPLIED MECHANICS

PhD THESIS

Academic Year 2011-2012

Seimon Powell

Non-reflecting boundary conditions and tensile instability in smooth particle hydrodynamics

Supervisor: Prof. Rade Vignjevic

January 2012

Abstract

This thesis aimed at the understanding and further development of smoothed particle hydrodynamics (SPH). The first part described the implementations of non-reflecting boundary conditions for elastic-waves in SPH. The second part contains a stability analysis of the semi-discrete SPH equations and a new method for stabilising basic SPH in tension.

Acknowledgements

First I must thank Rade for allowing me to start, and continuing to support me to the end. Thanks also to the members of the Applied Mechanics department, staff and students who have been ever-ready to give time to help.
I must also thank my family and most of all Goher. Ta.

Contents

List of Figures

Glossary

AB/s	Artificial boundary/ies
AMR	Adaptive mesh refinement
ASPH	Adaptive smoothed particle hydrodynamics
BP/s	Boundary particle/s
BSM	Bridging scale method
CFL	Courant, Friedrichs and Lewy
E-M	Engquist-Majda
FD	Finite difference
FE	Finite element
IBP/s	Inner boundary particle/s
MCM	Meshfree continuum mechanics (SPH code)
MD	Molecular dynamics
MLS	Moving least squares
NCSPH	Normalised corrected smoothed particle hydrodynamics
NCXSPH	Normalised corrected smoothed particle hydrodynamics with velocity smoothing
NRBC	Non-reflecting boundary condition
OBP/s	Outer boundary particle/s
ODE	Ordinary differential equations
PDE	Partial differential equation
PML	Perfectly matched layer
RHS	Right-hand side

RKPM	Reproducing kernel particle method
RSPH	Regularised smoothed particle hydrodynamics
SPH	Smoothed particle hydrodynamics
S-SPH	Stabilised smoothed particle hydrodynamics
TL-SPH	Total Lagrangian smoothed particle hydrodynamics
XSPH	Smoothed particle hydrodynamics with velocity smoothing

Introduction

Smoothed particle hydrodynamics (SPH) is a technique for the numerical solution of partial differential equations. It is meshfree and therefore has advantages over grid-based methods in modelling many phenomena that undergo large deformations in a Lagrangian framework. However, it has several important drawbacks; the particle discretisation introduces an instability which most often manifests as an unphysical clumping of particles under tension, leading to purely numerical fracture.

The implementation of boundary conditions is another weakness. SPH does not interpolate nodal values exactly i.e. it is not a projection operator and thus the imposition of Dirichlet boundary conditions is complicated. Additionally, the ability of SPH to accurately approximate derivatives near a boundary is retarded by a deficiency in the number of particles used in the approximation.

Finally, SPH simulations can be more computationally intensive than a comparable finite difference code. The main reasons being the additional cost of searching for and updating a list of particle neighbours and the fact that numerical differentiation of a particular field variable at a point requires the contribution of more neighbouring points than would be used on a grid. These are the downsides of a meshfree method.

Each of the final three chapters in this thesis addresses in some way one of the three main drawbacks listed above.

Chapter 1 consists of a general introduction to SPH and its terminology. Special attention is given to the derivation of the kernel differentiation formulae and their application to the

conservation equations of continuum mechanics. The SPH conservation of mass equation is derived in a moving reference frame and is found to automatically include a previously ad hoc correction term. Finally a description of the Cranfield MCM (meshfree continuum mechanics) code is given, in particular the time integration algorithm.

Chapter 2 starts with a detailed derivation of one of the most commonly used non-reflecting boundary conditions (NRBCs) in other numerical methods. There follows the details of the implementation and testing of the boundary condition in SPH.

Chapter 3 is a stability analysis of SPH. The semi-discrete SPH equations in 1D are linearised and subjected to a stability analysis. An energy conserving form of SPH is derived and is subject to a Lyapunov stability analysis, and conditions are given that guarantee stability (in the Lyapunov sense) for the conservative equations.

Chapter 4 describes a novel method to stabilise basic SPH. The linear stability analysis of the previous chapter is extended to include the proposed method. It is tested and shown to be stable under tension.

Chapter 1

Smoothed Particle Hydrodynamics

Smoothed particle hydrodynamics (SPH) is a meshfree particle method; instead of a mesh the problem domain is discretised by a set of interpolation points. These points have no fixed connectivity; their interaction is governed only by their proximity. The points are referred to as particles because they have a mass and a velocity. Spatial derivatives are approximated by analytical differentiation of special kernel functions centred at each particle. The particles' velocity is identical to the material velocity i.e. the particles follow the material. This and the absence of a fixed mesh means that SPH is a Lagrangian method which is nevertheless tolerant of large deformations. SPH was first devised for modelling gas dynamics in astrophysics by Gingold and Monaghan [31, 30] and independently by Lucy [61]. Later SPH was applied to solid mechanics by Libersky [56, 81]. As well as continued use in astrophysics, further applications in continuum mechanics include: free surface flows [1], multi-phase flows [72], impact [90, 18] and detonation .

1 Kernel approximation

The main distinguishing feature of SPH is the method by which derivatives are approximated. Kernel differentiation does not require a computational grid and this is the advantage of SPH over grid-based methods. The usual derivation of the kernel approx-

imation formulae [71, 57] is to approximate a function, or derivative of a function, with an integral and then to approximate the integral as a volume-weighted sum. By the definition of the Dirac distribution, for a function $f : \Omega \to \mathbb{R}$

$$f(\mathbf{x}) = \int_{\Omega} f(\mathbf{x}')\delta(\mathbf{x} - \mathbf{x}')\mathrm{d}\mathbf{x}'. \tag{1.1}$$

By replacing the delta function with a suitable kernel function an approximation to $f(\mathbf{x})$ is obtained

$$f(\mathbf{x}) \approx \langle f(\mathbf{x}) \rangle = \int_{\Omega_{\mathbf{x}}} f(\mathbf{x}')W\left(|\mathbf{x} - \mathbf{x}'|, h\right)\mathrm{d}\mathbf{x}'. \tag{1.2}$$

We define $\Omega_{\mathbf{x}}$ to be the compact support of the kernel centered at $\mathbf{x}$. The angled brackets signify kernel approximation and h is a parameter as explained below. The kernel function is chosen or constructed such that the following conditions are met:

1. $\int_{\Omega_{\mathbf{x}}} W\left(|\mathbf{x} - \mathbf{x}'|, h\right)\mathrm{d}\mathbf{x}' = 1$.
2. $\lim_{h\to 0} \int_{\Omega_{\mathbf{x}}} f(\mathbf{x}')W\left(|\mathbf{x} - \mathbf{x}'|, h\right)\mathrm{d}\mathbf{x}' = \int_{\Omega_{\mathbf{x}}} f(\mathbf{x}')\delta(\mathbf{x} - \mathbf{x}')\mathrm{d}\mathbf{x}'$, so that $\lim_{h\to 0} \langle f(\mathbf{x}) \rangle = f(\mathbf{x})$.
3. $W\left(|\mathbf{x} - \mathbf{x}'|, h\right) > 0$ if $|\mathbf{x} - \mathbf{x}'| < 2h$ and $W\left(|\mathbf{x} - \mathbf{x}'|, h\right) = 0$ otherwise.

Note also that the kernel is a function of $|\mathbf{x} - \mathbf{x}'|$ and is therefore radially symmetric. Equation (1.2) effectively replaces the original function value with a weighted average or smoothed value. The parameter h is called the smoothing length because increasing h dilates the compact support of the kernel and increases the smoothing effect of the approximation.

The earliest SPH papers used a Gaussian kernel but later Monaghan proposed using B-splines which have the advantage of compact support [67]. One of these is the cubic B-spline,

$$W(r, h) = \frac{c}{h}\begin{cases} 1 - \frac{3}{2}r^2 + \frac{3}{4}r^3 & : r < 1 \\ \frac{1}{4}(2 - r)^3 & : 1 \leq r < 2 \\ 0 & : r \geq 2, \end{cases} \tag{1.3}$$

where $r = \frac{|\mathbf{x}-\mathbf{x}'|}{h}$ and $c = \frac{2}{3}$, $\frac{10}{7\pi}$ or $\frac{1}{\pi}$ in 1D, 2D or 3D, respectively. Unless otherwise indicated, this is the kernel used throughout this work. Which of the many kernels that have been devised is the best is still an open question. Fulk [29] analysed 20 different kernels, including variations on Gaussian kernels, B-splines and kernels with two humps. The bell-shaped kernels are reported to be better, but of those no one kernel is found to be significantly superior (by the criteria described therein). A Wendland kernel is reported to improve stability in a free surface flow simulation [62]. The improvement in stability is linked to the Wendland kernel's positive-definite Fourier transform by [19], see also chapter 3 below where the same link is made indirectly.

1.1 Discrete approximation and consistency

An important consideration for any approximation is the order of consistency - defined as the ability to reproduce exactly a polynomial function of a given order. The properties defined above guarantee first-order consistency; a linear function is reproduced exactly,

$$\begin{aligned}\langle a\mathbf{x}+b\rangle =& a\overbrace{\int_\Omega \mathbf{x}' W\left(|\mathbf{x}-\mathbf{x}'|,h\right)\mathrm{d}\mathbf{x}'}^{=\mathbf{x}} + b\overbrace{\int_\Omega W\left(|\mathbf{x}-\mathbf{x}'|,h\right)\mathrm{d}\mathbf{x}'}^{=1}\\ =& a\mathbf{x}+b.\end{aligned}$$

The second integral is equal to unity by construction and the first is equal to $\mathbf{x}$ because the symmetry of the kernel about the point $\mathbf{x}$ means that $(\mathbf{x}-\mathbf{x}')\,W\left(|\mathbf{x}-\mathbf{x}'|,h\right)$ is an odd function and therefore $\int_\Omega (\mathbf{x}-\mathbf{x}')\,W\left(|\mathbf{x}-\mathbf{x}'|,h\right)\mathrm{d}\mathbf{x}' = 0$.

To approximate the spatial derivative of a function we begin with (1.2) but now approximate the gradient of a function,

$$\langle \nabla f(\mathbf{x})\rangle = \int_\Omega [\nabla f(\mathbf{x}')] W\left(|\mathbf{x}-\mathbf{x}'|,h\right)\mathrm{d}\mathbf{x}'. \tag{1.4}$$

Integrating by parts (1.4) becomes

$$\langle \nabla f(\mathbf{x})\rangle = -\int_\Omega f(\mathbf{x}')\nabla W\left(|\mathbf{x}-\mathbf{x}'|,h\right)\mathrm{d}\mathbf{x}' + \int_\Omega \nabla\left[f(\mathbf{x}')W\left(|\mathbf{x}-\mathbf{x}'|,h\right)\right]\mathrm{d}\mathbf{x}'.$$

By the divergence theorem the second integral can be transformed into the surface integral $\int_{\partial\Omega} f(\mathbf{x}')W\left(|\mathbf{x}-\mathbf{x}'|,h\right)\mathrm{d}\mathbf{S}$. The kernel has compact support so if, $\Omega_{\mathbf{x}} \subset \Omega$ then the surface integral will be equal to zero because $W\left(|\mathbf{x}-\mathbf{x}'|,h\right)=0$ on $\partial\Omega$. Therefore the kernel approximation of $\nabla f(\mathbf{x})$ is

$$\langle \nabla f(\mathbf{x})\rangle = -\int_{\Omega} f(\mathbf{x}')\nabla_{x'} W\left(|\mathbf{x}-\mathbf{x}'|,h\right)\mathrm{d}\mathbf{x}'. \tag{1.5}$$

In practice f is only known at a finite set of interpolation points $\{\mathbf{x}_i\}_{i\in I}$, where $I=\{1,\ldots,N\}$ is an index set. We will refer to the elements of I as particles. For example we may write "particle i has position $\mathbf{x}_i$ and velocity $\mathbf{v}_i$". This provides a convenient notation and is perhaps clearer than writing "the particle *at* $\mathbf{x}_i$ etc..". A particle i has mass m_i and density ρ_i so that a volume $V_i=\frac{m_i}{\rho_i}$ can be defined. Only a subset of the particles contribute to the approximation at each interpolation point. The particles within this contributing subset (the neighbourhood) are referred to as neighbours. The set of all the neighbours of particle i will be denoted by $N(i)\subset I$. This is defined as $N(i)=\{\forall j\in I \text{ s.t. } |\mathbf{x}_i-\mathbf{x}_j|<2h\}$ i.e. those particles for which the kernel function $W\left(|\mathbf{x}_i-\mathbf{x}_j|,h\right)$ is non-zero.

In SPH the integral approximations (1.2) and (1.5) are in turn approximated by a volume weighted sum. The discrete approximation of f at $\mathbf{x}_i$ is therefore,

$$\langle f\left(\mathbf{x}_i\right)\rangle = \sum_{j\in N(i)} f\left(x_j\right) W\left(|\mathbf{x}_i-\mathbf{x}_j|,h\right) V_j, \tag{1.6}$$

and of the derivative,

$$\langle \nabla f\left(\mathbf{x}_i\right)\rangle = -\sum_{j\in N(i)} f\left(x_j\right) \nabla_j W\left(|\mathbf{x}_i-\mathbf{x}_j|,h\right) V_j. \tag{1.7}$$

Where ∇_i denotes differentiation with respect to the variable $\mathbf{x}_i$, i.e. in 3D $\nabla_i = \left(\frac{\partial}{\partial x_i^1},\frac{\partial}{\partial x_i^2},\frac{\partial}{\partial x_i^3}\right)$. Henceforth the convention that $W\left(|\mathbf{x}_i-\mathbf{x}_j|,h\right)V_j = W_{ij}$ will be adopted and the arguments, $\mathbf{x}_i$, $\mathbf{x}_j$ and h, and the particle volume, V_k, will only be referred to explicitly if necessary for clarity.

Equation (1.7) can also be obtained by differentiation of (1.6) instead of direct from the

integral form: If $r = |\mathbf{x}_i - \mathbf{x}_j|$ then

$$\nabla_i W_{ij} = \frac{\mathrm{d}}{\mathrm{d}r} W_{ij} \nabla_i r = \frac{\mathrm{d}}{\mathrm{d}r} W_{ij} \frac{(x_i - x_j)}{r},$$

but

$$\nabla_j W_{ij} = \frac{\mathrm{d}}{\mathrm{d}r} W_{ij} \nabla_j r = \frac{\mathrm{d}}{\mathrm{d}r} W_{ij} \frac{-(x_i - x_j)}{r}.$$

Therefore the derivative of the kernel is anti-symmetric; $\nabla_i W_{ij} = -\nabla_j W_{ij}$. The gradient of (1.6) is then found to be equal to (1.7):

$$\begin{aligned}
\nabla_i \langle f(\mathbf{x}) \rangle &= \sum_{j \in N(i)} f(\mathbf{x}_j) \nabla_i W_{ij} \\
&= -\sum_{j \in N(i)} f(\mathbf{x}_j) \nabla_j W_{ij} \qquad \text{by the anti-symmetry of the kernel derivative} \\
&= \langle \nabla_i f(\mathbf{x}) \rangle \qquad \text{by equation (1.7).}
\end{aligned}$$

In the remainder $\nabla W_{km} = \nabla_k W_{km}$ i.e. if no indication is otherwise given, the gradient will be assumed to be taken with respect to the first index in W_{km}. Therefore equation (1.7) will be written

$$\langle \nabla f(\mathbf{x}_i) \rangle = \sum_{j \in N(i)} f(\mathbf{x}_j) \nabla W_{ij}. \tag{1.8}$$

1.2 Reproducing conditions

The discrete approximation, equation (1.6), is not zero-order consistent for a general arrangement of particles. This is because normalisation and anti-symmetry are not necessarily preserved by the discretisation i.e. $\sum_{j \in N(i)} W_{ij} \neq 1$ and $\sum_{j \in N(i)} \nabla W_{ij} \neq 0$. A general quadratic polynomial function of a vector $\mathbf{x}_i$ can be written

$$f(\mathbf{x}_i) = a + \mathbf{b} \cdot \mathbf{x}_i + \mathbf{x}_i \cdot \mathbf{C} \mathbf{x}_i \tag{1.9}$$

where a is a scalar, $\mathbf{b}$ is a vector, and $\mathbf{C}$ is matrix. A cubic polynomial would involve a third-order tensor coefficient and higher order polynomials correspondingly higher order coefficients. Denote the components of the vector $\mathbf{x}_i$ as x_i^α for $\alpha = 1, 2, 3$. We define a

p^{th}-order tensor $T_{\alpha_1 \ldots \alpha_p}$ so that a n^{th}-order polynomial can be written as

$$f(\mathbf{x}_i) = T + \sum_{p=1}^{n} T_{\alpha_1 \ldots \alpha_p} x_i^{\alpha_1} \ldots x_i^{\alpha_p}, \tag{1.10}$$

where summation over repeated α_i is implied. To derive the reproducing conditions we substitute (1.10) into equation (1.6) and interchange the order of summation;

$$\begin{aligned}
\langle f(\mathbf{x}_i) \rangle &= \sum_{j \in N(i)} f(\mathbf{x}_j) W_{ij} \\
&= \sum_{j \in N(i)} \left\{ T + \sum_{p=1}^{n} T_{\alpha_1 \ldots \alpha_p} x_j^{\alpha_1} \ldots x_j^{\alpha_p} \right\} W_{ij} \\
&= T \sum_{j \in N(i)} W_{ij} + \sum_{p=1}^{n} T_{\alpha_1 \ldots \alpha_p} \left\{ \sum_{j \in N(i)} x_j^{\alpha_1} \ldots x_j^{\alpha_p} W_{ij} \right\}.
\end{aligned} \tag{1.11}$$

It follows that if, for all i,

$$\sum_{j \in N(i)} W_{ij} = 1, \tag{1.12a}$$

$$\sum_{j \in N(i)} W_{ij} x_j^{\alpha_1} = x_i^{\alpha_1}, \tag{1.12b}$$

and that for $p = 2$ to k

$$\sum_{j \in N(i)} W_{ij} x_j^{\alpha_1} \ldots x_j^{\alpha_p} = x_i^{\alpha_1} \ldots x_i^{\alpha_p}. \tag{1.12c}$$

Then the first k terms of the n^{th}-order polynomial (1.10) will be reproduced exactly. It is of more interest here that the gradient of a function is accurately approximated. The approximation $\langle \nabla f \rangle$ can be found by substituting (1.10) into (1.8),

$$\begin{aligned}
\left\langle \frac{\partial f}{\partial x_i^\beta} \right\rangle &= T \sum_{j \in N(i)} \frac{\partial W_{ij}}{\partial x_i^\beta} + \sum_{p=1}^{n} T_{\alpha_1 \ldots \alpha_p} \left\{ \sum_{j \in N(i)} x_j^{\alpha_1} \ldots x_j^{\alpha_p} \frac{\partial W_{ij}}{\partial x_i^\beta} \right\} \\
&= T \sum_{j \in N(i)} \frac{\partial W_{ij}}{\partial x_i^\beta} + T_{\alpha_1} \left\{ \sum_{j \in N(i)} x_j^{\alpha_1} \frac{\partial W_{ij}}{\partial x_i^\beta} \right\} + \text{h.o.t}
\end{aligned}$$

Therefore if the following conditions hold the gradient of a linear polynomial (in this case $\frac{\partial f}{\partial x_i^\beta} = T_\beta$) will be evaluated exactly.

$$\sum_{j \in N(i)} \nabla W_{ij} = \mathbf{0} \qquad \text{or} \qquad \sum_{j \in N(i)} \frac{\partial W_{ij}}{\partial x_i^\beta} = 0 \tag{1.13a}$$

and

$$\sum_{j\in N(i)} \mathbf{x}\otimes\nabla W_{ij} = \mathbf{I} \qquad \text{or} \qquad \sum_{j\in N(i)} x_j^{\alpha_1}\frac{\partial W_{ij}}{\partial x_i^{\beta}} = \delta_{\alpha_1\beta}. \tag{1.13b}$$

1.2.1 Correcting for consistency

To restore zero-order consistency we can use Shepard functions; set

$$\tilde{W}_{ij} = \frac{W_{ij}}{\sum_{k\in N(i)} W_{ik}} \tag{1.14}$$

then

$$\sum_{j\in N(i)} \tilde{W}_{ij} = \frac{\sum_{j\in N(i)} W_{ij}}{\sum_{k\in N(i)} W_{ik}} = 1.$$

Alternatively the derivative can be corrected directly by the addition of an extra term, due to Monaghan [68, 66], to equation (1.8),

$$\langle\nabla f(\mathbf{x}_i)\rangle = \sum_{j\in N(i)} \left(f(\mathbf{x}_j) - f(\mathbf{x}_i)\right)\nabla W_{ij}. \tag{1.15}$$

Note that the correction term is equal to zero in integral form

$$-\sum_{j\in N(i)} f(\mathbf{x}_i)\nabla W_{ij} \approx f(\mathbf{x}_i)\int_{\Omega} W\left(|\mathbf{x}_i - \mathbf{x}'|\right)\mathrm{d}\mathbf{x}' = 0.$$

With this correction applied any constant-valued function's gradient will clearly be correctly evaluated to $\mathbf{0}$. This [71] is sometimes justified by writing

$$g\nabla f = \nabla(gf) - f\nabla g \tag{1.16}$$

where g is a differentiable function chosen to suit the circumstances. Each derivative in (1.16) is then approximated with equation (1.8). To get to (1.15), for example, set $g \equiv 1$. As a derivation this is not particularly satisfying as it gives no clue why this should be an improvement.

Correcting to enforce higher orders of consistency is always possible. Liu and Liu [57] present a method that reproduces a polynomial of order n. In 1D the smoothing function is taken as

$$W_{ij} = \sum_{m=0}^{n} a_m(x_i, h)\left(\frac{x_i - x_j}{h}\right)^m \tag{1.17}$$

and the coefficients a_m are chosen to enforce the consistency conditions (1.12). In practice this involves solving, in 1D, an $n \times n$ linear system for each particle at every time step. Unfortunately the smoothing functions are not guaranteed to be symmetric or positive definite which can produce unphysical behaviour such as a negative density. The reproducing kernel particle method (RKPM) [58, 59] follows similar principles to (1.17); the difference being that the original kernel function is modified by a correcting function to reproduce a polynomial of a given order.

Moving least squares (MLS) is another method [20, 8, 51], capable of an arbitrary order of consistency. Local approximations for each particle of the form $\langle f \rangle = \sum_{i=1,n} p_i(x) a_i(x)$ are assumed, where n is the required order of the approximation. The $p_i(x)$ are elements of a set of basis functions, for example, in 1D, to enforce second-order consistency $p_i \in \{1, x, x^2\}$. The a_i are the coefficients found by minimising a functional for each particle

$$J_i = \sum_{j \in N(i)} W_{ik} \left\{ \left(\sum_{k=1,n} p_k \left(x_j\right) a_k \left(x_i\right) \right) - f\left(x_j\right) \right\}^2 \tag{1.18}$$

where $f(x)$ is the function to be approximated. As an example, the simplest case is to choose $p_i = 1$ as the single basis function. Then (1.18) becomes

$$J_i = \sum_{j \in N(i)} W_{ik} \left(a\left(x_i\right) - f\left(x_j\right)\right)^2 .$$

By differentiating with respect to a and setting the result equal to zero the optimal coefficients (a) are found

$$\frac{\mathrm{d}J_i}{\mathrm{d}a} = 2 \sum_{j \in N(i)} W_{ij} \left(a\left(x_i\right) - f\left(x_j\right)\right)$$

so that

$$a\left(x_i\right) \sum_{k \in N(i)} W_{ik} = \sum_{j \in N(i)} f\left(x_j\right) W_{ij}$$

$$a\left(x_i\right) = \sum_{j \in N(i)} \frac{f\left(x_j\right) W_{ij}}{\sum_{k \in N(i)} W_{ik}} = \sum_{j \in N(i)} f\left(x_j\right) \tilde{W}_{ij}$$

exactly reproducing the Shepard function approximation from (1.14). In fact, it can be shown [9] that the approximations obtained by enforcing the consistency conditions (1.12) on the kernel in the manner of the RKPM are equivalent to MLS.

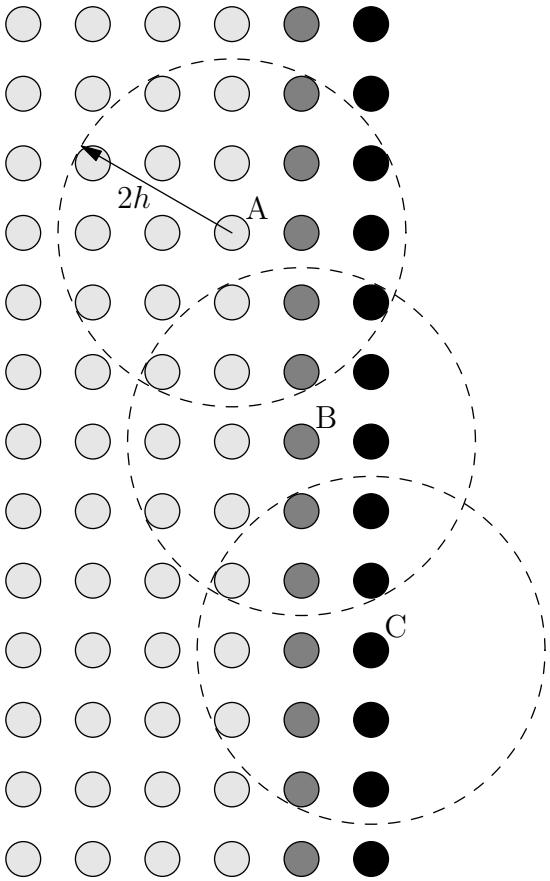

Figure 1.1: Particle deficiency: Particle A has a full set of neighbours and particle C, on the boundary, is deficient. Particle B, nominally on the interior, also has an incomplete set of neighbours.

Instead of requiring consistency as an end in itself, some authors have derived first-order consistent conditions as a consequence of requiring conservation of linear and angular momentum [13] or of preserving the homogeneity and isotropy of space. From the latter, normalised corrected SPH (NCSPH) [89] is derived. The resulting conditions are equations (1.12a) and (1.13b) and the kernel is modified to enforce these conditions. If $\tilde{W}_{ij}$ is the corrected kernel from (1.14) then the normalised-corrected kernel is

$$\tilde{\nabla}\tilde{W}_{ij} = \nabla\tilde{W}_{ij} \cdot \left(\sum_{k \in N(i)} \mathbf{x}_k \otimes \nabla\tilde{W}_{ik} \right)^{-1} . \tag{1.19}$$

This is the formulation that is used in the MCM[a] code and it is to be understood that in subsequent chapters the first-order consistent method used is NCSPH.

[a]Meshless continuum mechanics, the Cranfield university SPH code.

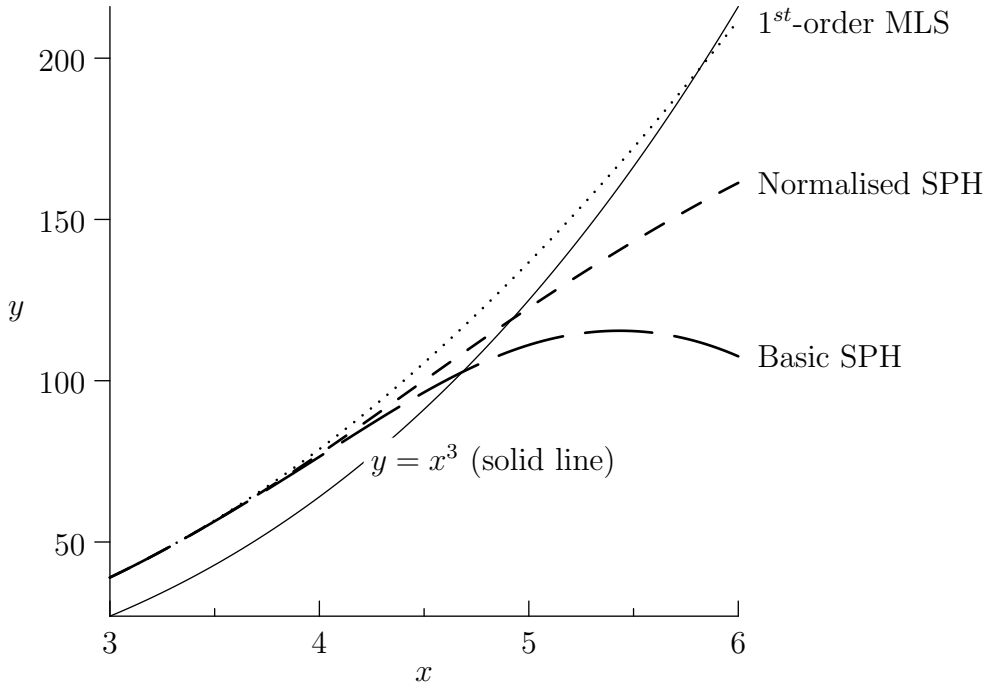

Figure 1.2: Approximation of $f(x) = x^3$ near boundary using seven evenly-spaced particles from $x = 0.0$ to $x = 6.0$ with a smoothing length $h = 2.0$. Note that normalised SPH uses the Shepard function kernel - equation (1.14).

1.3 Boundary conditions

Imposing boundary conditions in SPH can be difficult. In the first instance the "boundary" in SPH is ambiguous. A computational mesh has a well-defined boundary and nodes on it will remain there. In contrast, in SPH there is no fixed connection between particles and the influence of the boundary extends into the interior (see figure 1.1). Additionally, SPH does not interpolate nodal values exactly i.e. $\langle f(\mathbf{x}_i)\rangle \neq f(\mathbf{x}_i)$ which means that Dirichlet conditions cannot simply be prescribed on the boundary. Various strategies have had to be invented to overcome these limitations. For example, the impostion of zero-velocity wall-type boundary conditions can be achieved by using ghost particles [56, 81] or by the creation of a repulsive force to prevent particles penetrating the boundary [69]. Another difficulty is that equation (1.2), i.e. kernel approximation, is only valid if the kernel support is completely within the problem domain Ω. Otherwise the function being

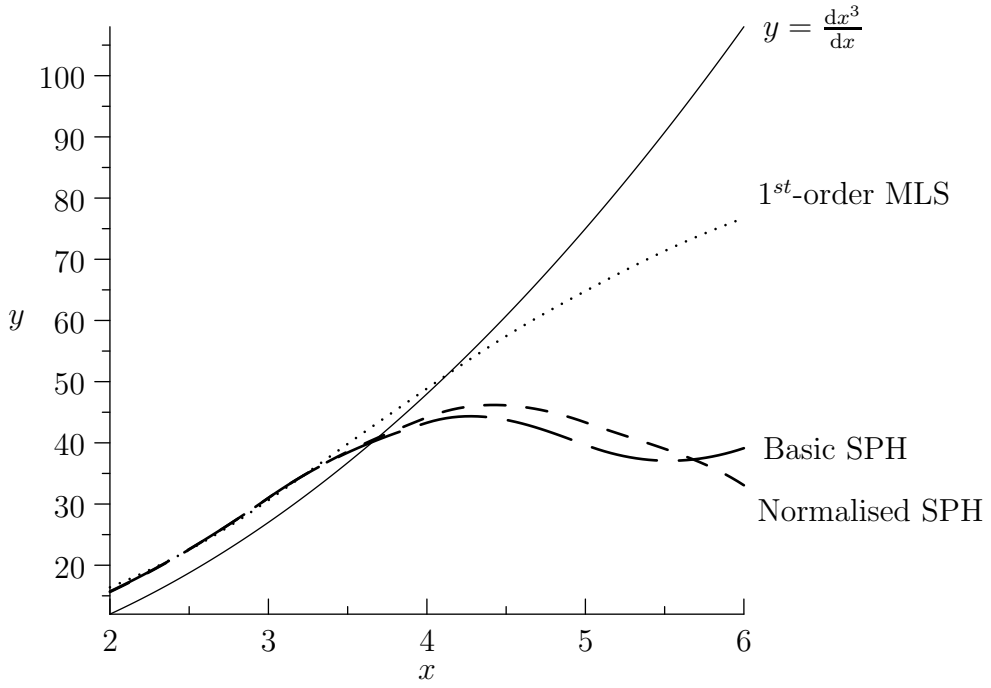

Figure 1.3: Approximation of $f'(x) = \frac{\mathrm{d}x^3}{\mathrm{d}x}$ near boundary using seven evenly-spaced particles from $x = 0.0$ to $x = 6.0$ with a smoothing length $h = 2.0$. Note zero-order correction from equation (1.15) applied to basic SPH.

approximated is effectively,

$$\tilde{f}(\mathbf{x}) = \begin{cases} f(\mathbf{x}) & : \text{ in } \Omega \\ 0 & : \text{ otherwise.} \end{cases} \tag{1.20}$$

This means that near a boundary there is a deficiency of particles and the approximation behaves as if extra particles with a zero value exist outside of the domain. The resulting inaccuracy in the approximation of a function and its derivative is illustrated in figures 1.2 and 1.3, respectively. Note how the approximation worsens closer to the boundary and is only partly mitigated by using a higher order method - in this case linear least squares. For a free surface this error actually approximates the correct zero-stress boundary condition. This automatic treatment of free surface boundary conditions is very useful in many applications and its absence is a drawback of higher order methods.

1

1.4 Smoothing length

In SPH it is important that the smoothing length (h) is correctly chosen. If it is too large the approximated field is over-smoothed and detail is lost, and the computation is slowed as particles acquire too many neighbours. If h is too small then particles have too few neighbours and accuracy suffers. A smoothing length of between one and two times the particle spacing, Δx, is generally regarded as striking the appropriate balance. Given a uniform square grid of fixed particles Δx can be defined unambiguously as the smallest distance between two particles. However an initially uniform arrangement of particles will soon become disordered. If the problem involves significant strain, using the original smoothing length will result in particles with too many or too few neighbours. To maintain accuracy and efficiency, various authors have proposed changing the smoothing length to reflect changes in particle distribution.

The first papers describing SPH [31, 61] used a universal smoothing length, equal for each particle, but allowed the length to change as the gas expanded or contracted. It was later suggested [32, 43] that each particle's smoothing length should change independently to better reflect local changes in particle configuration and, by implication, density. Hernquitz and Katz [43] modify the smoothing length so as to keep the number of neighbours approximately constant throughout the simulation; a similar approach is used in [75]. Instead of keeping the number of neighbouring particles constant Kitsionas and Whitworth [50] use the total mass of the neighbours. This is done in combination with a particle-splitting algorithm (see chapter 2) and they report that the alternative approach gives much better results. One possible factor in the improvement may be that the smoothing length will tend to vary more gradually from the coarser to the finer sub-domains.

In [32] the authors set the smoothing length as inversely proportional to the number of neighbours. More common [71, 14, 57] is using equation (1.21),

$$h_i = h_i^0 \left(\frac{\rho_i^0}{\rho_i} \right)^{1/d}, \tag{1.21}$$

where h_i and ρ_i are, respectively, the i particle's smoothing length and density at the current time and d is the number of dimensions. One more alternative [11] is to differentiate (1.21) with respect to time and evolve the smoothing length with

$$\frac{\mathrm{d}h}{\mathrm{d}t} = -\frac{h}{d\rho}\frac{\mathrm{d}\rho}{\mathrm{d}t}. \tag{1.22}$$

Modification of the smoothing length as outlined above is intended to improve the accuracy of SPH by maintaining an optimal neighbourhood size for each particle. Formally, if the smoothing length is to depend on position then extra terms must be included in the gradient of the kernel;

$$\frac{\mathrm{d}W}{\mathrm{d}\mathbf{x}} = \frac{\partial W}{\partial \mathbf{x}} + \frac{\partial W}{\partial h}\frac{\mathrm{d}h}{\mathrm{d}\mathbf{x}}. \tag{1.23}$$

Analysis in [25] suggests that if the smoothing length varies on a scale close to h then the extra, ∇h, term can safely be ignored, and this is the usual practice. However it has been reported [42, 74] that large errors, especially in energy conservation, can arise when the ∇h term is neglected and conservation improves with the addition of the extra term. Others too have obtained better accuracy in a shock tube simulation [79] and for dam breaking [14].

The density of a particle is calculated either directly by summation over the particle's neighbours,

$$\rho_i = \sum_{j \in N(i)} m_j W_{ik}(h), \tag{1.24}$$

or via the continuity equation

$$\dot{\rho}_i = \sum_{j \in N(i)} \frac{m_j}{\rho_i} \left(\mathbf{v}_i - \mathbf{v}_j\right) \nabla W_{ij}(h). \tag{1.25}$$

If the smoothing length and density are related then, for example, (1.21) together with (1.24) or (1.25) are coupled non-trivially. Usually the smoothing length is updated using the density at the previous time step, alternatively, the non-linear system can be approximately solved using an iterative method [14, 79]. Increased accuracy is reported at the cost of increased computational effort.

An important consideration when using a variable smoothing length is the need to ensure that particle interactions remain symmetric. In standard SPH the momentum equation is

$$\dot{\mathbf{v}}_i = \sum_{j \in N(i)} m_k \left(\frac{\sigma_i}{\rho_i^2} + \frac{\sigma_j}{\rho_j^2} \right) \nabla W_{ij}(h). \tag{1.26}$$

The anti-symmetry of (1.26) ensures conservation of linear momentum; a variable, particle specific, smoothing length breaks this anti-symmetry and linear momentum is no longer conserved. Two alternative methods are to replace $\nabla W_{ij}(h_j)$ with $\nabla W_{ij}(h_{ij})$ where h_{ij} is symmetric, for example, $h_{ij} = \frac{1}{2}(h_i + h_j)$[25] or to average the kernel function directly [43]

$$\nabla W_{ij}(h_i, h_j) = \frac{1}{2} \left[\nabla W_{ij}(h_j) + \nabla W_{ji}(h_i) \right]. \tag{1.27}$$

Other alternatives for a symmetric smoothing length are given in [57].

Adaptive SPH (ASPH) [77, 83] takes the idea of variable smoothing lengths a step further. The scalar smoothing length is replaced with a tensor G. The normally spherical domain of influence for each particle is replaced by an ellipsoid. This method is designed to cope with uniaxial or otherwise highly non-uniform strains. A spherical support domain expands or contracts uniformly. This may result in a deficiency of particles contributing to the approximation perpendicular to the axis of greatest compression. The elliptical domain is claimed to better reflect the changes in particle distribution and to improved accuracy. The difficulties associated with a variable smoothing length apply equally to ASPH. Particle interactions are made symmetrical using (1.27) and the effect of neglecting the ∇h term is mitigated by periodically smoothing the smoothing tensor itself to ensure that the variation of h is kept reasonably constant across a few smoothing lengths.

2 Implementation

For future reference this section will present the continuity equations and their SPH discretisations followed by a brief description of the time integration algorithm used by the Cranfield MCM SPH code.

The conservation equations for mass, momentum and energy are, respectively:

$$\dot{\rho} = -\rho \nabla \cdot \mathbf{v}, \tag{1.28}$$

$$\rho \dot{\mathbf{v}} = \nabla \sigma, \tag{1.29}$$

$$\rho \dot{E} = \sigma : \nabla \mathbf{v}. \tag{1.30}$$

These must be supplemented with a constitutive equation in order to be well-posed. The next step is to approximate the spatial derivatives in the above equations in order to derive the particle equations.

2.1 SPH spatial discretisation

Note that in this section (2) the particle volume $V_i = \frac{m_i}{\rho_i}$ will be included in the formulae explicitly.

2.1.1 Density

There are two options for updating the density in SPH. The first is to use a kernel approximation,

$$\langle \rho_i \rangle = \sum_{j \in N(i)} \rho_j W_{ij} \frac{m_j}{\rho_j} = \sum_{j \in N(i)} m_j W_{ij}. \tag{1.31}$$

Alternatively we can use the continuity equation and approximate the divergence of the velocity using kernel differentiation;

$$\langle \dot{\rho}_i \rangle = \sum_{j \in N(i)} (\mathbf{v}_i - \mathbf{v}_j) \cdot \nabla W_{ij} \frac{m_j}{\rho_j}. \tag{1.32}$$

In practice the rate of deformation tensor ($\mathbf{D}$) is needed to update the stress this is approximated with

$$\langle \mathbf{D}_i \rangle = \frac{1}{2} \left(\mathbf{L}_i + \mathbf{L}_i^T \right), \tag{1.33}$$

where

$$\mathbf{L}_i = \sum_{j \in N(i)} (\mathbf{v}_i - \mathbf{v}_j) \otimes \nabla W_{ij} \frac{m_j}{\rho_j}.$$

2.1.2 Momentum

Applying the kernel differentiation formula (1.15) to the conservation equation would give a particle momentum equation of the form

$$\langle \dot{\mathbf{v}}_i \rangle = \frac{1}{\rho_i} \sum_{j \in N(i)} \frac{m_j}{\rho_j} (\sigma_j - \sigma_i) \cdot \nabla W_{ij}. \tag{1.34}$$

However this is not often used as the forces between particles are not symmetric, violating Newton's third law. Therefore a symmetric form which conserves momentum locally is preferred

$$\langle \dot{\mathbf{v}}_i \rangle = \frac{1}{\rho_i} \sum_{j \in N(i)} \frac{m_j}{\rho_j} (\sigma_j + \sigma_i) \cdot \nabla W_{ij}, \tag{1.35}$$

or

$$\langle \dot{\mathbf{v}}_i \rangle = \sum_{j \in N(i)} m_j \left(\frac{\sigma_j}{\rho_j^2} + \frac{\sigma_i}{\rho_i^2} \right) \cdot \nabla W_{ij}. \tag{1.36}$$

2.1.3 Energy

The continuity of energy equation is approximated with

$$\left\langle \dot{E}_i \right\rangle = \frac{\sigma_i}{\rho_i^2} : \sum_{j \in N(i)} m_j (\mathbf{v}_i - \mathbf{v}_j) \otimes \nabla W_{ij}. \tag{1.37}$$

2.1.4 SPH formulated in a moving reference frame [88]

The corrections applied to the kernel differentiation formulae are in some sense arbitrary. The justification is that without correction, kernel differentiation is not accurate. It is possible to derive equation (1.32) without resorting to ad hoc correction if the equations of motion are considered in a moving reference frame attached to a particular particle. Consider a coordinate system attached to a particle i moving at velocity $\mathbf{v}_i$. In the referential coordinate system the velocity of another particle, j, will be $\mathbf{v}_j^R = \mathbf{v}_j - \mathbf{v}_i$, it follows that $\mathbf{v}_i^R = 0$. The total derivative of a function is

$$\frac{Df}{Dt} = \frac{\partial f}{\partial t} + \mathbf{v} \cdot \nabla f.$$

We define the referential derivative to be

$$\frac{\tilde{D}f}{Dt} = \frac{\partial f}{\partial t} + \mathbf{v}_i \cdot \nabla f$$

and therefore

$$\frac{Df}{Dt} = \frac{\tilde{D}f}{Dt} + \mathbf{v}^R \cdot \nabla f.$$

The continuity equation (1.28) can be written in terms of the referential derivative;

$$\begin{aligned} \frac{\tilde{D}\rho}{Dt} &= -\rho \nabla \cdot \mathbf{v} - \mathbf{v}^R \cdot \nabla \rho \\ &= -\nabla \cdot (\rho \mathbf{v}) + \mathbf{v}_i \cdot \nabla \rho. \end{aligned} \tag{1.38}$$

The uncorrected kernel approximation (1.8) of $\nabla \cdot (\rho \mathbf{v})$ and $\nabla \rho$ can now be substituted into (1.38) and we find,

$$\begin{aligned} \left\langle \frac{D\rho_i}{Dt} \right\rangle &= -\sum_{j \in N(i)} \rho_j \mathbf{v}_j \cdot \nabla W_{ij} \frac{m_j}{\rho_j} + \mathbf{v}_i \cdot \sum_{j \in N(i)} \rho_j \nabla W_{ij} \frac{m_j}{\rho_j} \\ &= \sum_{j \in N(i)} m_j \left(\mathbf{v}_j - \mathbf{v}_i \right) \cdot \nabla W_{ij}. \end{aligned} \tag{1.39}$$

Note that at the particle the referential and total derivative coincide, $\frac{\tilde{D}\rho_i}{Dt} = \frac{D\rho_i}{Dt}$. Thus the correction term has appeared naturally in equation (1.39) without resorting to arbitrary correction. For details of how the same idea can be applied to the momentum equation and numerical examples with the resulting equations see [88].

2.2 Time integration

The MCM code uses an explicit leap-frog time integration scheme. As an explicit method it is only conditionally stable and the time step (Δt) must be adjusted in order to satisfy the CFL condition [73]. The integration scheme uses the time derivative of a variable at an intermediate time step to advance the variable to the next time step,

$$\begin{aligned} f^n &= f^{n-1} + \Delta t^{n-1/2} \dot{f}^{n-1/2} \\ f^{n+1/2} &= f^{n-1/2} + \Delta t^n \dot{f}^n, \end{aligned} \tag{1.40}$$

where each superscript refers to the timestep at which f is known. To illustrate, consider the wave equation in 1D

$$\frac{\partial^2 u}{\partial x^2} = \frac{\partial^2 u}{\partial t^2}. \tag{1.41}$$

Introduce supplementary variables $s = \frac{\partial v}{\partial x}$ and $v = \frac{\partial u}{\partial t}$ then (1.41) becomes

$$\frac{\partial v}{\partial t} = \frac{\partial s}{\partial x}, \tag{1.42a}$$

$$\frac{\partial s}{\partial t} = \frac{\partial v}{\partial x}. \tag{1.42b}$$

The kernel approximations of the spatial derivatives at timestep n and particle i are $\langle s_x \rangle_i^n$ and $\langle v_x \rangle_i^n$ and the leap-frog scheme advances s_i and v_i through time as follows;

$$v_i^{n+1/2} = v_i^{n-1/2} + \Delta t \left\langle s_x \right\rangle_i^n, \tag{1.43a}$$

$$s_i^n = s_i^{n-1} + \Delta t \left\langle v_x \right\rangle_i^{n+1/2}. \tag{1.43b}$$

The wave equation is a special case of the equations solved by the full MCM code and the algorithm is in essence as in equation (1.43). The general operation of the code proceeds as algorithm 1.1 below (see [18] for full details).

Algorithm 1.1 Leap-frog time integration in MCM

while $current\_time \leq end\_time$ **do**

Perform neighbour search

for $i = 1$ to Number of Particles **do**

Calculate $\langle \mathbf{D} \rangle_i^{n-1/2}$ and $\langle \dot{\rho} \rangle_i^{n-1/2}$ ▷ Equations (1.32) and (1.33)

$\rho_i^n \leftarrow \rho_i^{n-1} + \Delta t^{n-1/2} \langle \dot{\rho} \rangle_i^{n-1/2}$ ▷ Update density

Calculate $\langle \dot{\sigma} \rangle_i^{n-1/2}$ ▷ Constitutive equation

$\sigma_i^n \leftarrow \sigma_i^{n-1} + \Delta t^{n-1/2} \langle \dot{\sigma} \rangle_i^{n-1/2}$ ▷ Update stress

Calculate $\mathbf{a}_i^n$ ▷ Equation (1.36)

end for

$\Delta t^n \leftarrow \Delta t^{n-1}$; $\Delta t^{n+1/2} \leftarrow \Delta t^{n-1/2}$

for $i = 1$ to Number of Particles **do**

$\mathbf{v}_i^{n+1/2} \leftarrow \mathbf{v}_i^{n-1/2} + \Delta t^n \mathbf{a}_i^n$

$\mathbf{x}_i^n \leftarrow \mathbf{x}_i^{n-1} + \Delta t^{n+1/2} \mathbf{v}_i^{n+1/2}$

end for

$current\_time \leftarrow current\_time + \Delta t^n$

end while

Chapter 2

Non-Reflecting Boundary Conditions

1 Introduction

There are many problems where the natural domain of the problem is too large for computer simulation to be practical. As a consequence, artificial boundaries (ABs) must be introduced to truncate the computational domain. For example, in SPH an AB may be used to simulate a continuous flow of fluid down a channel; particles are deleted at the outlet and new particles are created at the inlet [55, 26]. In this chapter we seek to apply an artificial boundary condition in SPH which can absorb elastic waves generated in the interior of some domain. Artificial boundary conditions which are designed to absorb incoming waves, not necessarily elastic waves, are often called non-reflecting boundary conditions (NRBCs). Such a boundary condition is useful in, for example, seismology or impact problems and could extend the applicability of SPH in these, and other, areas. Note that boundary conditions in general, and NRBCs in particular, are not well developed in SPH, but where examples of NRBCs used in SPH (or other particle methods) exist in the literature they will be mentioned where appropriate during the introduction. However there is an extensive body of theoretical, finite difference (FD) and, to a lesser extent, finite element (FE) literature dedicated to NRBCs, for detailed reviews see [34, 33, 86, 40].

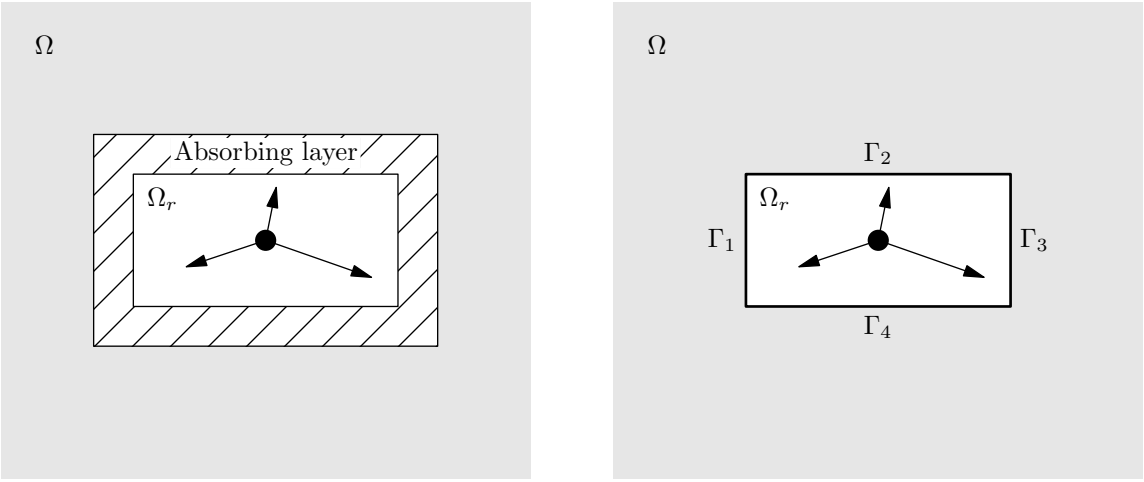

(a) (b)

Figure 2.1: A domain Ω is restricted to Ω_r and a NRBC must be applied. In (a) an absorbing layer is situated outside Ω_r that is designed to damp incoming waves. In (b) a boundary condition is imposed on $\delta\Omega_r = \bigcup_{i=1}^{4} \Gamma_i$ that is solved alongside the PDE defined in the interior.

In figure 2.1 two general methods for constructing NRBCs are represented. In the first, represented in figure 2.1a, an absorbing layer that is designed to damp waves entering from the interior surrounds Ω_r. To achieve the desired absorbtion at the boundary the equations of motion inside the absorbing layer are modified in some way. In [78], an SPH simulation of wave impact on a ship, an absorbing layer is implemented upstream to absorb the wave after it has passed the ship. The boundary condition consists of a sponge layer of particles where the velocity is linearly damped towards zero. This method is easy to implement but requires the addition of a relatively thick layer of particles. The difficulty inherent in absorbing layer formulations is that at the interface between Ω_r and the absorbing layer, outgoing waves will tend to produce spurious reflections. This problem is solved by using a perfectly matched layer (PML) for which there are no spurious interfacial reflections; PMLs are, theoretically, reflectionless. The PML method was invented by Berenger [12] to absorb electromagnetic waves and has since been applied to elastic waves [17, 2]. Consider an absorbing layer in the space $x > 0$ and a problem domain in $x \leq 0$, then the PDE inside the layer is modified to include damping terms

applied only to the components of, for example, the velocity parallel to the x-axis. The damping parameters can then be choosen to exponentially attenuate waves entering the absorbing layer. Perfectly matched layers are reported to give good results even for the absorption of surface waves [27].

For the second broad type of boundary condition, represented in figure 2.1b, there is a further division between global and local boundary conditions. Global boundary conditions are more accurate, even exact, but are only applicable for certain boundary geometries e.g. spherical boundaries. In addition they are non-local in space and/or time, requiring information from the whole boundary and previous time-steps. An example is the Dirichlet to Naumann (DtN) map [48, 36] where the analytical solution of the PDE on the exterior domain, i.e. in $\Omega \setminus \Omega_r$, provides a boundary condition for $\delta\Omega_r$. The requirement that the exterior problem be solved analytically restricts the boundary geometry; in practice a circular or spherical boundary is used. Further, the condition is non-local in space but it can be localised, though at the cost of no longer being exact, see [35] and for elastic waves [41].

We finally consider local NRBCs; the approach used can be characterised as follows: the problem domain Ω is truncated to Ω_r and $\delta\Omega_r$ becomes an AB that is designed to absorb outgoing (that is leaving Ω_r) waves. Consider for example the 2D wave equation defined on $\Omega \subseteq \mathbb{R}^2$

$$\frac{\partial^2 u}{\partial t^2} = \frac{\partial^2 u}{\partial x^2} + \frac{\partial^2 u}{\partial y^2} \qquad \text{for } (x, y) \in \Omega. \tag{2.1}$$

In truncating the domain (2.1) is replaced by another problem:

$$\begin{aligned} \frac{\partial^2 u}{\partial t^2} &= \frac{\partial^2 u}{\partial x^2} + \frac{\partial^2 u}{\partial y^2} \qquad \text{for } (x, y) \in \Omega_r \\ \mathcal{L}u &= 0 \qquad \text{for } (x, y) \in \delta\Omega_r, \end{aligned} \tag{2.2}$$

where $\mathcal{L}$ is some differential operator. In principal the, as yet unspecified, PDE on the boundary ($\mathcal{L}u = 0$) is solved alongside the interior problem. The hope is that the solution obtained for (2.2) is sufficiently close to the solution for the original problem (2.1). The advantage of local NRBCs is that there are no theoretical restrictions on

the boundary geometry. They are also relatively easy to implement, computationally inexpensive and, except for some more recent high-order implementations, do not require any extra particles to be placed around the domain. There has been some previous work done in SPH using local NRBCs. In [55] the authors apply a boundary condition based on characteristic variables where at the boundaries appropriate characteristic variables are prescribed. This method relies on the flow being quasi-one dimensional. A similar method but applied to the shallow water equations is used in [87]. Finally in [23] the authors implement, not in SPH but in the related vortex particle method, a non-reflecting boundary of the Engquist-Majda (E-M) type (see § 1.1) for acoustic waves. Particle deficiency near the boundary requires that a one-sided kernel is used near the boundary to accurately calculate the derivative. It is a boundary condition of this type, due originally to [16], which we apply to SPH in this chapter and detailed derivations are given below.

1.1 The Engquist-Majda NRBCs

This section will re-derive, in detail, a local NRBC which can absorb elastic waves. See appendix A § 3 for an introduction to elastic waves. There is a close association between the scalar wave equation and elastic waves and we therefore start by discussing NRBCs for the wave equation in 1D and 2D. We give two derivations for the NRBCs for the wave equation (in 1D and 2D). One follows the original derivation given by Engquist and Majda in [24]. They first derive an exact, but non-local boundary condition which is localised by approximation. The second follows the method given in [6] to derive a NRBC for elastic waves; and [21] for electro-magnetic waves (Maxwell's equations), and for acoustic waves in a 2D flow (linearised Euler equations). This method is conceptually simpler. The idea is to try and minimise the reflection coefficient of a incident plane wave by choosing the coefficients of a linear constant coefficient boundary condition.

1.1.1 One-dimensional wave equation

A particularly simple NRBC exists for the 1D wave equation which is local and perfectly absorbing. We derive this condition in detail in order to introduce the ideas needed when deriving a local NRBC in 2D. Consider the one dimensional wave equation on a semi-infinite domain $(-\infty, 0]$;

$$\frac{\partial^2 u}{\partial t^2} = c^2 \frac{\partial^2 u}{\partial x^2} \qquad \text{with} \qquad \mathcal{L}u|_{x=0} = 0. \tag{2.3}$$

where $\mathcal{L}$ is an, as yet unspecified, differential operator. The task is to choose $\mathcal{L}$ in such a way that there is no reflection. Or, equivalently, that a right moving wave (i.e. towards $x = 0$) is absorbed by the boundary condition. A right moving harmonic wave with amplitude A, angular frequency ω, and wave number $k = \omega/c$ has the form

$$u(x,t) = Ae^{i(kx-\omega t)}. \tag{2.4}$$

We will show that the boundary condition defined by

$$\mathcal{L} = \frac{\partial}{\partial x} - ik = \frac{\partial}{\partial x} - \frac{i\omega}{c}, \tag{2.5}$$

will absorb, perfectly, a wave of the form (2.4). First notice that multiplication of (2.4) by $-i\omega$ is equivalent to differentiation with respect to time $\frac{\partial}{\partial t}$;

$$\frac{\partial}{\partial t} Ae^{i(kx-\omega t)} = -i\omega Ae^{i(kx-\omega t)}.$$

Equation (2.5) can therefore be rewritten;

$$\mathcal{L} = \frac{\partial}{\partial x} + \frac{1}{c}\frac{\partial}{\partial t}. \tag{2.6}$$

It can be seen by substitution of (2.4) into (2.6) that $\mathcal{L}$ defined thus will cancel this right moving wave. Indeed for any right moving wave of the form $f(x - ct)$;

$$\mathcal{L}f(x-ct) = f' - \frac{1}{c}cf' = 0.$$

In anticipation of the 2D case to follow a general solution to (2.3) can be written as a superposition of harmonic waves,

$$u(x,t) = \int_0^\infty A(\omega) e^{i(\frac{\omega}{c}x - \omega t)} \mathrm{d}\omega. \tag{2.7}$$

The boundary condition for all ω is then

$$\mathcal{L}u\big|_{x=0} = \frac{\partial u}{\partial x} - \int_0^\infty i\frac{\omega}{c}A(\omega)e^{i(\frac{\omega}{c}x-\omega t)}\mathrm{d}\omega = 0. \tag{2.8}$$

It can be confirmed easily that this will exactly cancel waves like (2.7) because

$$\frac{\partial u}{\partial x} = \frac{\partial}{\partial x}\int_0^\infty A(\omega)e^{i(\frac{\omega}{c}x-\omega t)}\mathrm{d}\omega = \int_0^\infty i\frac{\omega}{c}A(\omega)e^{i(\frac{\omega}{c}x-\omega t)}\mathrm{d}\omega.$$

Note too that

$$\frac{\partial u}{\partial t} = \frac{\partial}{\partial t}\int A(\omega)e^{i(\frac{\omega}{c}x-\omega t)}\mathrm{d}\omega = -\int_0^\infty i\omega A(\omega)e^{i(\frac{\omega}{c}x-\omega t)}\mathrm{d}\omega. \tag{2.9}$$

Comparison of the above with (2.8) reveals that the boundary condition may be rewritten

$$\mathcal{L}\big|_{x=0} = \frac{\partial u}{\partial x} + \frac{1}{c}\frac{\partial u}{\partial t} = 0 \tag{2.10}$$

exactly recovering the boundary condition derived by considering only a harmonic wave of a single angular frequency ω.

To illustrate further we consider the reflection coefficient of a harmonic wave incident to $x = 0$. In general the solution will have a transmitted and reflected part so that

$$u(x,t) = A^R e^{ik(x+ct)} + A^T e^{ik(x-ct)}. \tag{2.11}$$

where A^R and A^T are the amplitudes of the reflected and transmitted wave respectively. As $\mathcal{L}$ is linear if it is applied at $x = 0$ we find,

$$\mathcal{L}u\big|_{x=0} = A^R\mathcal{L}\left(e^{ik(x+ct)}\right) + A^T\mathcal{L}\left(e^{ik(x-ct)}\right) = 0. \tag{2.12}$$

By definition the reflection coefficient is

$$R = \left|\frac{A^R}{A^T}\right| = \left|\frac{\mathcal{L}\left(e^{ik(x-ct)}\right)}{\mathcal{L}\left(e^{ik(x+ct)}\right)}\right|.$$

To be perfectly absorbing the reflection coefficient should be zero. Therefore as $\mathcal{L}\left(e^{ik(x-ct)}\right) = 0$, and $\mathcal{L}\left(e^{ik(x+ct)}\right) \neq 0$, the reflection coefficient R is equal to zero, indicating that no reflection occurs.

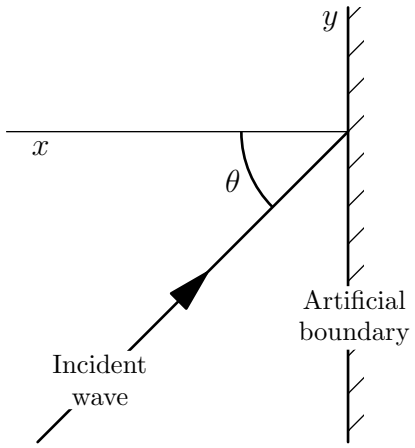

Figure 2.2: Plane wave incident to artificial boundary at $x = 0$.

1.1.2 Two-dimensional wave equation

We now consider the 2D wave equation defined on the space $x \leq 0$, it will be seen that in this case only an approximate local boundary condition can be found.

$$\frac{\partial^2 u}{\partial t^2} = c^2 \frac{\partial^2 u}{\partial x^2} + c^2 \frac{\partial^2 u}{\partial y^2} \qquad \text{with} \qquad \mathcal{L}u|_{x=0} = 0. \tag{2.13}$$

A plane harmonic wave moving has the form

$$u(x, y, t) = Ae^{i(\mathbf{k}\cdot\mathbf{x} - \omega t)}. \tag{2.14}$$

The wave vector $\mathbf{k}$ is defined;

$$\mathbf{k} = k\mathbf{n} = \frac{\omega}{c}\mathbf{n}. \tag{2.15}$$

The vector $\mathbf{n}$ is the unit vector parallel to to phase velocity. The notation

$$\mathbf{n} = (\alpha, \beta) = (\sin\theta, \cos\theta)$$

will be used where θ is the angle between the x-axis and phase velocity. By substituting (2.14) into (2.13) we find the dispersion relation,

$$\omega^2 = c^2 \left(k_1^2 + k_2^2\right),$$

for the wave equation. Solving for k_1;

$$k_1 = \pm\sqrt{\frac{\omega^2}{c^2} - k_2^2} = \pm\frac{\omega}{c}\sqrt{1 - \beta^2}. \tag{2.16}$$

The wave we wish to absorb is moving towards the right so $k_1 > 0$ (or equivalently $\alpha > 0$), thus the positive root must be taken.

Using (2.16) equation (2.14) can be rewritten as a function of k_2 and ω only;

$$u(x, y, t) = Ae^{i\sqrt{\omega^2/c^2 - k_2^2}x + ik_2 y - i\omega t}. \tag{2.17}$$

A boundary condition which exactly cancels (2.17) is, exactly as in to the 1D case above,

$$\mathcal{L} = \frac{\partial}{\partial x} - i\sqrt{\frac{\omega^2}{c^2} - k_2^2} = \frac{\partial}{\partial x} - i\frac{\omega}{c}\sqrt{1 - \beta^2}. \tag{2.18}$$

As in the previous section multiplication by $-i\omega$ is equivalent to $\frac{\partial}{\partial t}$ and therefore the boundary condition is equivalent to

$$\mathcal{L} = \frac{\partial}{\partial x} + \frac{1}{c}\sqrt{1 - \beta^2}\frac{\partial}{\partial t}. \tag{2.19}$$

For a wave arriving normal to the boundary $\beta = 0$ so the boundary condition is the same as for the 1D equation. This boundary condition will only perfectly absorb waves that hit the boundary at the "correct" angle.

To try to produce a NRBC that can absorb waves at any angle of incidence we can again represent the solution to (2.13) as a superposition of harmonic waves.

$$u(x, y, t) = \iint A(\omega, k_2)\, e^{i\sqrt{\omega^2/c^2 - k_2^2}x + ik_2 y - i\omega t}\, \mathrm{d}\omega\, \mathrm{d}k_2. \tag{2.20}$$

Note that certain restrictions are given for the function $A(\omega, k)$ in [24]. Therefore one only needs to define $\mathcal{L}$ such that

$$\mathcal{L}|_{x=0}\frac{\partial u}{\partial x} - \iint i\sqrt{\omega^2/c^2 - k_2^2}\, A(\omega, k_2)\, e^{i\sqrt{\omega^2/c^2 - k_2^2}x + ik_2 y - i\omega t}\, \mathrm{d}\omega\, \mathrm{d}k_2 = 0. \tag{2.21}$$

Unfortunately this is not a local condition, nor does it reduce to one as in the 1D case. Define the function that appears as the second term in the boundary condition (i.e. not $\frac{\partial}{\partial x}$) as $\mathcal{P}$. Previously, equation (2.9), we had that

$$\frac{1}{c}\frac{\partial u}{\partial t} = \mathcal{P}. \tag{2.22}$$

Therefore the locality of the boundary condition was recovered. Unfortunately a similar operation where, for some differential operator $\mathcal{D}$,

$$\mathcal{D}u = \mathcal{P}$$

so that

$$\mathcal{L} = \frac{\partial}{\partial x} - \mathcal{D} = 0$$

cannot be found[a].

The problem is the square root ($\sqrt{\omega^2/c^2 - k_2^2}$). Faced with this, the authors of [24] approximate the square root function by using a Padé expansion [10] having shown that a Taylor expansion leads to an ill-posed boundary condition. Expanding $i\omega\sqrt{1-\beta^2}$ in powers of β^2 one finds for the first- and second-order approximations:

$$1^{\text{st}}\text{- order:} \qquad \frac{\partial}{\partial x} - \frac{i\omega}{c}\sqrt{1-\beta^2} = \frac{\partial}{\partial x} - \frac{i\omega}{c} + O(\beta^2) \tag{2.23a}$$

$$2^{\text{nd}}\text{- order:} \qquad \frac{\partial}{\partial x} - \frac{i\omega}{c}\sqrt{1-\beta^2} = \frac{\partial}{\partial x} - \frac{i\omega}{c} + \frac{i\omega}{c}\frac{1}{2}\beta^2 + O(\beta^4) \tag{2.23b}$$

We now replace multiplication by $-i\omega$ and $\frac{i\omega}{c}\beta$ by their equivalent operations - $\frac{\partial}{\partial t}$ and $\frac{\partial}{\partial y}$, respectively, to find the boundary conditions. The first-order condition, is once again,

$$\frac{\partial}{\partial x} + \frac{1}{c}\frac{\partial}{\partial t} = 0. \tag{2.24}$$

For the second-order condition, equation (2.23b) is first multiplied by $-\frac{i\omega}{c}$;

$$-\frac{i\omega}{c}\frac{\partial}{\partial x} + \left(-\frac{i\omega}{c}\right)^2 - \frac{1}{2}\left(\frac{i\omega\beta}{c}\right)^2 = 0.$$

Multiplication is then converted to differentiation so that the second-order condition is

$$\frac{1}{c}\frac{\partial}{\partial x\partial t} + \frac{1}{c^2}\frac{\partial^2}{\partial t^2} - \frac{1}{2}\frac{\partial^2}{\partial y^2} = 0. \tag{2.25}$$

A hierarchy of more accurate boundary conditions can be derived depending on how far one takes the Padé expansion.

[a] Obviously we exclude $\mathcal{D} = \frac{\partial}{\partial x}$.

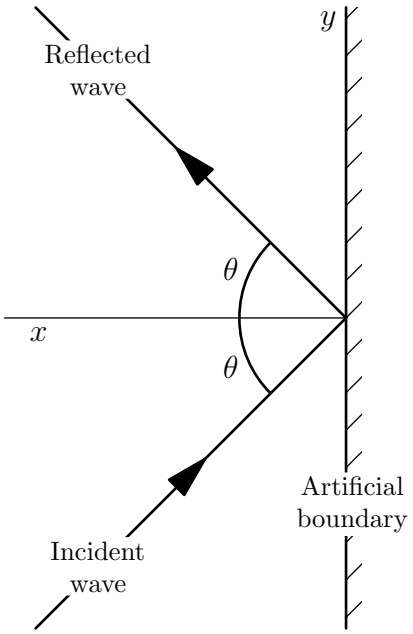

Figure 2.3: Incident and reflected wave at artificial boundary ($x = 0$) for wave equation.

The boundary conditions can also be derived directly, i.e. not through approximation of an exact condition by considering the reflection of a harmonic wave from the boundary. The procedure involves assuming the boundary condition has a particular form,

$$\mathcal{L} = \frac{\partial}{\partial t} + a\frac{\partial}{\partial x} + b\frac{\partial}{\partial y} = 0. \tag{2.26}$$

and then choosing the coefficient, a, to minimise the reflection. First, note that a wave incident on a boundary, $x = 0$, will reflect at an angle such that the incident angle, θ, and reflected angle, ϕ, are related by the formula

$$\frac{\sin\theta}{\sin\phi} = \frac{c_{\text{ref}}}{c_{\text{inc}}}, \tag{2.27}$$

where c_{inc} and c_{ref} are the incoming and reflected phase speeds. This relation is true because the component of the wave vector perpendicular to the boundary must remain constant [54]. In the present case $c_{\text{ref}} = c_{\text{inc}}$ so that the angle of incidence and reflection are also equal (see figure 2.3). For elastic waves however the phenomenon of mode conversion [47] (see also below) means that the incoming and reflected phase speeds may differ. The solution at $x = 0$ can be written as the sum of an incoming/transmitted and reflected plane harmonic wave,

$$u(x, y, t) = A^T e^{i(k_1 x + k_2 y - \omega t)} + A^R e^{i(p_1 x + p_2 y - \omega t)}, \tag{2.28}$$

where $\mathbf{k}$ and $\mathbf{p}$ are the wave vectors. By equation (2.27) $k_2 = p_2$. The dispersion relation (2.16) implies that,

$$p_1^2 + p_2^2 = k_1^2 + k_2^2$$

and therefore $p_1 = \pm k_1$. The positive root gives the incoming wave so for the reflected wave $p_1 = -k_1$ and (2.28) becomes

$$u(x, y, t) = A^T e^{i(k_1 x + k_2 y - \omega t)} + A^R e^{i(-k_1 x + k_2 y - \omega t)}, \tag{2.29}$$

Recall that by definition

$$\mathbf{k} = \frac{\omega}{c} (\cos\theta, \sin\theta) = \frac{\omega}{c} (\alpha, \beta),$$

so that when we apply the operator (2.26) to (2.29) we find

$$\mathcal{L}u\big|_{x=0} = A^T \left(1 + a\frac{\sqrt{1-\beta^2}}{c} - b\frac{\beta}{c}\right) + A^R \left(1 - a\frac{\sqrt{1+\beta^2}}{c} - b\frac{\beta}{c}\right) = 0, \tag{2.30}$$

where the common factor $-i\omega e^{i(k_2 y - \omega t)}$ has been cancelled. The reflection coefficient is $R = \left|A^R/A^T\right|$ and we seek to choose a and b so that $R = O(\beta^n)$ for n as large as possible. For the first-order condition the best that can be achieved is $n = 2$ [21]. We use the approximation, familiar from the above, $\sqrt{1-\beta^2} = 1 + O(\beta^2)$ and find;

$$R = \left|\frac{A^R}{A^T}\right| = \left|\frac{1 - a\frac{1}{c} - b\frac{\beta}{c} + O(\beta^2)}{1 + a\frac{1}{c} - b\frac{\beta}{c} + O(\beta^2)}\right|. \tag{2.31}$$

By inspection if $a = c$ and $b = 0$ the numerator of (2.31) is $O(\beta^2)$ and the denominator is $O(1)$ so that $R = O(\beta^2)$ as required.

Higdon [44] showed that the p^{th}-order E-M boundary condition is equivalent to

$$\left(\frac{\partial}{\partial x} + \frac{1}{c}\frac{\partial}{\partial t}\right)^p u = 0. \tag{2.32}$$

For example, for $p = 2$, (2.32) is

$$\frac{\partial^2 u}{\partial x^2} + \frac{2}{c}\frac{\partial^2 u}{\partial x \partial t^2} + \frac{1}{c^2}\frac{\partial^2 u}{\partial t^2} = 0.$$

But u is a solution of the wave equation so that

$$\frac{\partial^2 u}{\partial x^2} = \frac{1}{c^2}\frac{\partial^2 u}{\partial t^2} - \frac{\partial^2 u}{\partial y^2},$$

and therefore

$$\frac{1}{c^2}\frac{\partial^2 u}{\partial t^2} - \frac{\partial^2 u}{\partial y^2} + \frac{2}{c}\frac{\partial^2 u}{\partial x \partial t^2} + \frac{1}{c^2}\frac{\partial^2 u}{\partial t^2} = \frac{1}{c}\frac{\partial}{\partial x \partial t} + \frac{1}{c^2}\frac{\partial^2}{\partial t^2} - \frac{1}{2}\frac{\partial^2}{\partial y^2} = 0.$$

This is the second-order E-M condition (2.25). In the same paper Higdon also introduced a generalisation to (2.32);

$$\left[\prod_{i=1}^{p}\left(\cos\alpha_i \frac{\partial}{\partial x} + \frac{1}{c}\frac{\partial}{\partial t}\right)\right] u = 0. \tag{2.33}$$

This will absorb right moving waves hitting the boundary, $x = 0$, at any angle α_i for $i = 1$ to p. Clearly any plane wave

$$u = e^{i\omega(\cos\theta x/c + \sin\theta y/c - t)},$$

will be annhialated by one of the factors in (2.33) if $\theta = \alpha_i$ for any $i = 1$ to p. It is suggested that in this way a boundary condition may be tuned to account for *a priori* knowledge of dominant wave directions. Note that the E-M boundary conditions are a special case of (2.33) with $\alpha_i = 0$ for all i.

1.1.3 Boundary condition for a general configuration

Thus far we have always assumed that a right moving wave is incident to the a boundary at $x = 0$, there is in fact no difference if we consider a boundary $x = a$, for some constant a. For waves travelling from right to left or those incident from above or below to a boundary $y = a$ the boundary conditions must be modified in a straightforward way; easily derived by reapeating the above analysis with the appropriate changes in the initial assumptions. The changes necessary for the first-order E-M condition are illustrated in figure 2.4.

The most general case is for a wave incident to a boundary surface defined by a normal $\mathbf{n} = (n_1, n_2) = (\cos\phi, \sin\phi)$. In all of the derivations above we considered a right moving wave with wave vector $\mathbf{k} = (k_1, k_2)$ and a reflected wave with wave vector $\mathbf{p} = (-k_1, k_2)$. A simple way to derive the correct NRBC for the present case is to rotate $\mathbf{k}$ and

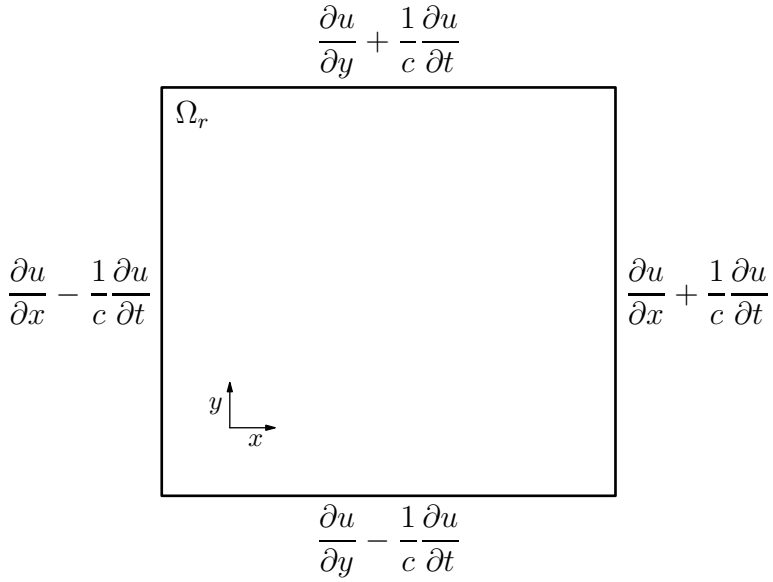

Figure 2.4: Modification of first-order E-M NRBC for the sides of a rectangular domain.

$\mathbf{p}$ by ϕ degrees and calculate the action of the general first-order homogeneous boundary condition (2.26) on the total displacement as above. First note that the rotated wave vectors can be found by multiplication by the rotation matrix

$$\mathbf{R}_\phi = \begin{pmatrix} \cos\phi & -\sin\phi \\ \sin\phi & \cos\phi \end{pmatrix} = \begin{pmatrix} n_1 & -n_2 \\ n_2 & n_1 \end{pmatrix}.$$

Therefore the total displacement including the reflected and transmitted part is

$$u = A^T e^{i((n_1k_1 - n_2k_2)x + (n_2k_1 + n_1k_2)y - \omega t)} + A^R e^{i(-(n_1k_1 + n_2k_2)x + (-n_2k_1 + n_1k_2)y - \omega t)}. \tag{2.34}$$

If the boundary condition is applied to (2.34) and all the common factors are cancelled we find

$$A^T \left(-1 + \frac{a}{c}(n_1\alpha - n_2\beta) + \frac{b}{c}(n_2\alpha + n_1\beta) \right) + A^R \left(-1 - \frac{a}{c}(n_1\alpha + n_2\beta) + \frac{b}{c}(-n_2\alpha + n_1\beta) \right) = 0, \tag{2.35}$$

where $\mathbf{k} = (\alpha,\ \beta)$. We once again use the approximation $\alpha = \sqrt{1-\beta^2} = 1 + O(\beta^2)$ and the reflection coefficient is

$$R = \left| \frac{A^R}{A^T} \right| = \left| \frac{-1 + \frac{a}{c}(n_1 - n_2\beta) + \frac{b}{c}(n_2 + n_1\beta)}{-1 - \frac{a}{c}(n_1 + n_2\beta) + \frac{b}{c}(-n_2 + n_1\beta)} \right|. \tag{2.36}$$

If $a = cn_1$ and $b = cn_2$ then the reflection coefficient is $O(\beta^2)$ and the general first-order NRBC is

$$\frac{\partial u}{\partial t} + c(\mathbf{n} \cdot \nabla) u = 0. \tag{2.37}$$

It will be seen that this agrees with the specific examples given in figure 2.4.

The high-order boundary conditions i.e. (2.32) or (2.33) with $p \geq 3$ or 4 though offering arbitrarily high accuracy are generally considered impractical because of the need to approximate higher order derivatives. More recent papers however provide a means to apply these conditions to an arbitrary order without calculating derivatives of higher than second-order. This is done by introducing extra degrees of freedom into the calculaton, either by defining extra non-physical variables on the boundary [34] or by adding extra grid points around the outside of the domain [39]. Unfortunately accurate calculation of even second derivatives in SPH can be difficult especially on the boundary.

1.1.4 P- and S-waves

A characteristic of elasticity in an infinte medium is that waves can propagate at two distinct speeds. These are P-waves, with phase speed c_p, and S-waves, with phase speed c_s where $c_p > c_s$. The displacements associated with P-waves are parallel to the phase velocity, for S-waves the displacements are normal to the phase velocity. In addition there can exist Rayleigh waves on the free surface of an elastic body with phase speed $c_r < c_s$. Particles on the surface when a Rayleigh wave is propagating to the right follow a counter-clockwise elliptical path. Further information on elastic waves can be found in appendix A and the references cited there.

For reference the equations of linear elasticity can be written in the form

$$\frac{\partial^2 \mathbf{u}}{\partial t^2} = c_s^2 \Delta \mathbf{u} + \left(c_p^2 - c_s^2\right) \nabla \left(\nabla \cdot \mathbf{u}\right). \tag{2.38}$$

Or in index notation

$$\frac{\partial^2 u_i}{\partial t^2} = c_s^2 \frac{\partial^2 u_i}{\partial x_j \partial x_j} + \left(c_p^2 - c_s^2\right) \frac{\partial^2 u_j}{\partial x_i \partial x_j}. \tag{2.39}$$

A plane P-wave has the form;

$$\mathbf{u} = \mathbf{A} e^{i(\mathbf{k}_p \cdot \mathbf{r} - \omega t)}, \tag{2.40a}$$

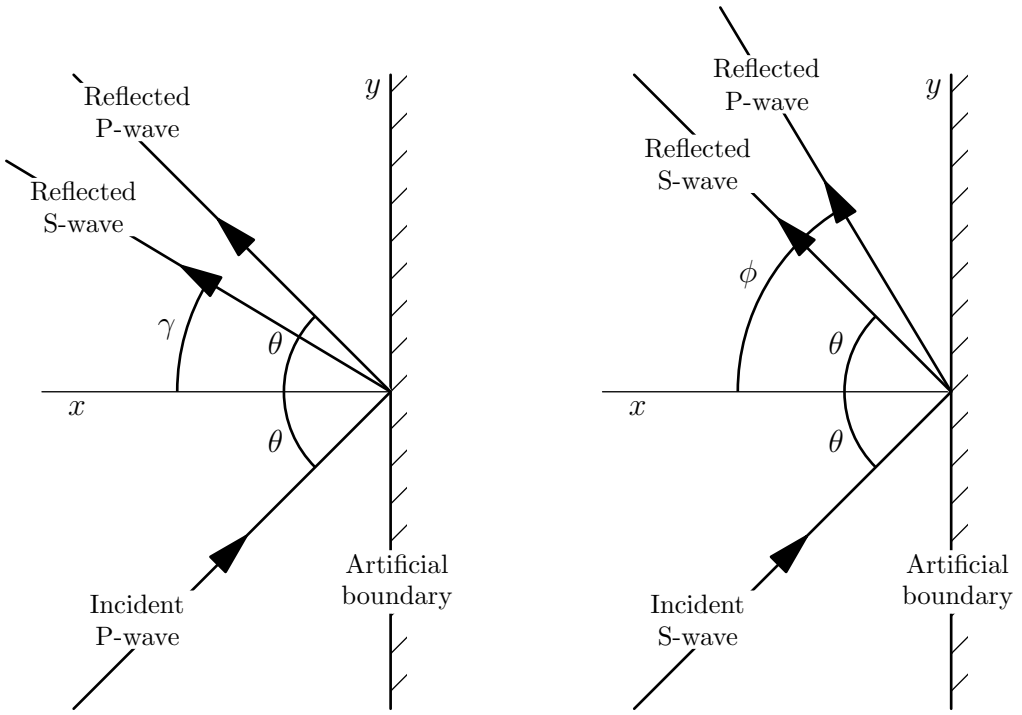

Figure 2.5: Mode conversion of plane elastic waves on reflection from a boundary. In (a) $\sin\gamma = \frac{c_s}{c_p}\sin\theta$ and (b) $\sin\phi = \frac{c_p}{c_s}\sin\theta$.

where the vector amplitude is parallel to the wave vector, $\mathbf{A} = |\mathbf{A}|\,\hat{\mathbf{k}}_p$, and the "hat" denotes the unit vector i.e. $\hat{\mathbf{a}} = \mathbf{a}/|\mathbf{a}|$. Similarly for a plane S-wave, in 2D,

$$\mathbf{u} = \mathbf{B}e^{i(\mathbf{k}_s\cdot\mathbf{r}-\omega t)}, \tag{2.40b}$$

with $\mathbf{B} = |\mathbf{B}|\,(\mathbf{t}\times\hat{\mathbf{k}}_s)$ where $\mathbf{t} = (0,0,1)$ so that $\mathbf{B} = (-k_{2,s}, k_{1,s}, 0)$ is in the xy-plane and perpendicular to the wave vector $\mathbf{k}_s$.

A complication of the reflection of elastic waves is that unless the wave vector is normal to the boundary the reflected wave will be a combination of a P-wave and an S-wave regardless of whether the incident wave was a pure P- or S-wave. The angle of reflection is governed by equation (2.27). This phenomenon, known as *mode conversion*, is illustrated in figure 2.5. By a generalisation of the p^{th}-order boundary condition (2.33), in [45] Higdon suggests the following boundary condition to absorb right moving waves at $x = 0$;

$$\left(\frac{\partial}{\partial t} + c_p\frac{\partial}{\partial x}\right)\left(\frac{\partial}{\partial t} + c_s\frac{\partial}{\partial x}\right)\mathbf{u} = 0. \tag{2.41}$$

It is clear by substitution of (2.40a) or (2.40b) into (2.41) that it will perfectly absorb a normally incident P-wave, S-wave, or a superposition thereof (by linearality of the boundary condition). Clayton and Engquist [16] derive a first-order (and a second-order) boundary condition for elastic waves in 2D. The first-order condition, for right moving waves incident to $x = 0$ is;

$$\begin{aligned}\left(\frac{\partial}{\partial t} + c_p\frac{\partial}{\partial x}\right) u_1 =& 0 \\ \left(\frac{\partial}{\partial t} + c_s\frac{\partial}{\partial x}\right) u_2 =& 0.\end{aligned} \tag{2.42}$$

This is derived by assuming the first-order boundary condition will take the form

$$\begin{pmatrix} a & 0 \\ 0 & b \end{pmatrix} \frac{\partial \mathbf{u}}{\partial t} + \frac{\partial \mathbf{u}}{\partial x} = 0. \tag{2.43}$$

They then perform a Fourier transform on equations (2.38) and (2.43). They approximate the square root term that appears in the transformed elasticity equation and try to match the coefficients of the two equations so that the boundary condition and the PDE are both satisfied on the boundary. The boundary condition is then transformed back into the time domain. The same procedure is used to find a second-order boundary condition;

$$\left\{ \frac{\partial^2}{\partial t^2} + \begin{pmatrix} c_p & 0 \\ 0 & c_s \end{pmatrix} \frac{\partial^2}{\partial x \partial t} + \begin{pmatrix} 0 & c_p - c_s \\ c_p - c_s & 0 \end{pmatrix} \frac{\partial^2}{\partial y \partial t} + \frac{1}{2} \begin{pmatrix} \frac{c_p - 2c_s}{c_p} & 0 \\ 0 & \frac{c_s - 2c_p}{c_s} \end{pmatrix} \frac{\partial^2}{\partial y^2} \right\} \mathbf{u} = 0. \tag{2.44}$$

The reflection coefficient for the first-order boundary condition for the wave equation is of $O(\sin^2\theta)$. We will show that (2.42) is $0(\sin\theta)$, however the boundary condition

$$\left\{ \frac{\partial}{\partial t} + \begin{pmatrix} c_p & 0 \\ 0 & c_s \end{pmatrix} \frac{\partial}{\partial x} + \begin{pmatrix} 0 & c_p - c_s \\ c_p - c_s & 0 \end{pmatrix} \frac{\partial}{\partial y} \right\} \mathbf{u} = 0, \tag{2.45}$$

given in [84], can make the reflection coefficient $O(\sin^2\theta)$ without resorting to second derivatives.

We must consider four seperate coefficients; one for an incident P-wave and one for a reflected P-wave (PP), an incident P-wave and reflected S-wave (PS), an incident S-wave

and reflected S-wave (SS), and finally an incident S-wave and reflected P-wave (SP). Consider a incident P- or S-wave with wave vector $\mathbf{k}$ with $\hat{\mathbf{k}} = (\alpha, \beta) = (\cos\theta, \sin\theta)$. For an incident P-wave the reflected P-wave will have wave vector $\mathbf{k}_p$ with $\hat{\mathbf{k}}_p = (-\alpha, \beta)$ and reflected S-wave with wave vector $\mathbf{k}_s$ with $\hat{\mathbf{k}}_s = (-\zeta, \eta) = (-\cos\gamma, \sin\gamma)$ (see figure 2.5a). For an incident S-wave, the reflected P-wave has wave vector $\mathbf{d}_p$ with $\hat{\mathbf{d}}_p = (-\nu, \xi) = (-\cos\phi, \sin\phi)$ and the reflected S-wave has wave vector $\mathbf{d}_s$ with $\hat{\mathbf{d}}_s = (-\alpha, \beta)$ (see figure 2.5b). The total displacement at the boundary for an incident P-wave with wave vector will be

$$\mathbf{u} = A_0 \begin{pmatrix} \alpha \\ \beta \end{pmatrix} e^{i(\mathbf{k}\cdot\mathbf{r}-\omega t)} + A_p \begin{pmatrix} -\alpha \\ \beta \end{pmatrix} e^{i(\mathbf{k}_p\cdot\mathbf{r}-\omega t)} - A_s \begin{pmatrix} \eta \\ \zeta \end{pmatrix} e^{i(\mathbf{k}_s\cdot\mathbf{r}-\omega t)}. \tag{2.46a}$$

For an S-wave;

$$\mathbf{u} = A_0 \begin{pmatrix} -\beta \\ \alpha \end{pmatrix} e^{i(\mathbf{k}\cdot\mathbf{r}-\omega t)} + A_p \begin{pmatrix} -\nu \\ \xi \end{pmatrix} e^{i(\mathbf{d}_p\cdot\mathbf{r}-\omega t)} - A_s \begin{pmatrix} \beta \\ \alpha \end{pmatrix} e^{i(\mathbf{d}_s\cdot\mathbf{r}-\omega t)}. \tag{2.46b}$$

From equation (2.27) and $\alpha^2 + \beta^2 = 1$ we find the relations

$$\begin{aligned} \nu &= \sqrt{1 - \frac{c_p^2}{c_s^2}\beta^2}, \qquad \xi = \frac{c_p}{c_s}\beta, \\ \zeta &= \sqrt{1 - \frac{c_s^2}{c_p^2}\beta^2}, \qquad \eta = \frac{c_s}{c_p}\beta. \end{aligned} \tag{2.47}$$

In general applying a linear differential operator, $\mathcal{L}$, to (2.46) gives, for u_1 and u_2,

$$\begin{aligned} \mathcal{L}u_1 =& A_o F_1 + A_p F_2 + A_s F_3 = 0 \\ \mathcal{L}u_2 =& A_o G_1 + A_p G_2 + A_s G_3 = 0. \end{aligned} \tag{2.48}$$

Where the functions F_1, F_2, and F_3 are the result of applying $\mathcal{L}$ to the first component (u_1), of each harmonic wave in (2.46) and each G is defined analogously but applied to the second component (u_2). We can solve (2.48) for A_p/A_0 and A_s/A_o to find the reflection coefficients, note these apply equally to (2.46a) and (2.46b),

$$\left|\frac{A_p}{A_0}\right| = \left|\frac{G_1F_3 - F_1G_3}{G_3F_2 - F_3G_2}\right|, \tag{2.49a}$$

$$\left|\frac{A_s}{A_0}\right| = \left|\frac{G_1F_2 - F_1G_2}{G_2F_3 - F_2G_3}\right|. \tag{2.49b}$$

Equations (2.49) can be used to calculate the reflection coefficient for any, linear, boundary condition. The calculation is simpler if it is remembered that the y-component of the wave vector must remain constant so that a common factor of $e^{i(k_2 y-\omega t)}$ may be cancelled and $x = 0$ so that $e^{ik_1 x} = 1$. Finally recall from the above that for a harmonic wave $f(x, y, t)$ with wave vector $\mathbf{k} = \frac{\omega}{c}(\alpha, \beta)$ the following operations are equivalent;

$$\begin{aligned}\frac{\partial}{\partial t} f =& -i\omega \times f,\\ \frac{\partial}{\partial x} f =& \frac{i\omega\alpha}{c} \times f,\\ \frac{\partial}{\partial y} f =& \frac{i\omega\beta}{c} \times f.\end{aligned}$$

If the boundary condition only contains derivatives of the same order, as is the case here, then the term $i\omega$ will be a common factor that can be cancelled.

Therefore for [16] we find for (2.46a) using the relations from (2.47) and the approximation $\sqrt{1+\beta^2} = 1 + O(\beta^2)$

$$\begin{aligned} F_1 &= -\alpha + \alpha^2 = O(\beta^2) & G_1 &= -\beta + \frac{c_s}{c_p}\alpha\beta = O(\beta^2)\\ F_2 &= \alpha + \alpha^2 = O(1) & G_2 &= -\beta - \frac{c_s}{c_p}\alpha\beta = O(\beta)\\ F_3 &= \zeta + \frac{c_p}{c_s}\zeta\eta = O(\beta) & G_3 &= \eta + \eta^2 = O(\beta).\end{aligned}$$

The above can be substituted into (2.49a) and it is found that the numerator is order $O(\beta^3)$ and the denominator is $O(\beta)$ so that overall $PP = O(\beta^2)$. For (2.49b) the reflection coefficient is $PS = O(\beta)$.

For (2.46b) we find

$$\begin{aligned} F_1 &= \beta - \frac{c_p}{c_s}\beta\alpha = O(\beta) & G_1 &= \alpha - \alpha^2 = O(\beta^2)\\ F_2 &= \nu + \nu^2 = O(1) & G_2 &= -\xi - \frac{c_s}{c_p}\nu\xi = O(\beta)\\ F_3 &= \beta + \frac{c_p}{c_s}\beta\alpha = O(\beta) & G_3 &= \alpha + \alpha^2 = O(1).\end{aligned}$$

Similary to the previous case by substitution of the above into (2.49) we find that $SP = O(\beta)$ and $SS = O(\beta^2)$.

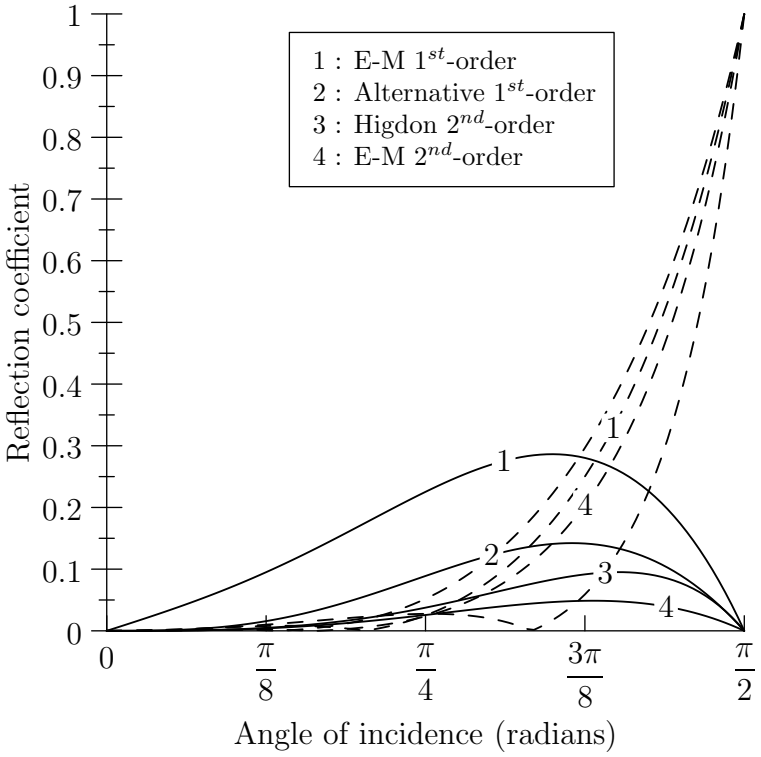

Figure 2.6: Reflection coefficient for incident P-wave. Dashed lines are the P-wave and solid lines the S-wave.

To compare the reflection coefficients for the various boundary conditions refer to figure 2.6.

2 Implementation

2.1 Identification of boundary particles

In order to apply boundary conditions in SPH it is obviously necessary to identify the particles on the boundary. In SPH this must include not only the particles on the very outside of the domain but also those near enough to be affected by particle deficiency (see chapter 1 § 1.3). Moreover it is desirable for the identification of boundary particles, and the calculation of the surface normals at those particles, to be automated as far as possible. This relieves the necessity of including such information in the input file. And allows, if desired, for the updating of boundary particles and their surface normals as the computation progresses. For clarity all the particles on or near enough to the boundary to be affected by particle deficiency will be referred to as boundary particles (BPs), the

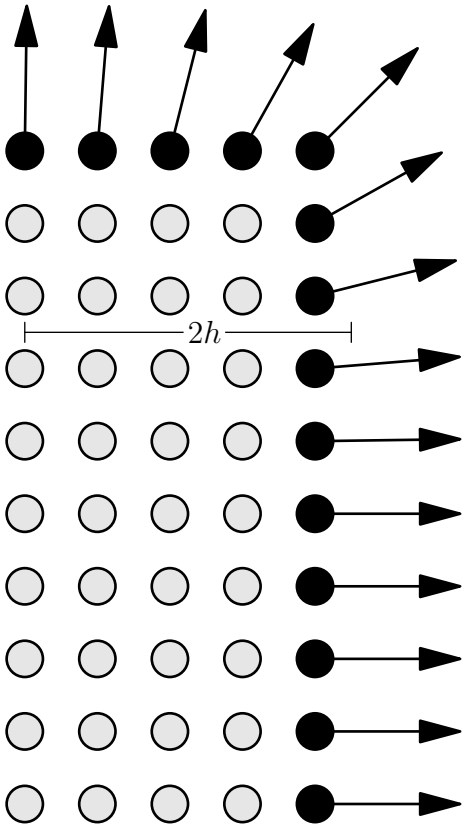

Figure 2.7: Surface normal vectors calculated for the top-right corner of a rectangular domain, with regular particle arrangement, using equation (2.51).

outer layer of particles will be referred to as outer boundary particles (OBPs) and the BPs that are not OBPs are inner boundary particles (IBPs).

To identify boundary particles Randles and Libersky, in [81], assign the same integer, I_i, to each particle i that make up a particular, distinct object or material. Then if

$$I_i \not\approx \sum_{j \in N(i)} I_j W_{ij}, \tag{2.50}$$

i is designated as a boundary particle. To approximate the surface normal they calculate

$$\mathbf{e}_i = \langle \nabla \mathbf{1} \rangle = \sum_{j \in N(i)} \nabla W_{ij}, \tag{2.51}$$

then the normal is $\mathbf{n}_i = -\hat{\mathbf{e}}_i = -\mathbf{e}_i / |\mathbf{e}_i|$. This is an SPH approximation of the gradient of a constant field and should, of course, be equal to zero. Instead of using (2.50) we have found that $|\mathbf{e}_i|$ can be used to find boundary particles. Indeed the error associated with calculating $\langle \nabla \mathbf{1} \rangle$ is greater than that associated with $\langle \mathbf{1} \rangle$, thereby indicating boundary particles more clearly. The exact criterion used is that i is a boundary particle if

$$\langle \mathbf{e}_i \rangle > C \max_{\forall k} \langle \mathbf{e}_k \rangle . \tag{2.52}$$

Where C is a constant, by trial and error $C = 0.75$ is found to work well. This test will only flag particles on the "true" boundary i.e. those particles in the very outer layer of the domain. For stability reasons we must also definitively exclude some particles from the boundary; those that are within the neighbourhood of an OBP but have full kernel support. Particles are excluded if

$$\langle \mathbf{e}_i \rangle > D \min_{\forall k} |\mathbf{e}_k| \,. \tag{2.53}$$

Again by trial and error we use $D = 10$. Finally it is found that the boundary normal is only accurately approximated for OBPs. Therefore once the OBPs have been identified we must recalculate $\mathbf{e}_i$ for all of the IBPs while excluding the OBPs from the calculation. This identifies a second layer of particles further inside the domin than the OBPs but to the outside of the rest of the domain. The surface normals can then be set for this second layer. Similarly a third layer is identified by excluding the OBPs and the second layer and recalculating $\mathbf{e}_i$. This is repeated untill all of the BPs, i.e. those affected by particle deficiency, have had an accurate surface normal set. The whole procedure is outlined in algorithm 2.1. In the next section the problems used to test the NRBCs will primarily consist of 2D rectangular blocks with particles arranged on a regular grid, figure 1.3. For problems of this nature the algorithm 2.1 is found to be especially accurate (for the initial configuration at least) for two reasons:

1. The regularity of the grid in the initial configuration means that, for a non-BP i,

   $$\mathbf{e}_i = 0$$

   to within rounding error. Therefore the tolerance of the algorithm when identifying non-BPs, and by implication BPs, is larger. In contrast, particle disorder introduces errors, in the form of mis-identification of boundary particles, into the procedure.

2. On a straight edge of the regular grid, symmetry of the particle arrangement means the surface normal, away from the corners, is calculated exactly (again to within rounding error).

Algorithm 2.1 Identify boundary particles

for $i = 1$ **to** Number of Particles **do**

$\mathbf{e}_i \leftarrow \sum_{j \in N(i)} \nabla W_{ij}$

end for

$max \leftarrow 0.75 \times \max_{\forall i} |\mathbf{e}_i|$

$min \leftarrow 10 \times \min_{\forall i} |\mathbf{e}_i|$

for $i = 1$ **to** Number of Particles **do**

if $|\mathbf{e}_i| > max$ **then**

$BP \leftarrow BP \cup i$ ▷ BP is the set of boundary particles

$\mathbf{n}_i \leftarrow -\hat{\mathbf{e}}_i$

end if

for $j \in N(i) \setminus BP$ **do**

if $|\mathbf{e}_j| > min$ **then** ▷ Exclude particles with full neighbourhood

$BN \leftarrow BN \cup j$ ▷ BN is the set of neighbours of boundary particles

end if

end for

end for

2.2 NRBC in SPH

For practical implementation of a NRBC in the SPH code we must first derive an expression for the boundary condition that is valid for a wave incident to a boundary defined by the outward normal, $\mathbf{n}$. In section 1.1.3 it was shown that the first-order E-M boundary condition for an acoustic wave incident to a plane defined by a unit normal $\mathbf{n}$ is

$$\frac{\partial u}{\partial t} + c\left(\mathbf{n} \cdot \nabla\right) u = 0. \tag{2.37}$$

Analogously, for an elastic wave the general first-order E-M condition is the simultaneous differential equation,

$$\left(\frac{\partial \mathbf{u}}{\partial t} + c_p\left(\mathbf{n} \cdot \nabla\right) \mathbf{u}\right) \cdot \mathbf{n} = 0 \tag{2.54a}$$

$$\left(\frac{\partial \mathbf{u}}{\partial t} + c_s\left(\mathbf{n} \cdot \nabla\right) \mathbf{u}\right) \cdot \mathbf{t} = 0. \tag{2.54b}$$

Algorithm 2.2 Calculate boundary normals

while $BN \not\equiv \emptyset$ **do**

for $i \in BN$ **do**

$\mathbf{e}_i \leftarrow \sum_{i \in N(i) \setminus BP} \nabla W_{ij}$ ▷ Exclude $j \in BP$ from calculation

if $|\mathbf{e}_i| > max$ **then**

$\mathbf{n}_i \leftarrow -\hat{\mathbf{e}}_i$

$BP \leftarrow BP \cup i$

$BN \leftarrow BN \setminus i$

end if

end for

end while

It may be seen by substitution of the appropriate normal vector, $\mathbf{n}$, that the expected boundary conditions are generated. For example, if $\mathbf{n} = (0, 1)$ then $\mathbf{t} = (1, 0)$ and (2.54) becomes

$$\frac{\partial u_2}{\partial t} + c_p \frac{\partial u_2}{\partial y} = 0$$
$$\frac{\partial u_1}{\partial t} + c_s \frac{\partial u_1}{\partial y} = 0.$$

In general if a second-order boundary condition for a right moving wave incident to a boundary at $x = 0$ is

$$\frac{\partial u_1}{\partial t} + G_1 \left(\mathbf{u}_x, \mathbf{u}_y, \mathbf{u}_{xx}, \mathbf{u}_{yy}, \mathbf{u}_{yx} \right) = 0 \tag{2.55}$$
$$\frac{\partial u_2}{\partial t} + G_2 \left(\mathbf{u}_x, \mathbf{u}_y, \mathbf{u}_{xx}, \mathbf{u}_{yy}, \mathbf{u}_{yx} \right) = 0, \tag{2.56}$$

for linear functions G_1 and G_2. Then for a boundary perpendicular to $\mathbf{n}$, if the normal derivative is $\mathbf{u_n} = (\mathbf{n} \cdot \nabla) \mathbf{u}$ and the tangental derivative is $\mathbf{u_t} = (\mathbf{t} \cdot \nabla) \mathbf{u}$, equation (2.55) becomes;

$$\left(\frac{\partial \mathbf{u}}{\partial t} + G_1 \left(\mathbf{u_n}, \mathbf{u_t}, \mathbf{u_{nn}}, \mathbf{u_{tt}}, \mathbf{u_{tn}} \right) \right) \cdot \mathbf{n} = 0, \tag{2.57}$$
$$\left(\frac{\partial \mathbf{u}}{\partial t} + G_2 \left(\mathbf{u_n}, \mathbf{u_t}, \mathbf{u_{nn}}, \mathbf{u_{tt}}, \mathbf{u_{tn}} \right) \right) \cdot \mathbf{t} = 0. \tag{2.58}$$

To summarise, to transform a boundary condition derived for a right moving wave incident to a boundary at $x = 0$, to one appropriate for absorbing waves incident to a boundary defined by an outward normal $\mathbf{n}$, the following substitutions should take place:

$$\begin{aligned}
\frac{\partial}{\partial x} &\to (\mathbf{n} \cdot \nabla) = n_1 \frac{\partial}{\partial x} + n_2 \frac{\partial}{\partial y} \\
\frac{\partial}{\partial y} &\to (\mathbf{t} \cdot \nabla) = n_2 \frac{\partial}{\partial x} - n_1 \frac{\partial}{\partial y} \\
u_1 &\to \mathbf{u} \cdot \mathbf{n} \\
u_2 &\to \mathbf{u} \cdot \mathbf{t}.
\end{aligned}$$

For the first-order conditions that we will be considering below it is more convenient to work with the velocity, $\mathbf{v}$, rather than the displacement, $\mathbf{u}$. The velocity gradient is already calculated in the code, see algorithm 1.1 (on 21), and moreover the particle displacements are not normally calculated. The boundary conditions is therefore differentiated with respect to time, so that (2.54) becomes

$$\left(\frac{\partial \mathbf{v}}{\partial t} + c_p \left(\mathbf{n} \cdot \nabla \right) \mathbf{v} \right) \cdot \mathbf{n} = 0 \tag{2.59a}$$

$$\left(\frac{\partial \mathbf{v}}{\partial t} + c_s \left(\mathbf{n} \cdot \nabla \right) \mathbf{v} \right) \cdot \mathbf{t} = 0, \tag{2.59b}$$

where we have assumed that $\dot{\mathbf{n}} \approx 0$. Combining (2.59a) and (2.59b) we have

$$\frac{\partial \mathbf{v}}{\partial t} = -c_p \left(\left(\mathbf{n} \cdot \nabla \right) \mathbf{v} \cdot \mathbf{n} \right) \mathbf{n} - c_s \left(\left(\mathbf{n} \cdot \nabla \right) \mathbf{v} \cdot \mathbf{t} \right) \mathbf{t}, \tag{2.60}$$

where we have used the fact that for any vector $\mathbf{b} = (\mathbf{b} \cdot \mathbf{n})\,\mathbf{n} + (\mathbf{b} \cdot \mathbf{t})\,\mathbf{t}$. This boundary condition gives a relationship between the partial derivative of the velocity with respect to time, $\frac{\partial \mathbf{v}}{\partial t}$ and the velocity gradient. In SPH the momentum equation, (1.29), is defined in terms of the material derivative,

$$\dot{\mathbf{v}} = \frac{\mathrm{D}\mathbf{v}}{\mathrm{D}t} = \frac{\partial \mathbf{v}}{\partial t} + \mathbf{v} \cdot \nabla \mathbf{v}. \tag{2.61}$$

Re-arranging we have

$$\frac{\mathrm{D}\mathbf{v}}{\mathrm{D}t} - \mathbf{v} \cdot \mathbf{v} = \frac{\partial \mathbf{v}}{\partial t},$$

which may then be substituted into (2.60) to find the particle acceleration;

$$\frac{\mathrm{D}\mathbf{v}}{\mathrm{D}t} = -c_p\left(\left(\mathbf{n}\cdot\nabla\right)\mathbf{v}\cdot\mathbf{n}\right)\mathbf{n} - c_s\left(\left(\mathbf{n}\cdot\nabla\right)\mathbf{v}\cdot\mathbf{t}\right)\mathbf{t} + \mathbf{v}\cdot\nabla\mathbf{v}. \tag{2.62}$$

Consider again, the E-M boundary condition for a right moving wave incident to a boundary defined by $x = 0$,

$$\left(\frac{\partial}{\partial t} + \mathbf{A}\frac{\partial}{\partial x}\right)\mathbf{u} = 0, \tag{2.63}$$

where $\mathbf{A} = \left(\begin{smallmatrix} c_p & 0 \\ 0 & c_s \end{smallmatrix}\right)$. The particle acceleration in this case is therefore, from (2.62),

$$\frac{\mathrm{D}\mathbf{v}}{\mathrm{D}t} = -\mathbf{A}\frac{\partial}{\partial x} + \mathbf{v}\cdot\nabla\mathbf{v}. \tag{2.64}$$

Further if the particle velocity is normal to the boundary, $\mathbf{v} = |\mathbf{v}|\,\mathbf{n} = |\mathbf{v}|\,(1,0)$ and one substitutes this into (2.64), we find,

$$\frac{\mathrm{D}\mathbf{v}}{\mathrm{D}t} = -\mathbf{A}\frac{\partial\mathbf{v}}{\partial x} + |\mathbf{v}|\,\mathbf{n}\cdot\nabla\mathbf{v} = \begin{pmatrix} -c_p + |\mathbf{v}| & 0 \\ 0 & -c_s + |\mathbf{v}| \end{pmatrix}\frac{\partial\mathbf{v}}{\partial x}. \tag{2.65}$$

Therefore if the particle velocity is much smaller that the speed of sound the convective term $(\mathbf{v}\cdot\nabla\mathbf{v})$, should be negligible, but (2.65) implies that at higher particle velocities changing to the material derivative becomes more important.

2.3 Time integration

For the boundary particles the velocity gradient, $\mathbf{L}$, is used to calculate the acceleration, through equation (1.33). In the leap-frog scheme described in chapter 1§2.2 the particle stress and velocity are held at different time levels, the derivative of one being used to advance the other to the next time step. However, for boundary particles the NRBC uses the velocity gradient, rather than the divergence of the stress, to calculate the acceleration. It will be seen therefore that the acceleration and the velocity are held on the same time level, see 2.3. This has deleterious consequences for the stability as the velocity of each boundary particle is being advanced using the forward Euler method,

$$v_i^{n+1/2} = v_i^{n-1/2} + \Delta t a_i^{n-1/2}, \tag{2.66}$$

Algorithm 2.3 Time integration for boundary particles

while $current\_time \leq end\_time$ **do**

Perform neighbour search

for $i = 1$ to Number of Boundary Particles **do**

Calculate $\langle \mathbf{D} \rangle_i^{n-1/2}$ and $\langle \dot{\rho} \rangle_i^{n-1/2}$

$\rho_i^n \leftarrow \rho_i^{n-1} + \Delta t^{n-1/2} \langle \dot{\rho} \rangle_i^{n-1/2}$

Calculate $\langle \dot{\sigma} \rangle_i^{n-1/2}$ ▷ Constitutive equation

$\sigma_i^n \leftarrow \sigma_i^{n-1} + \Delta t^{n-1/2} \langle \dot{\sigma} \rangle_i^{n-1/2}$ ▷ Need σ for neighbouring particles to see

Calculate $\mathbf{a}_i^{n-1/2}$ ▷ Uses $\langle \mathbf{L} \rangle_i^{n-1/2}$ so at the half step

end for

for $i = 1$ to Number of Boundary Particles **do**

$\mathbf{v}_i^{n+1/2} \leftarrow \mathbf{v}_i^{n-1/2} + \Delta t^n \mathbf{a}_i^{n-1/2}$

$\mathbf{x}_i^n \leftarrow \mathbf{x}_i^{n-1} + \Delta t^{n+1/2} \mathbf{v}_i^{n+1/2}$

end for

$current\_time \leftarrow current\_time + \Delta t^n$

end while

which is unconditionally unstable [73]. There are two solutions which stabilise the method. The first, implied above, is that each boundary particle have neighbours which are not themselves boundary particles. This is why when calculating boundary particles those particles with a complete set of neighbours are not included as boundary particles. The disadvantge of this is that greater care must be taken in calculating boundary particles.

An alternative time-integration method which is easy to implement is the upwind method [73]. In practice this requires that when calculating $\langle \mathbf{L}_i \rangle$ for a boundary particle, only particles further to the interior of the material should be used. Consider a 1D example with all the particles numbered sequentially from left to right. If a particle i is part of the NRBC absorbing waves moving to the right then

$$\langle \mathbf{L}_i \rangle = \sum_{j<i} (\mathbf{v}_j - \mathbf{v}_i) \otimes \nabla W_{ij}. \tag{2.67}$$

However, one can see that calculated in this way $\mathbf{L}_i$ will be approximated as if i were a particle on the extreme end of the domain. Consequently the approximation will be poor and every particle in the boundary will suffer from the same poor approximation. For this reason the upwind type scheme must be used with a normalised kernel.

The cost of implementing the NRBCs are negligible if the identification of the boundary particles is done only on initialisation. In the examples considered below the boundary normals were calculated only once. The boundary in these examples does not deform significantly and it is found that the minor deformation that does take place is more deleterious to the accuracy of algorithm 2.2 than to the NRBC.

That said, all that is left for the NRBC is to calculate the acceleration using information we already have, the velocity gradient, instead of having to solve the momentum equation. Theoretically then the truncated solution should be more efficient than the same problem run without a NRBC. This assumes that one is using a first-order boundary condition, a second-order condition using the first and second derivatives of the displacement. Unless we are using a higher order method for the main integration loop, the second-order boundary conditions will surely be more expensive than solving the momentum equation.

3 Numerical examples

3.1 1D problems

This section presents a simple 1D test for the NRBC involving the propagation of an elastic wave in a semi-infinite bar. Though simple, because in 1D the NRBC is theoretically perfectly absorbing, errors in the simulation can be attributed solely to the discretisation. In particular, the approximation of spatial derivatives near a boundary and the time integration scheme.

Consider the 1D wave equation on a semi-infinte bar in the domain $x \geq 0$ with a free

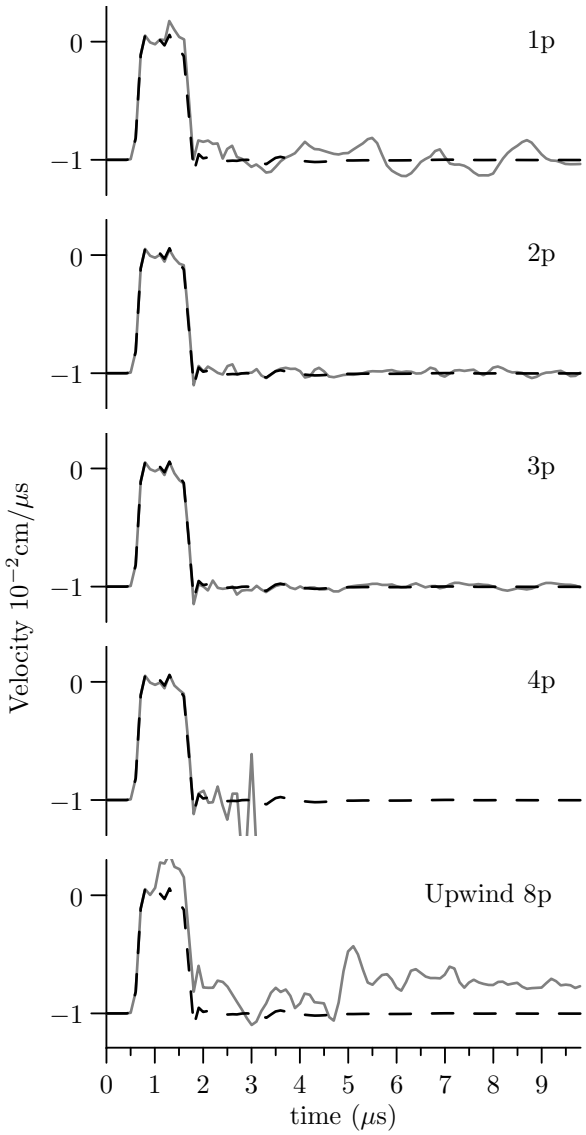

Figure 2.8: SPH: Velocity profile of particle 80. Solid line is the truncated solution with 100 particles. Dashed line is a reference solution with 800 particles and no NRBC. Number in upper right indicates number of particles where NRBC is applied. Bottom plot uses upwind time integration scheme (see main text page 48).

boundary at $x = 0$,

$$\begin{aligned} u_{tt} &= c^2 u_{xx} \\ u_x(0,t) &= 0 \\ u_t(x,0) &= \begin{cases} 0.01\text{cm}/\mu\text{s} & : x < 0.35\text{cm} \\ -0.01\text{cm}/\mu\text{s} & : x \geq 0.35\text{cm} \end{cases} \end{aligned} \tag{2.68}$$

with wave speed $c = \sqrt{\frac{E}{\rho}}$. We discretise the first 1cm of x using 100 equally-spaced particles, with particle spacing $\Delta x = 0.01$cm, numbered sequentially from left to right - particle 1 begins at $x_1 = 0.005$cm and particle 100 at $x_{100} = 0.995$cm. To simulate the

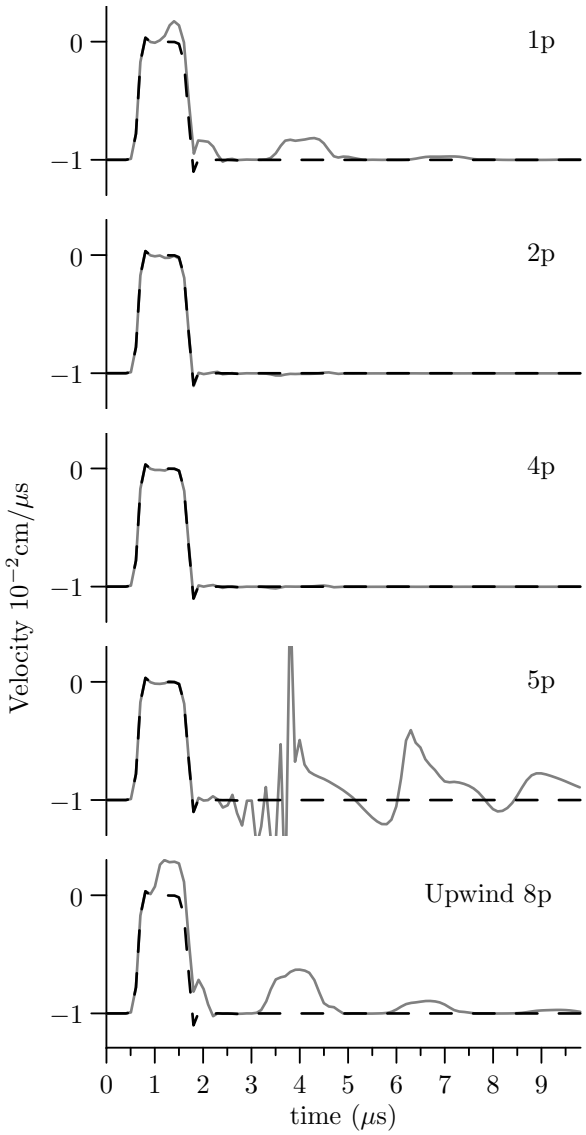

Figure 2.9: XSPH: Standard SPH with velocity smoothing. Further details as in figure 2.8.

semi-infinte bar we apply the 1D NRBC to n particles at the extreme right end, so that

$$u_{tt,i} = -c \left\langle u_{tx} \right\rangle_i \tag{2.69}$$

where

$$\left\langle u_{tx} \right\rangle_i = \sum_{j \in N(i)} (v_j - v_i) W'_{ij}, \tag{2.70}$$

and $u_{x,i} = v_i$.

To apply the initial condition the first 35 particles are prescribed an inital velocity of 0.01cm/μs and the remainder an inital velocity of -0.01cm/μs. A fixed smoothing length of $h = 1.3\Delta x$ is used. For comparison a reference solution is provided where the first 8cm

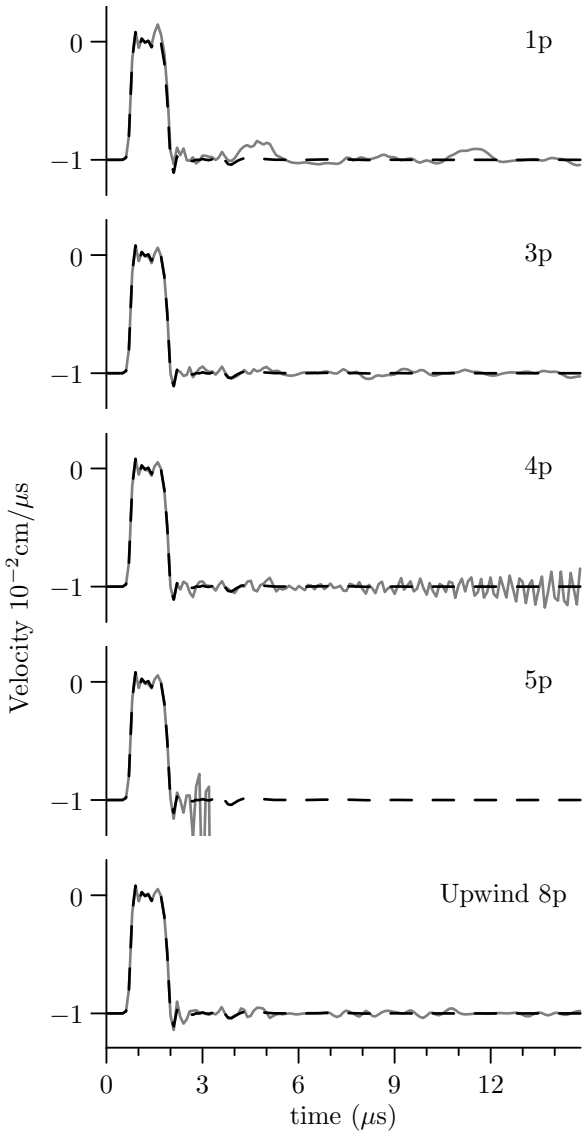

Figure 2.10: NCSPH: First-order complete version of SPH. Further details as in figure 2.8.

of the bar is simulated using 800 particles. The problem is not run long enough for waves reflected from the right hand side of the "reference" bar to affect the first 100 particles. This allows us to isolate the effect of the NRBC from other errors in the solution. Finally, the simulation is repeated using XSPH (with velocity smoothing), NCSPH and, NCXSPH (normalised corrected with velocity smoothing). For reference, the velocity is smoothed before updating the particle positions with,

$$\mathbf{v}_i \leftarrow \mathbf{v}_i + \epsilon \sum_{i \in N(j)} (\mathbf{v}_j - \mathbf{v}_i) W_{ij}, \tag{2.71}$$

where ϵ is a smoothing factor, in this work $\epsilon = 0.1$.

Figures 2.8-2.11 show the gross effect of varying the number of particles in the boundary

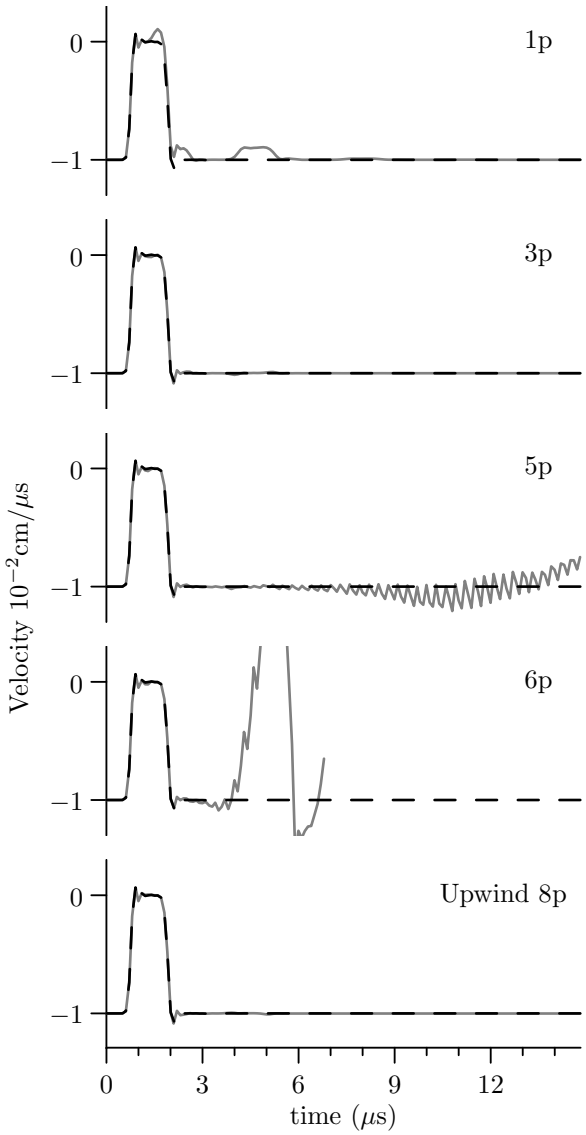

Figure 2.11: NCXSPH: First-order complete with velocity smoothing. Further details as in figure 2.8.

layer. With a smoothing length of $h = 1.3\Delta x$ each particle has four neighbours, two either side and consequently paticles 100 and 99 are deficient in neighbours. It is clear from the top plot in each figure (1p) that the boundary condition is not effective. This is no doubt caused by the fact that particle 99 "sees" the boundary and the incoming wave is reflected to some degree.

Too many particles in the boundary layer are seen to cause an instability. That this is due to the time integration scheme becoming in effect the forward Euler scheme, is confirmed by the stability of simulation when a different scheme (the upwind see above) is used with eight particles in the boundary layer. The upwind scheme is seen to be more

#Particles	Mean relative error ($\times 10^2$)			
	SPH	XSPH	NCSPH	NCXSPH
Reference	0.3474	0.0300	0.2243	0.0056
1	5.9729	1.3790	3.2605	0.8531
2	1.5015	0.1808	1.3068	0.0867
3	1.7273	0.0763	1.5451	0.0726
4	X	0.1401	7.5314	0.0733
5	X	X	X	13.7708
Upwind	30.9198	3.0328	1.2380	0.1078

Table 2.1: Relative error at particle 80 for $3\mu\text{s} < t < 20\mu\text{s}$. An X in the column indicates the simulation became unstable.

stable but for basic SPH (figures 2.8 and 2.9) it is very inaccurate because the gradient of the velocity for every particle in the boundary layer is approximated as inaccurately as that for the very end particle. For NCSPH because the kernel is normalised, the upwind scheme is not significantly worse than the basic algorithm. Smoothing the velocities has a stabilising effect and improves the accuracy (see below).

Define the relative error of the velocity at time-step k and particle i to be

$$E_i^k = \frac{|u_{t,i} - \langle u_t \rangle_i|}{|u_{t,i}|}. \tag{2.72}$$

To estimate the accuracy of the boundary condition we calculate the mean relative error at particle 80 for all time-steps such that $t > 3$. The first 3μs are omitted because the relative errors as the pulse is propagating through particle 80 are relatively large, and differences between the reference and truncated solutions are then obscured. The results of this calculation are shown in table 2.1 and the following can be ascertained:

- The best results for SPH and NCSPH are very similar. This is also true of XSPH and NCXSPH. Though the normalised and corrected versions appear to be more

forgiving in terms of accuracy and stability in regards to the thickness of the boundary layer.

- Velocity smoothing improves the accuracy of the reference simulation and this carries over to the truncated simulations.

- As is also apparent from the plots in figures 2.8 - 2.11 the upwind scheme is not appropriate for a non-normalised kernel.

- In all cases, as expected, the reference simulation is more accurate than the best achieved by the NRBC by between 2.5 to 13 times. This is despite the theoretically perfect absorption. An obvious explanation of the difference is inaccuracies in the approximation of the velocity gradient near the boundary - the probable cause of the inferior accuracy of the upwind scheme. Another factor is that the wave may propagate at a different sound speed in SPH than that predicted theoretically and used in the boundary condition.

Smoothing length. We now investigate the effect of varing the smoothing length on the efficacy of the boundary condition. Increases in h will obviously affect the number of particles that should be included in the boundary layer as the influence of the boundary extends further into the domain. For consistency we use NCSPH with velocity smoothing, and include $floor(2h/\Delta x) + 1$ particles in the boundary layer. This coincides with the optimum according to the previous test, where $h = 1.3\Delta x$, so $floor(2h/\Delta x)+1 = 3$. In all other respects, save the change in the smoothing length, this test is exactly as described above. It can be seen from 2.12 that the difference in the error between the reference and truncated solutions remains fairly constant irrespective of smoothing length. This indicates that the boundary condition is not dependent on a specific smoothing length to maintain its accuracy.

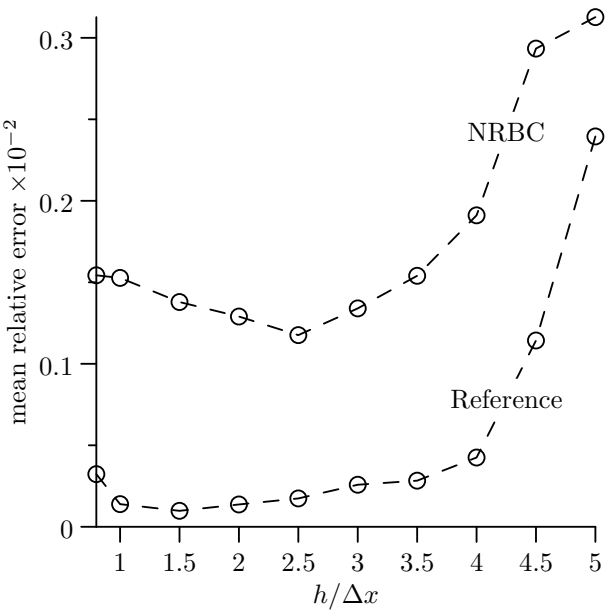

Figure 2.12: Relative error at particle 80 for $3\mu s < t < 10\mu s$ for large reference solution and for the truncated domain (NRBC).

3.2 2D problems

We now investigate the performance of NRBCs in 2D. In this case they are not even theoretically able to absorb all incident waves. It is expected therefore that the performance will be worse than in the 1D case above. As above we compare the truncated solution, i.e. one with a NRBC, to a larger reference solution. This allows us to analyse directly the effect of the boundary condition, and success may be judged by the difference seen between the two solutions. In all cases the linear elastic material model was used with density $\rho = 7.8$, Poisson ratio $\nu = 0.3$, and Young's modulus $E = 2.1$, all expressed in units of grams, centimeters, and micro-seconds. Addionally it is to be understood, given the results in 1D that unless otherwise stated all SPH simulations use NCSPH and velocity smoothing.

Various NRBCs were introduced above, some of first-order i.e. requiring only first derivatives in space. Others were of second-order i.e. requiring the approximation of second-order spatial derivatives. Below we will consider first-order methods exclusively. This is mainly because the author's efforts to implement a second-order condition that is *as* accurate and the first-order conditions have been in vain. This may be attributed to the difficult task of approximating higher derivatives accurately in the presence of particle

deficiency.

For reference we give the boundary conditions described above in their original version and in pseudo-code to describe their actual implementation in SPH. Note that for each particle i the gradient of velocity, $\mathbf{L}_i$, and the boundary normal, $\mathbf{n}_i$, is known when the boundary condition routine is called. For clarity we give the original boundary condition for a right moving wave incident to a vertical boundary.

1. The E-M first-order elastic boundary condition

$$\frac{\partial \mathbf{u}}{\partial t} + \begin{pmatrix} c_p & 0 \\ 0 & c_s \end{pmatrix} \frac{\partial \mathbf{u}}{\partial x} = 0. \tag{2.42}$$

for all boundary particles **do**

$\mathbf{t}[1] = \mathbf{n}_i[2]$; $\mathbf{t}[2] = -\mathbf{n}_i[1]$

$\mathbf{dv} = \mathbf{L}_i \cdot \mathbf{n}_i$

$\mathbf{a}_i = -c_p(\mathbf{dv} \cdot \mathbf{n}_i)\mathbf{n}_i - c_s(\mathbf{dv} \cdot \mathbf{t})\mathbf{t} + \mathbf{v}_i \cdot \mathbf{L}_i$

end for

2. The modified boundary condition given by [84],

$$\frac{\partial \mathbf{u}}{\partial t} + \begin{pmatrix} c_p & 0 \\ 0 & c_s \end{pmatrix} \frac{\partial \mathbf{u}}{\partial x} + \begin{pmatrix} 0 & c_p - c_s \\ c_p - c_s & 0 \end{pmatrix} \frac{\partial \mathbf{u}}{\partial y} = 0. \tag{2.45}$$

for all boundary particles **do**

$\mathbf{t}[1] = \mathbf{n}_i[2]$; $\mathbf{t}[2] = -\mathbf{n}_i[1]$

$\mathbf{dv} = \mathbf{L}_i \cdot \mathbf{n}_i$

$\mathbf{a}_i = c_p(\mathbf{dv} \cdot \mathbf{n}_i)\mathbf{n}_i + c_s(\mathbf{dv} \cdot \mathbf{t})\mathbf{t} + \mathbf{v}_i \cdot \mathbf{L}_i$

$\mathbf{dv} = \mathbf{L}_i \cdot \mathbf{t}$

$\mathbf{a}_i \leftarrow \mathbf{a}_i + (c_s - c_p)(\mathbf{dv} \cdot \mathbf{n}_i)\mathbf{n}_i + (c_p - c_s)(\mathbf{dv} \cdot \mathbf{t})\mathbf{t}$

end for

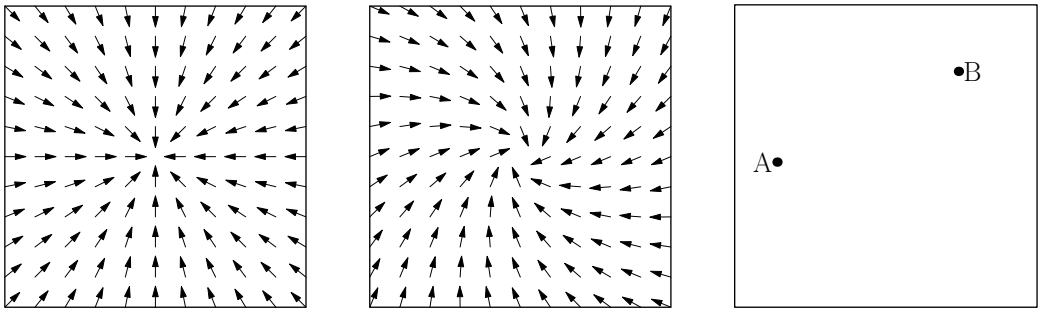

(a) Straight compression (b) Skewed compression (c) History particle locations

Figure 2.13: A 1cm×1cm elastic block. Initial velocity of all particles is either directed towards the center with equal magnitude (a). Or all velocity vectors are rotated (taking each particle as the origin) by $\pi/8$ radians (b). A NRBC is in place on all boundaries. Discretisation uses regular grid of 50×50 particles. Material is linear elastic with density $\rho = 7.8$, Young's modulus $E = 2.1$, and Poisson's ratio $\nu = 0.3$ (units are grams, centimetres and micro-seconds). For future reference the location of two particles A and B are indicated in (c).

3. Higdon's generalisation of E-M boundary conditions for the wave equation (2.33), suggests that given *a priori* knowledge of the problem it may be possible to "tune" the boundary condition. This is accomplished by using not the wave speeds c_p and c_s of an incident wave, but the wave speed normal to the boundary i.e. if the wave is travelling in the direction $\hat{\mathbf{k}}$ towards a boundary with normal n then, instead of c_p and c_s, one would substitute $\hat{\mathbf{k}} \cdot \mathbf{n} c_p$ and $\hat{\mathbf{k}} \cdot \mathbf{n} c_s$, respectively.

The next section will compare the above boundary conditions. For ease of reference they will be called, in order of their definition above, the P-(for plain) boundary condition, the M-boundary condition and the H-boundary condition. Plots below will be labelled accordingly.

3.2.1 Compression of a square elastic block

In this section we consider the problem of a square of particles each given an initial velocity of equal magnitude, $v_o = |\mathbf{v}_o|$. The velocity will either be directed directly towards the centre, as in figure 2.13a, or slightly off centre as in figure 2.13b. If $\mathbf{x}_m$ is the position vector of the square and $\mathbf{x}_{mi} = \mathbf{x}_m - \mathbf{x}_i$, then the initial velocity of each particle is

$$\mathbf{v}_i = v_0 \hat{\mathbf{x}}_{mi}, \tag{2.73}$$

in 2.13a, or

$$\mathbf{v}_i = v_0 \begin{pmatrix} \cos \pi/8 & -\sin \pi/8 \\ \sin \pi/8 & \cos \pi/8 \end{pmatrix} \cdot \hat{\mathbf{x}}_{mi}, \tag{2.74}$$

in figure 2.13b. We use the kinetic energy as a gross estimate of the effectiveness of the boundary condition. In figure 2.13a the kinetic energy for the first case is plotted. In this case we can see that the quantity reflected back into the domain, as a pecentage of the inital kinetic enrergy, is low. The greatest deviation from the reference solution for the P- and M-boundary conditions at around $t = 1.5$ is less than 0.25% of the initial kinetic energy whereas the H-condition is considerably more. In figure 2.15a one can see that the magnitiude of the velocity falls to zero, albeit with a spurious bump, this bump is roughly the same size for both particles. Similarly the pressure, figure 2.15b, rises to an equilibrium level and the boundary condition sustains the material under compression, though it is not uniform across the material. For both particles the final pressure is too high, but less so at particle B. The results for the "skewed" compression show that in this case the boundary condition performs less well, more energy is reflected back into the domain, figure 2.16. Also we find that the velocity of particles A and B do not go to zero as they should, this is at least in part due to a residual rotation of the body. There is more difference between the P- and M-boundary conditions with the kinetic energy. This may have been expected due to the nature of of the test as the M-condition should in theory be better at absorbing shear waves, see § 1.1.4.

In summary we may say that the P- and M-boundary conditions perform very similarly,

with a slight advantage for the M-condtion in the skewed case, probably because of its better theoretical ability to absorb S-waves. The H-condition is, perhaps surprisingly, the worst even though we had perfect knowledge of the wave directions.

3.2.2 Compression of central disc only

We wish to compare the performance of the proposed NRBC with that available in the FE program, LS-DYNA. The previous test is very convenient because the reference solution is particularly simple, but it cannot be used for the comparison because of LS-DYNA's implementation of NRBCs. Specifically, they are implemented by applying a normal and shear stress to the surface of the boundary elements [60]:

$$\begin{aligned} \sigma_n &= -\rho c_p \mathbf{v} \cdot \mathbf{n} \\ \sigma_t &= -\rho c_s \mathbf{v} \cdot \mathbf{t}. \end{aligned} \tag{2.75}$$

We can see that the applied force will therefore be proportional to the velocity. For this reason the previous test cannot be used as a fair comparison as the boundary is in motion from the beginning. Equation (2.75) will apply a force to the boundary immediately and the computed solution will not be as intended. Whether this behaviour is considered correct is a matter of debate. In the previous test the hypothetical infinite space surrounding the problem domain is supposed to be collapsing in on itself. The LS-DYNA boundary conditions assume it is at rest. Nevertheless, in this section a test indentical to that above, save that only particles/nodes within a distance of 0.25cm from the centre of the square are in motion initially i.e. if the centre of the square is at $\mathbf{x}_m$, define the vector $\mathbf{x}_{mi} = \mathbf{x}_m - \mathbf{x}_i$, then

$$\mathbf{v}_i = \begin{cases} v_0 \hat{\mathbf{x}}_{mi} & : |\mathbf{x}_{mi}| < 0.25 \\ 0 & : \text{otherwise} \end{cases}. \tag{2.76}$$

We compare the results for FE and SPH for two different initial conditons: where the speed of each particle within 0.25cm of the centre of the square is $v_0 = 0.01\text{cm}\mu\text{s}^{-1}$, and where $v_0 = 0.05\text{cm}\mu\text{s}^{-1}$. A comparison of the speed and pressure at the particle A and B

are given in figures 2.18 and 2.19, for the low and high speed versions respectively. One can see that the SPH and FE results for each case follow a similar pattern. The plots are not in perfect correspondence even at the beginning, say $t < 0.5\mu$s, when the boundary condition cannot have affected the motion at the particles in question. Nevertheless one can see that the FE and SPH results are broadly similar with perhaps the SPH particle near the corner, B, being noticeably worse than the corresponding node.

3.2.3 Transient surface impact

In the previous sections a NRBC was applied to the whole of the domain boundary, simulating an infinite domain. In an infinite homogeneous domain there only P- and S-waves to consider. For a semi-infinite domain the free surface introduces spacial difficulties, specifically the existence of Rayleigh waves that can propagate along the free surface but are exponentially damped towards the interior. For details see appendix A § 3.3, but in brief they travel at a velocity $c_r < c_s$, and whereas the displacement of particles under the action of a plane P- or S-wave is either parallel or normal, respectively, to the direction of propagation. For a Rayleigh wave the displacement is a mix of both components. Theoretically one could absorb an incoming Rayleigh wave with the Higdon-type boundary condition,

$$\frac{\partial \mathbf{u}}{\partial t} + c_r \frac{\partial \mathbf{u}}{\partial x} = 0. \tag{2.77}$$

But P- and S-waves still propagate along the surface and will be spuriously reflected because the wave speed c_r is not appropriate for their absorption. Following equation (2.33), one might then attempt, see [6], to use a condition which is a mix of the E-M condition and (2.77);

$$\left(\frac{\partial}{\partial t} + c_r \frac{\partial}{\partial x}\right)\left(\frac{\partial}{\partial t} + \begin{pmatrix} c_p & 0 \\ 0 & c_s \end{pmatrix} \frac{\partial}{\partial x}\right) \mathbf{u} = 0. \tag{2.78}$$

Theoretically this will absorb all normally incident P-, S- and Rayleigh waves. Unfortunately, it requires second derivatives and, if accurate approximation of the second-

derivative on a boundary is difficult, it is harder still on the corner where the free surface and the artificial boundary meet as particle deficiency is even more marked.

The problem considered here is described in 2.20. Essentially we truncate the reference domain to create a "narrow" domain with a NRBC abutting the free surface to investigate the absorption of surface waves. Or we create a "shallow" domain with a NRBC along the bottom to investigate the absorption of body waves generated at the surface. We consider two cases where the initial velocity of the "impact" is $0.1\text{cm}\mu\text{s}^{-1}$ and $0.5\text{cm}\mu\text{s}^{-1}$, referred to as "slow" and "fast", respectively. Note that in this case the boundary normal vectors along the artificial boundary have been assigned manually so that on the vertical boundary the normals are all $\mathbf{n} = (1, 0)$ and at the horizontal non-reflecting boundary we have $\mathbf{n} = (0, -1)$.

Absorption of surface waves. Figures 2.21 to 2.23 plot the pressure and x-and y-velocities of particles A and B. In all cases we can see, by the divergence of the dotted line (representing the solution on the truncated domain without NRBCs) when the P-wave first arrives from the truncated boundary. At this point there is little apparent disturbance in the NRBC solution. This is not surprising as at the free surface the problem is very much like that in the 1D case considered above where the boundary condition was seen to perform very well. The plots of the x- and y-velocities (figures 2.22 to 2.23) however show clearly, especially for the y-velocity, the arrival of a spurious reflection from the artificial boundary. This is not the P-wave, but the Rayleigh, and possibly S-, wave first seen at particle B at around 2μs and then beginning to affect particle A a micro second later. This is consistent with the approximate surface wave speed of $c_r = 0.32\text{cm}\mu\text{s}^{-1}$ calculated using the formula (A.36) from appendix A § 3.3. We can therefore conclude that the surface wave is absorbed quite poorly compared to the P-wave. The deviation from the reference solution, though marked is not absurd, and the boundary condition may find application when the exact behaviour of the surface is not the main point of interest. It should be noted that the reference solution needed 40,000 particles to be large enough such that the waves reflected from the boundary did

not reach the area of the truncated domain within the problem time. The narrow domain has only 5000 particles (50×100) and the shallow domain to be discussed below only 3000 (30×100).

Absorption of body waves generated at the surface. One can see from figures 2.24 and 2.25 that in general the boundary condition on the underside of the domain successfully absorbs the wave generated at the surface. Particle C directly below the impact shows that only a small reflection off the bottom has occurred, though a wave returning to C after hitting the underside would have been normally incident to the boundary and been absorbed well. As above the point where the dashed line deviates from the grey line shows when the P-wave reflected from a *free* boundary would have hit the particle. At this point the black line, associated with the NRBC only separates marginally from the reference solution. The particle on the surface B also follows the reference solution closely, whereas spurious reflections from the NRBC could have caused it to deviate from the reference solution. At 3μs the pressure at surface particle B starts to deviate from the reference solution. This is not a result of errors associated with the NRBC but the P-wave reflected from the far vertical boundary returning.

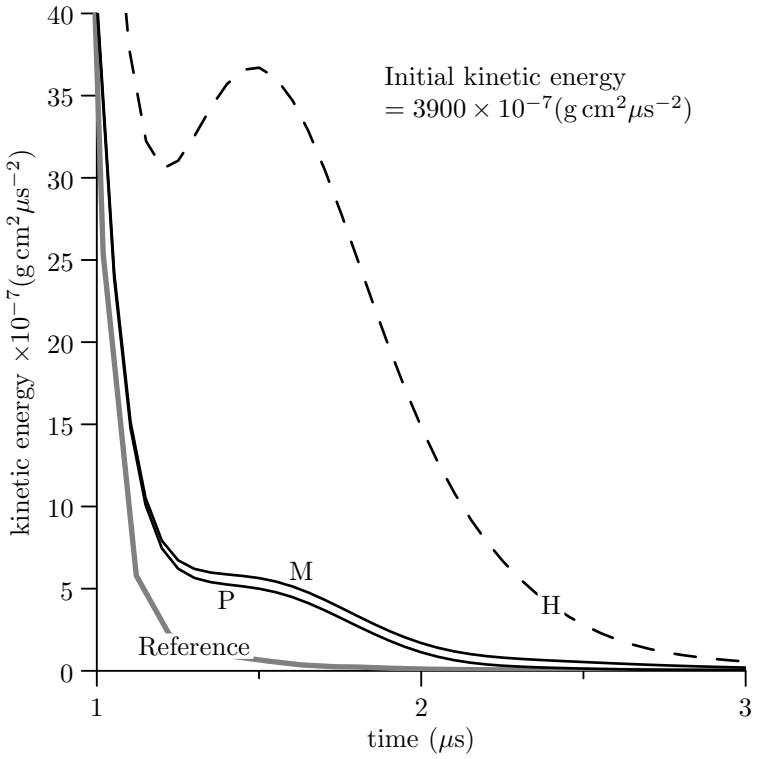

Figure 2.14: Kinetic energy square. Initial velocity of each particle $|\mathbf{v}_o| = 0.01\mathrm{cm}\mu\mathrm{s}^{-1}$, with direction as in 2.13a. Plots are labelled as explained on page 58.

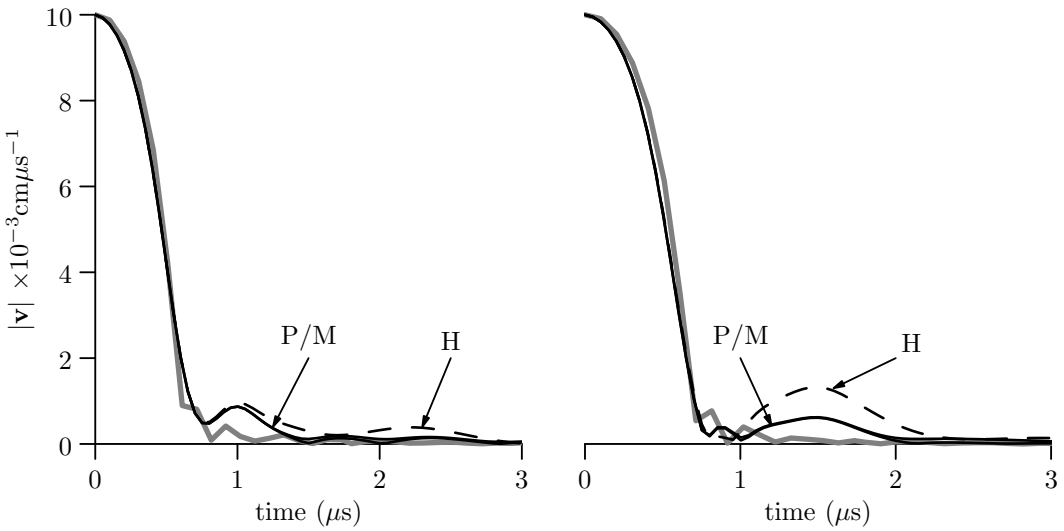

(a) Magnitude of velocity

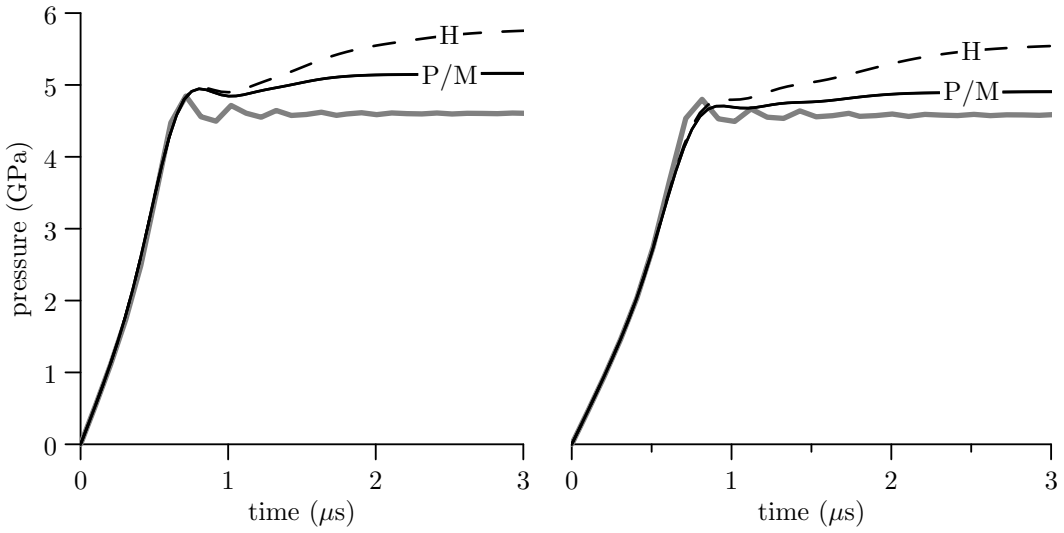

(b) Pressure

Figure 2.15: Time history plots at particles A and B. Plots on the left are taken at particle A in figure 2.13c, and those on the right from particle B. Unlabelled grey line is from the corresponding particles from the reference problem.

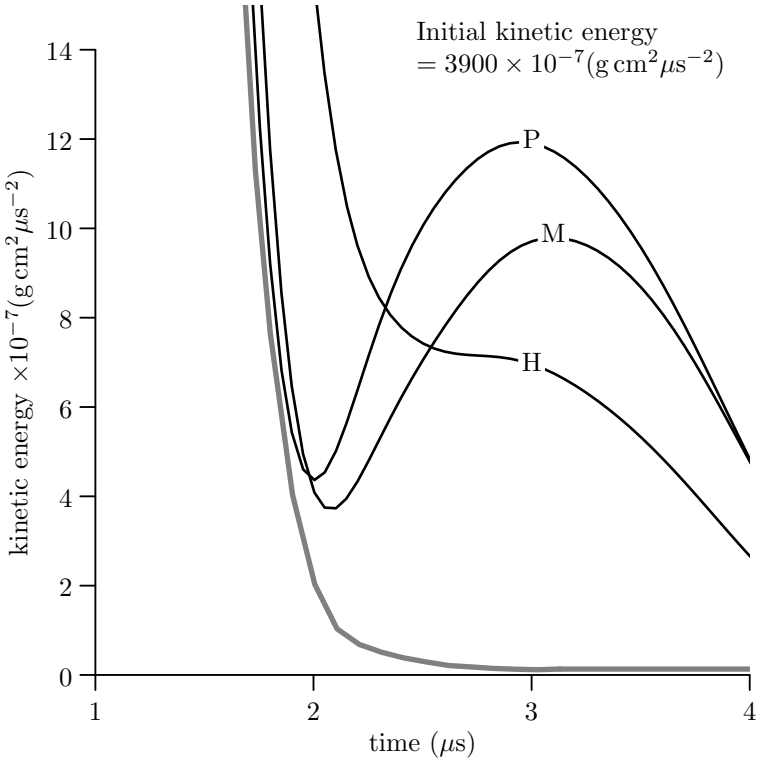

Figure 2.16: Kinetic energy square. Initial velocity of each particle $|\mathbf{v}_o| = 0.01\mathrm{cm}\mu\mathrm{s}^{-1}$, with direction as in 2.13b

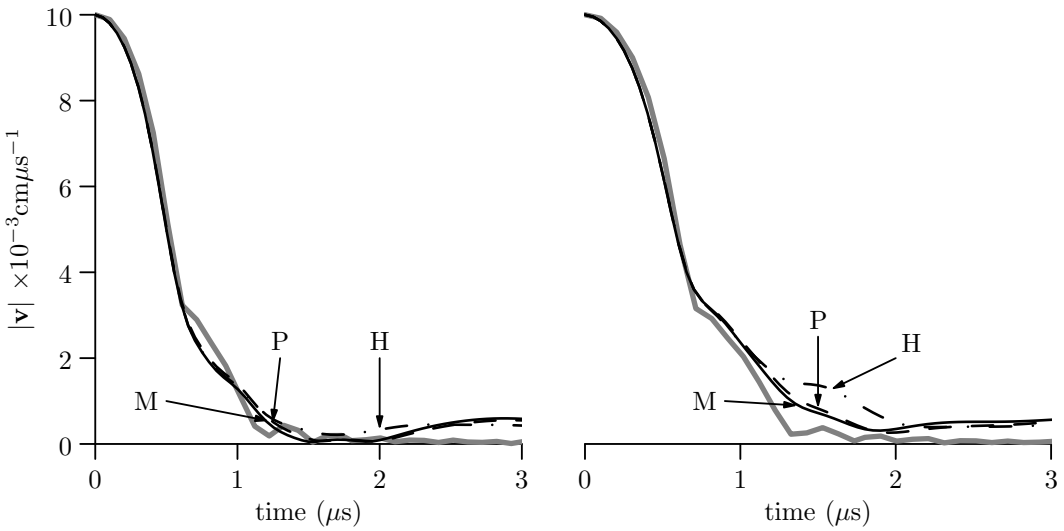

(a) Magnitude of velocity

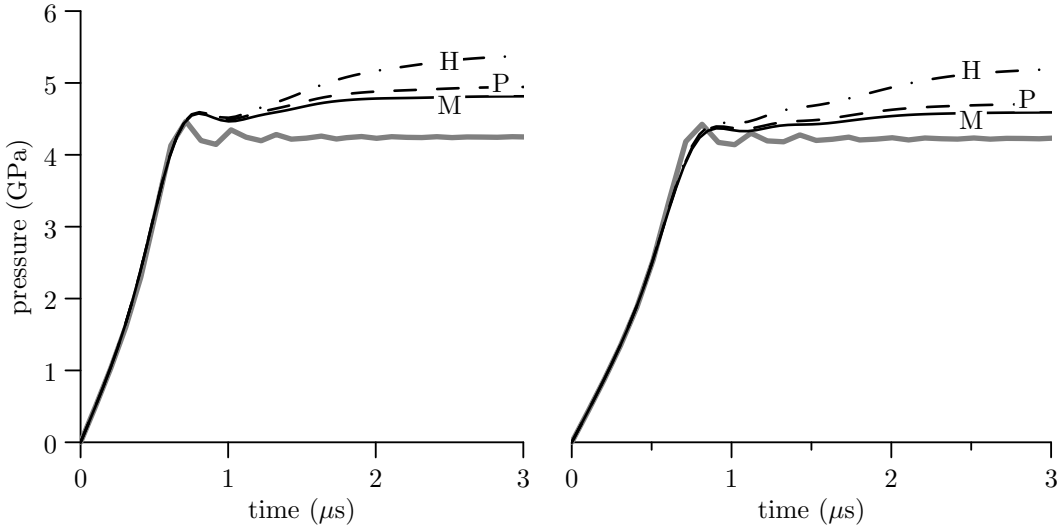

(b) Pressure

Figure 2.17: Time history plots at particles A and B. Plots on the left are taken at particle A in figure 2.13c, and those on the right from particle B. Unlabelled grey line is from the corresponding particles from the reference problem.

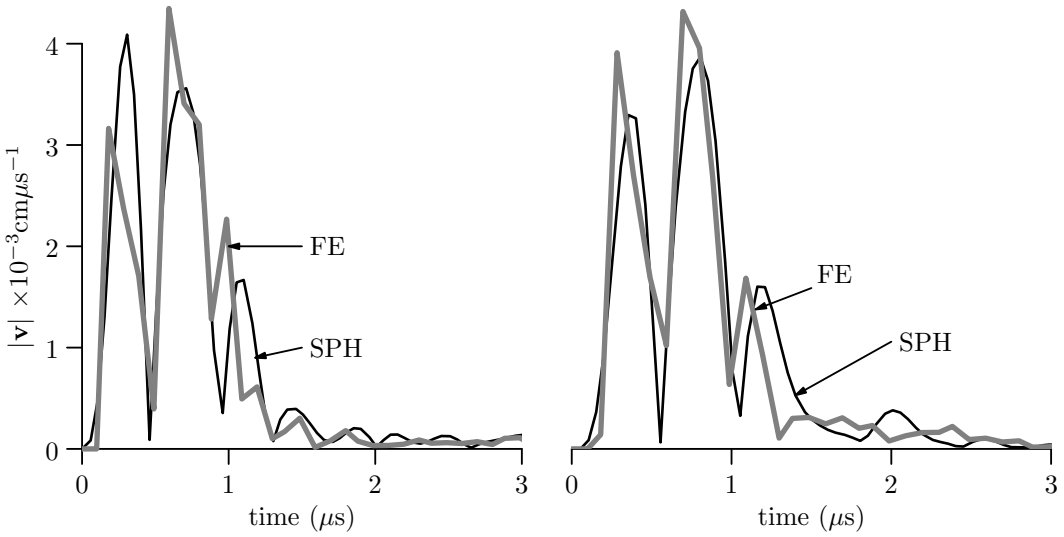

(a) Magnitude of velocity

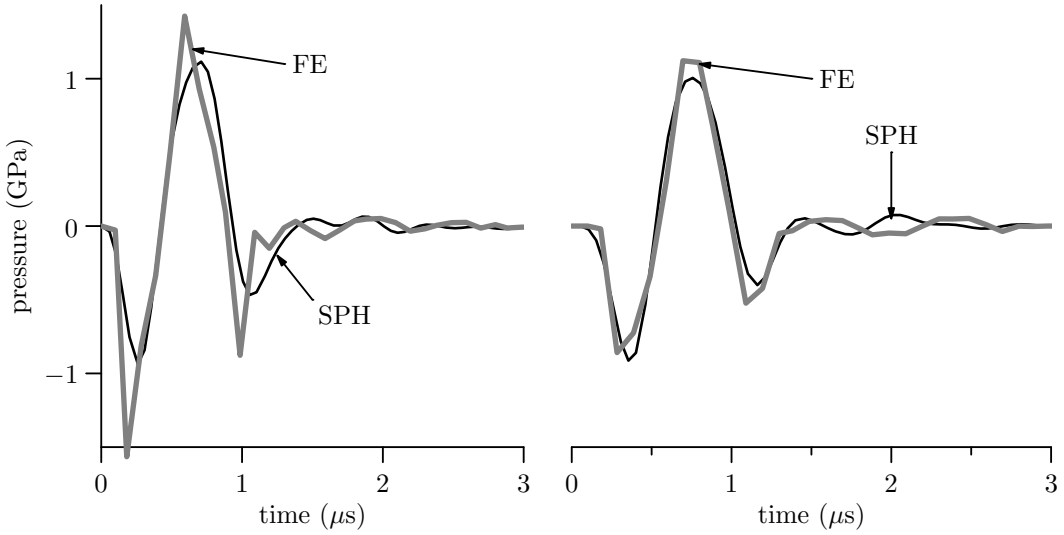

(b) Pressure

Figure 2.18: Compression of central portion of square. Initial velocity $|\mathbf{v}_o| = 0.01\mathrm{cm}\mu\mathrm{s}^{-1}$ for all particles within. Plots on the left are taken at particle A in figure 2.13c, and those on the right from particle B.

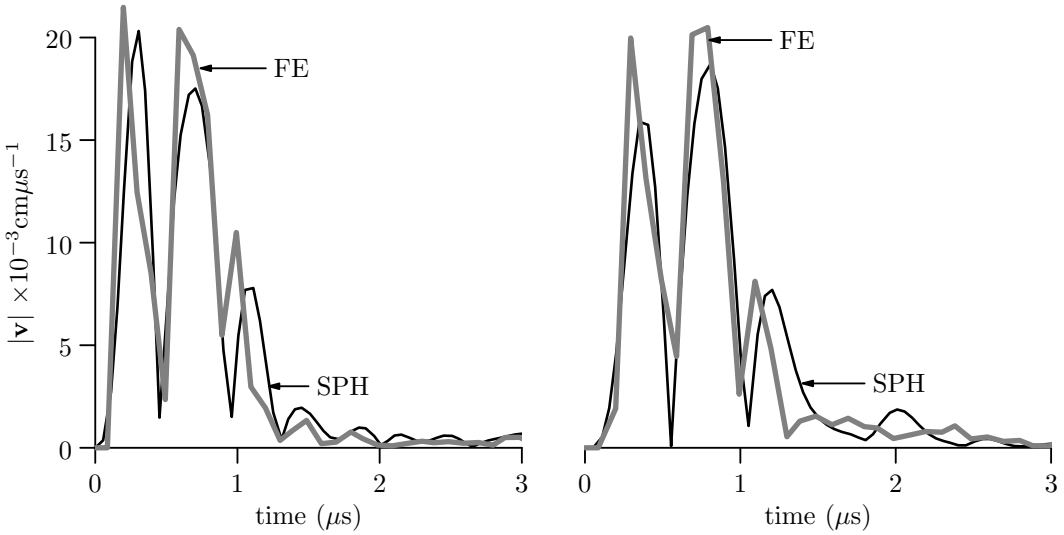

(a) Magnitude of velocity

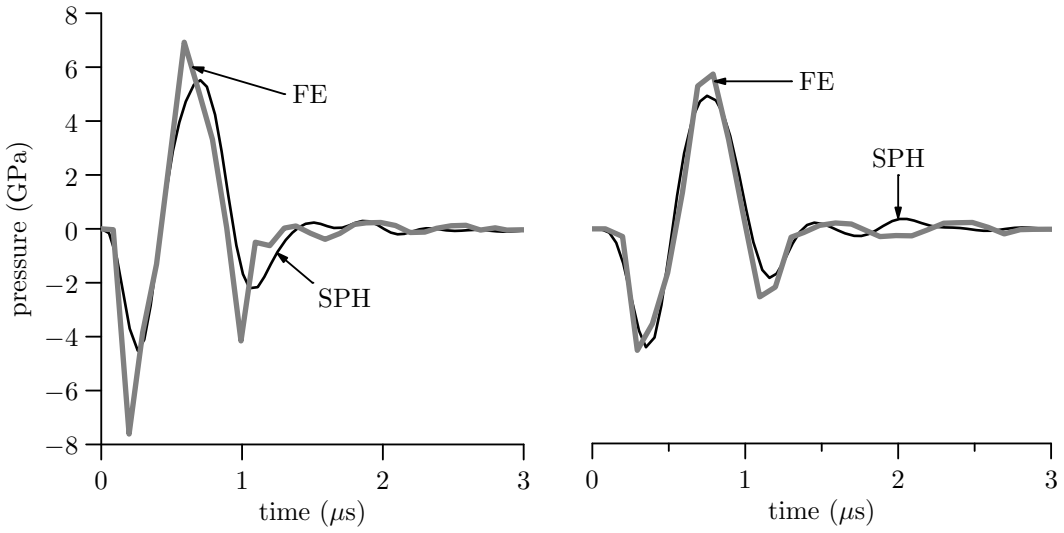

(b) Pressure

Figure 2.19: Compression of central portion of square. Initial velocity $|\mathbf{v}_o| = 0.05\mathrm{cm}\mu\mathrm{s}^{-1}$ for all particles. Plots on the left are taken at particle A in figure 2.13c, and those on the right from particle B.

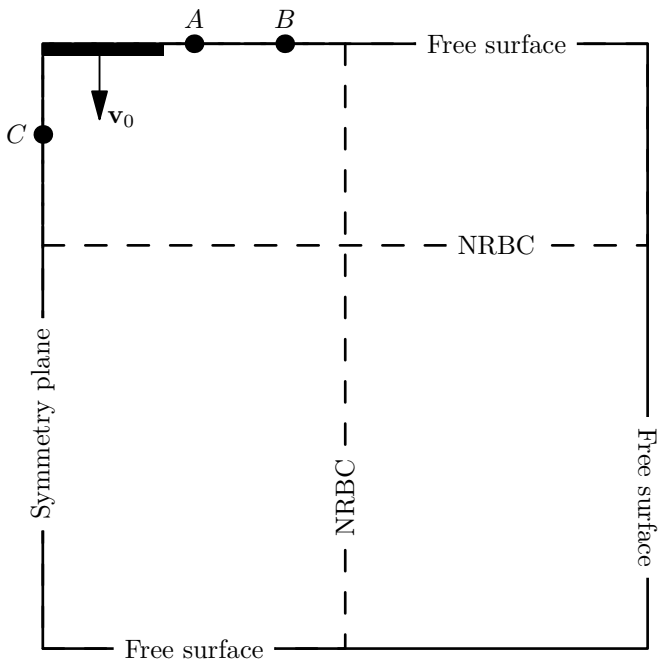

Figure 2.20: Reference domain 2cm×2cm elastic block. Truncated in one of two ways. Indicated by the two lines labelled "NRBC". One way we are left with a "shallow" domain of 100×30 particles; the other a "narrow" domain 50×100. A rectangle of 15×2 particles are prescribed an initial velocity in the negative y-direction. Particles A, B and C are labelled for future reference.

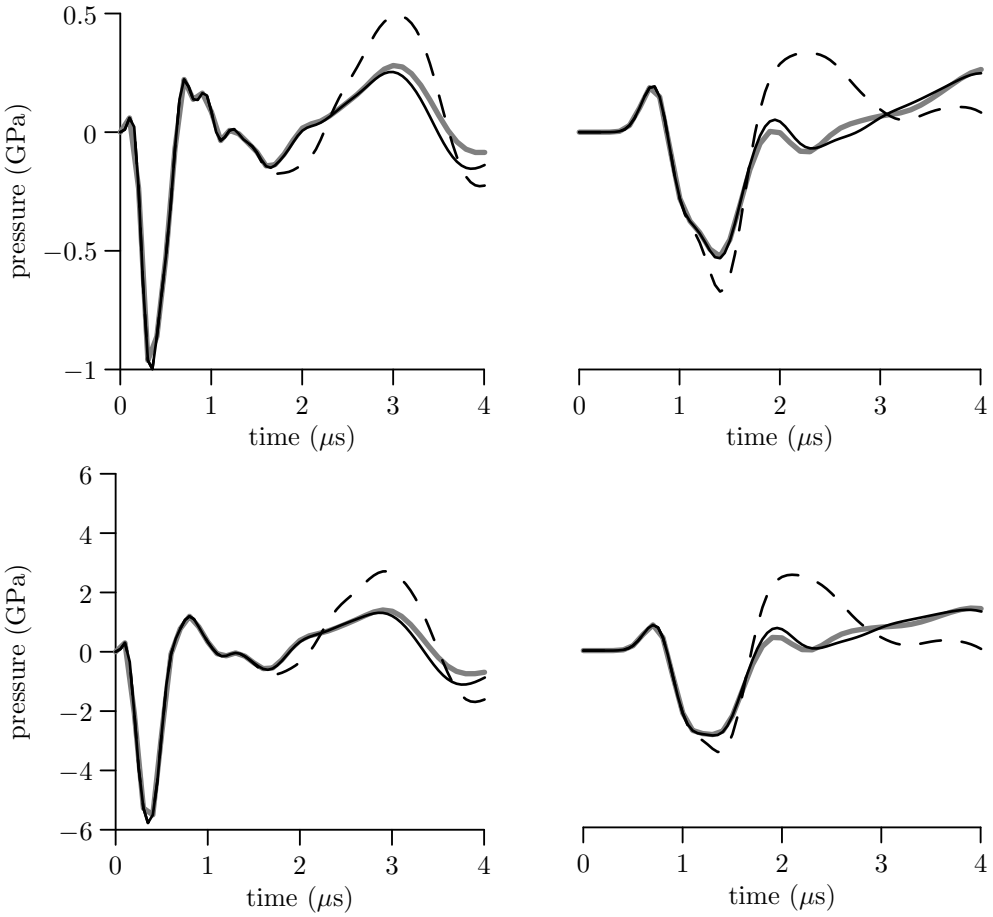

Figure 2.21: Narrow domain. Pressure at particles A (left column) and B (right column) for slow (top row) and fast (bottom row) impact. Grey line is the reference solution from a domain 4cm×4cm. Black line is the solution with NRBCs and the dashed line is the solution from the truncated domain with no NRBCs.

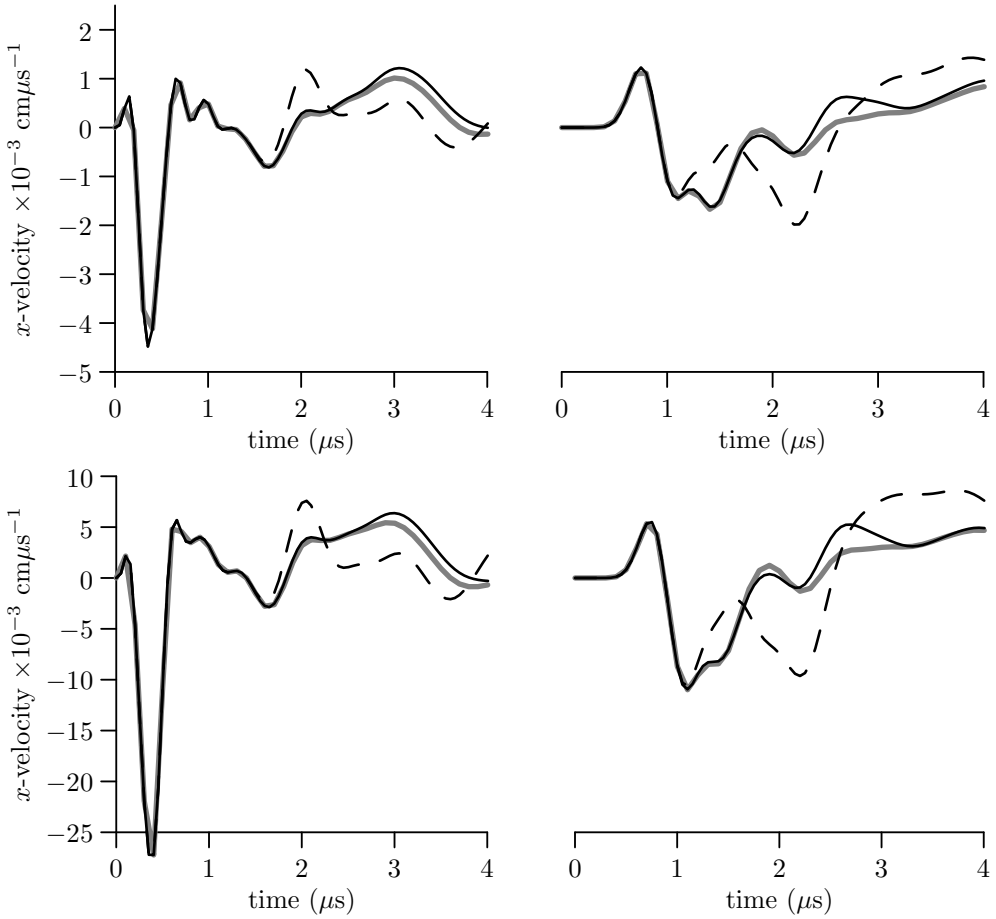

Figure 2.22: Narrow domain. x-velocity at particles A (left column) and B (right column) for slow (top row) and fast (bottom row) impact. Grey line is the reference solution, black line is solution with NRBCs and the dashed line is the solution from the truncated domain with no NRBCs.

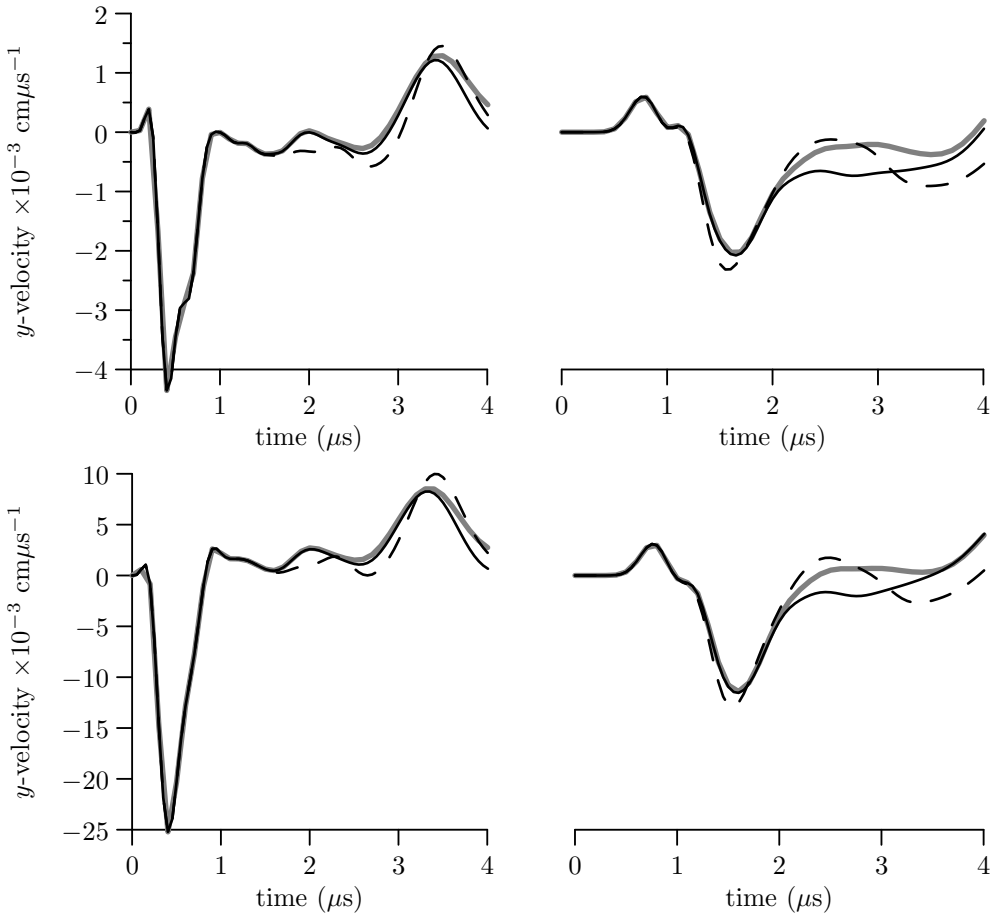

Figure 2.23: Narrow domain. y-velocity at particles A (left column) and B (right column) for slow (top row) and fast (bottom row) impact. Grey line is the reference solution, black line is the solution with NRBCs and the dashed line is the solution from the truncated domain with no NRBCs.

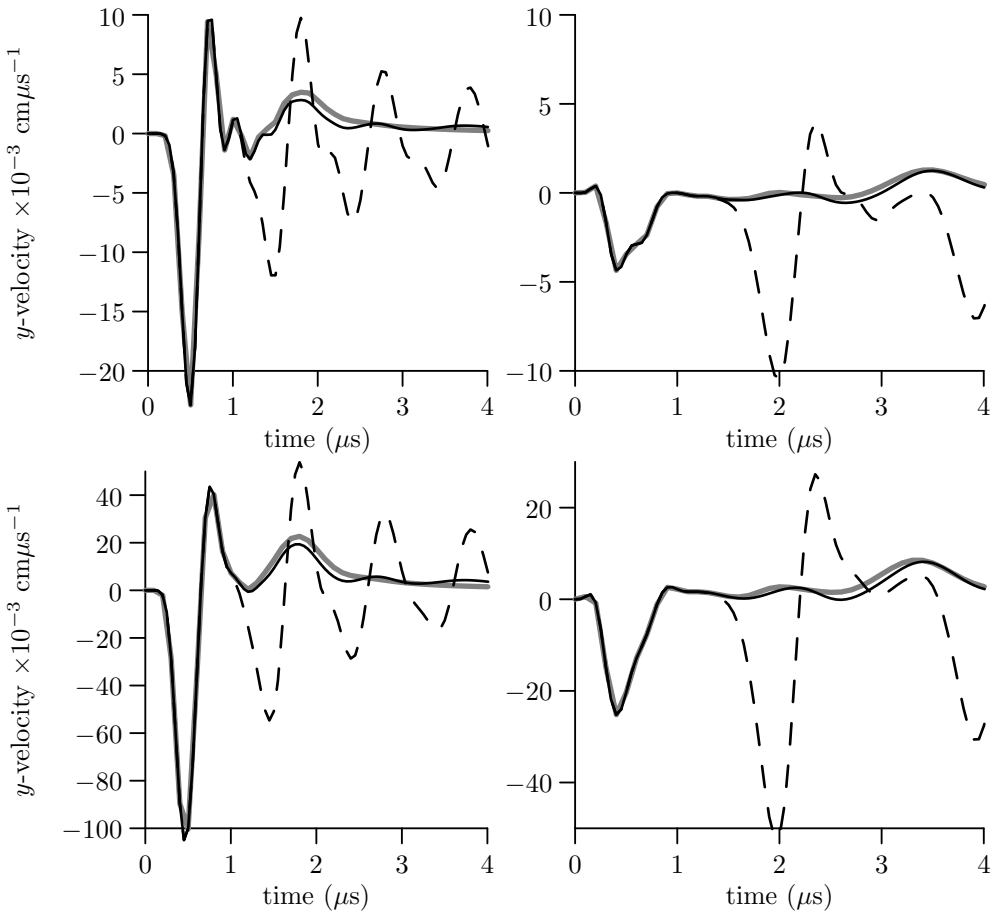

Figure 2.24: Shallow domain. y-velocity at particles C (left column) and A (right column) for slow (top row) and fast (bottom row) impact. Grey line is the reference solution, black line is the solution with NRBCs and the dashed line is the solution from the truncated domain with no NRBCs.

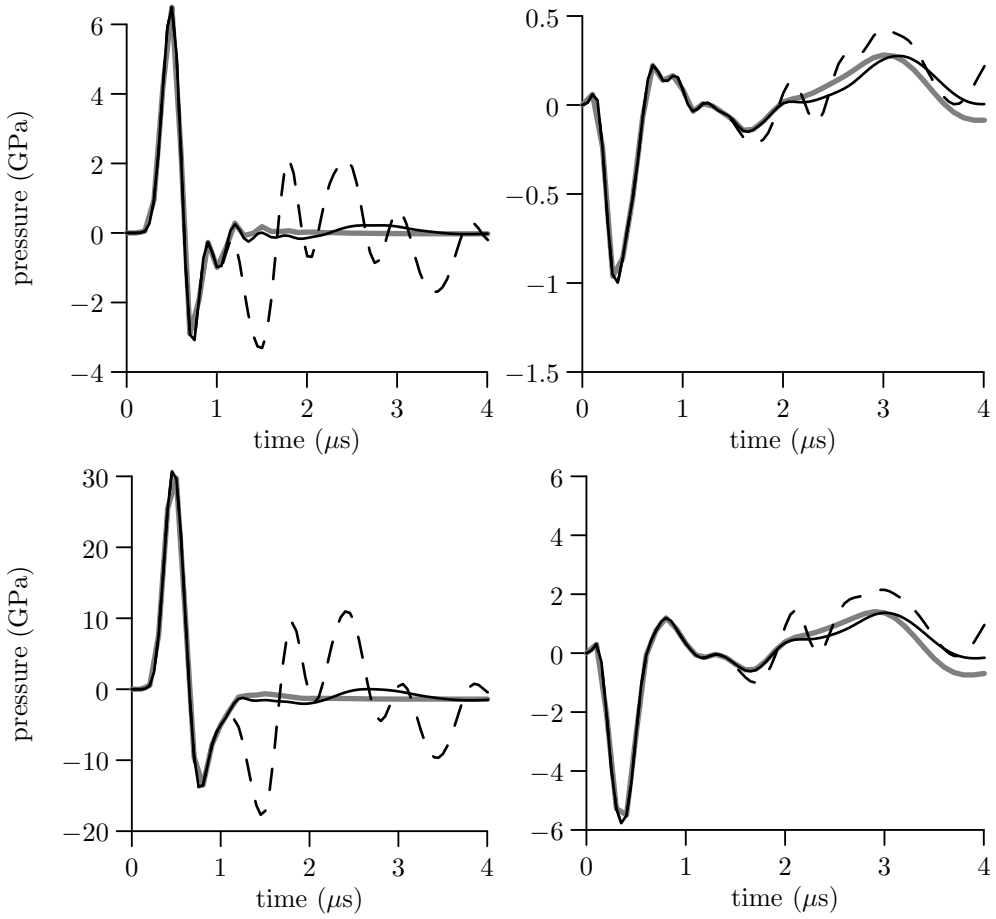

Figure 2.25: Shallow domain. Pressure at particles C (left column) and A (right column) for slow (top row) and fast (bottom row) impact. Grey line is the reference solution, black line is the solution with NRBCs and the dashed line is the solution from the truncated domain with no NRBCs.

Chapter 3

Stability Analysis of Semi-discretised SPH

1 Introduction

A well documented flaw in the basic formulation of SPH is an instability due to the particular nature of the space discretisation. Commonly this manifests as an unphysical clumping of particles under tension which can in turn result in purely numerical fracture. Many papers propose solutions to this problem but to the author's knowledge only [7, 85, 5] have a performed a stability analysis of SPH, all of which have been von Neumann analyses.

Total Lagrangian SPH (TL-SPH) [80, 89] reformulates conventional SPH in Lagrangian coordinates with a fixed set of neighbours for each particle. A stability analysis [7] shows that this formulation does not suffer from tensile instability. The disadvantage of a Lagrangian kernel is that it deforms as the material deforms, potentially nullifying an important advantage of meshfree methods. Monaghan introduced an artificial repulsive force acting over relatively short scales in order to prevent clumping [70]. This has the advantage of being relatively simple to implement, but careful tuning of parameters and velocity smoothing are necessary to prevent instability in solids. Another solution is

non-collocational SPH, first proposed by [22]. Stresses are calculated at a separate set of particles located between the standard SPH particles. In 1D this approach successfully removes tensile instability and has been extended to 2D in [82]. The difficulty in non-collocational SPH is placing the stress particles correctly, as one moves from 1D to 3D the complexity increases.

The first papers to analyse the stability of SPH were [85, 5]. Analysis is restricted to equally spaced particles in 1D with Eulerian kernels. Swegle et al. [85] derive a sufficient condition for SPH to be unstable; $W''\sigma > 0$. In tension ($\sigma > 0$) the position is unstable if the particles are so arranged that a kernel's second derivative is positive at neighbouring particles.

In a von Neumann type stability analysis [73] the equilibrium state is perturbed with a displacement field assumed to be of the form

$$u_n^j = \xi^n e^{-ikx}.$$

Here n refers to the time step, j is the particle index, and ξ is the amplification factor. If $|\xi| > 1$ then the perturbation will grow and the solution is unstable. In some special cases including, but not limited to, linear PDEs with constant coefficients, von Neumann stability analysis provides necessary and sufficient conditions for stability. For SPH however the conditions derived only provide a necessary condition for stability, or equivalently, a sufficient condition for instability. An intuitive explanation for the instability can be

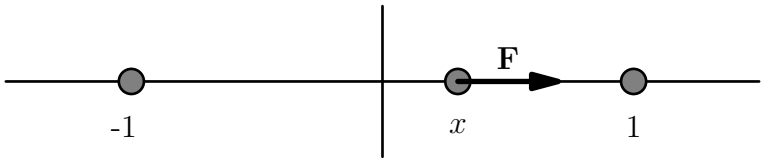

Figure 3.1: See main text.

given as follows. In figure 3.1 there are three particles in a line, assuming a constant stress the force on the centre particle for sufficiently small x is

$$\begin{aligned}\mathbf{F} &= \sigma\left[W'(-1,x) + W'(1,x)\right] \\ &\approx \sigma\left[W'(-1,0) + W'(1,0) + xW''(-1,0) + xW''(1,0)\right] \\ &= 2\sigma x W''(1,0)\,.\end{aligned}$$

If $W''\sigma > 0$ then the force, instead of acting to oppose the perturbation, reinforces the particle's motion. Additionally the forces in the discrete momentum equation are modified to enforce compliance with Newton's third law. Hence the particle at 1 will feel an equal but opposite force towards the centre particle and they will tend to clump. Obviously this does not replace a rigorous analysis.

Belytchko et al. [7] extended their analysis to SPH with Lagrangian kernels (Total Lagrangian SPH), non-collocational SPH and to a two dimensional case. Three distinct modes of instability are identified: tensile instability as identified by Swegle, instability due to the growth of zero-energy modes [85] and the instability present in the original PDEs. Total Lagrangian SPH does not suffer from tensile instability. Neither does non-collocational SPH in 1D, but the authors find that in 2D stability depends on the careful placement of the stress or slave nodes. Non-collocational SPH eliminates zero-energy modes and the authors state that a combination TL-SPH with stress point closely mirrors the instability properties of the PDE.

Instability is not restricted to states of tension. A so-called pairing instability can arise in fluid simulation especially when the number of neighbours is large [19]. The superior performance of Wendland kernels for free-surface flows has been noted in [62]. In [19] a linear stability analysis is performed and the superiority of Wendland kernels is linked to the positivity of their Fourier transform. In the present analysis a similar conclusion is reached i.e. that a kernel with a positive definite Fourier transform is generally stable under pressure.

2 Linear and Lyapunov stability analysis

The momentum equation in SPH can take various forms [57] but a representative example may be

$$\dot{\mathbf{v}}_i = \sum_{j \in N(i)} \left(\frac{\sigma_i}{\rho_i^2} + \frac{\sigma_j}{\rho_j^2} \right) \nabla W_{ij}. \tag{3.1}$$

If it is assumed that the RHS of (3.1) is a function of the particle displacements it is an example of a particular second order $N-$dimensional differential equation

$$\ddot{x}_i = f_i\left(x_1, \ldots, x_N\right). \tag{3.2}$$

The next sections, 2.1 and 2.2, present some selected general results pertaining to this kind of ODE that will then be applied directly to SPH.

The usual first step in a stability analysis is to linearise the system about some equilibrium point. The resulting linear system is easier to analyse and information about the behaviour of the original system near the equilibrium can be deduced. In section 2.1 it will be shown that in the case of (3.2) the linearised system does not provide necessary *and* sufficient conditions for the stability of the equilibrium. Nevertheless useful information can be obtained from the analysis, specifically a sufficient condition for instability (or equivalently a necessary condition for stability).

However a sufficient condition for stability can be derived via Lyapunov's method if in (3.2) the functions f_i can be derived from a potential energy function i.e. $f_i = -\frac{\partial U(\mathbf{x})}{\partial x_i}$. And further, the conditions derived for stability and instability in this case completely characterise the stability of the equilibrium position. That is to say, if a particular set of conditions are met the equilibrium is stable, if not, it is unstable.

We restrict the analysis to a semi-discretised version of the governing equations (i.e. time is continuous) so that the essential and special features of SPH can be understood in isolation.

2.1 Linear stability analysis

Equation (3.2) is equivalent to the first-order system

$$\begin{aligned} \dot{v}_i &= f_i\left(x_1, \ldots, x_N\right) \\ \dot{x}_i &= v_i. \end{aligned} \tag{3.3}$$

The result of linearising (3.3) about the origin is

$$\begin{aligned} \dot{v}_i &= \frac{\partial f_i^0}{\partial x_j} x_j \\ \dot{x}_i &= \delta_{ij} v_j \end{aligned} \tag{3.4}$$

where summation over a repeated index is implied and $\frac{\partial f_i^0}{\partial x_j} = \left.\frac{\partial f_i}{\partial x_j}\right|_{\mathbf{x}=\mathbf{0}}$ is the gradient evaluated at the origin. In block matrix form (3.4) is

$$\begin{pmatrix} \dot{\mathbf{v}} \\ \mathbf{v} \end{pmatrix} = \begin{pmatrix} \mathbf{0} & \mathbf{A} \\ \mathbf{I}_N & \mathbf{0} \end{pmatrix} \begin{pmatrix} \dot{\mathbf{x}} \\ \mathbf{x} \end{pmatrix}. \tag{3.5}$$

Where $\mathbf{A} \in \mathbb{R}^{N\times N}$ with components $A_{ij} = \frac{\partial f_i^0}{\partial x_j}$, $\mathbf{I}_N$ is the $N \times N$ identity matrix and $\mathbf{0}$ is an $N \times N$ matrix of zeros. Similarly $\mathbf{x} \in \mathbb{R}^N$ has components x_i with the vectors $\dot{\mathbf{x}}, \dot{\mathbf{v}}$ and $\mathbf{v}$ defined analogously. Define $\mathbf{B} = \left(\begin{smallmatrix} \mathbf{0} & \mathbf{A} \\ \mathbf{I}_N & \mathbf{0} \end{smallmatrix}\right)$ then the stability of the origin depends on the eigenvalues of $\mathbf{B}$ [3, 49], specifically if $\lambda \in \sigma(\mathbf{B})$ then:

1. If there exists a λ such that $\mathrm{Re}(\lambda) > 0$, the origin is unstable.

2. If for all λ, $\mathrm{Re}(\lambda) < 0$, the origin is asymptotically stable.

Theorem 3.1. *The system 3.2 is unstable unless the matrix $A_{ij} = \frac{\partial f_i}{\partial x_j}$ is negative definite or equivalently all of the eigenvalues of A_{ij} are negative.*

Proof. If $\mathbf{C}_{11}^{-1}$ exists the determinant of a block matrix $\left(\begin{smallmatrix} \mathbf{C}_{11} & \mathbf{C}_{12} \\ \mathbf{C}_{21} & \mathbf{C}_{22} \end{smallmatrix}\right)$ is [46]

$$\det \begin{pmatrix} \mathbf{C}_{11} & \mathbf{C}_{12} \\ \mathbf{C}_{21} & \mathbf{C}_{22} \end{pmatrix} = \det(\mathbf{C}_{11}) \det\left(\mathbf{C}_{22} - \mathbf{C}_{12}\mathbf{C}_{11}^{-1}\mathbf{C}_{21}\right). \tag{3.6}$$

The eigenvalues of a matrix $\mathbf{B}$ are the roots of the characteristic polynomial $\det(\mu\mathbf{I} - \mathbf{B})$. Applied to (3.5) i.e to a matrix $\mathbf{B} = \left(\begin{smallmatrix} \mathbf{0} & \mathbf{A} \\ \mathbf{I}_N & \mathbf{0} \end{smallmatrix}\right)$, formula (3.6) gives

$$\begin{aligned} \det(\mu\mathbf{I}_{2N} - \mathbf{B}) &= \det(\mu\mathbf{I}_N) \det\left(\mu\mathbf{I}_N - \mathbf{I}_N (\mu\mathbf{I}_N)^{-1} \mathbf{A}\right) \\ &= \mu \det(\mathbf{I}_N) \det\left(\mu\mathbf{I}_N - \mathbf{A}(\mu)^{-1}\right) \\ &= \det\left(\mu^2\mathbf{I}_N - \mathbf{A}\right). \end{aligned}$$

We find therefore that the set of eigenvalues of $\mathbf{B}$, denoted $\sigma(\mathbf{B})$ consists of the positive and negative square roots of the eigenvalues of $\mathbf{A}$. That is if for all $i = 1 \ldots N$, $\lambda_i \in \sigma(\mathbf{A})$ then

$$\sigma(\mathbf{B}) = \left\{ \sqrt{\lambda_1}, \ldots, \sqrt{\lambda_N}, -\sqrt{\lambda_1}, \ldots, -\sqrt{\lambda_N} \right\}. \tag{3.7}$$

Recall that if a single eigenvalue has a positive real part then the origin is unstable. If $\lambda = re^{i\theta}$ is an eigenvalue of $\mathbf{A}$ then $\mu = \pm r^{1/2} e^{i\theta/2}$ are eigenvalues of $\mathbf{B}$, the real parts are therefore $\mathrm{Re}(\mu) = \pm r^{1/2} \cos\frac{\theta}{2}$. Clearly because the positive and negative square roots are both eigenvalues one of the pair will have a positive real part unless $\cos\frac{\theta}{2} = 0$ [a]. In this case $\theta = \pi$ and $\lambda = -r$; all of the eigenvalues of $\mathbf{A}$ are real and negative or the system is unstable. □

Because the system is unstable, unless all of the eigenvalues of $\mathbf{B}$ have zero real-part, an immediate corollary of the above is that (3.2) cannot be asymptotically stable at the origin.

The requirement that $\frac{\partial f_i^0}{\partial x_j}$ be negative definite can be interpreted physically as follows. For small perturbations

$$\ddot{x}_i \approx \frac{\partial f_i^0}{\partial x_j} x_j.$$

If $\frac{\partial f_i^0}{\partial x_j}$ is negative definite then, by the definition of negative definiteness,

$$0 \geq x_i \frac{\partial f_i^0}{\partial x_j} x_j = x_i \ddot{x}_i. \tag{3.8}$$

Therefore, a necessary condition for stability is that for small displacements the projection of the acceleration vector on the displacement vector is negative. Acceleration must not act to reinforce the displacement.

Example 3.2 (Pendulum)**.** The equation of motion of a pendulum is

$$\ddot{x} = -\sin(x). \tag{3.9}$$

[a] We exclude the possibility that $r = 0$ on the grounds that a zero valued eigenvalue implies a singular matrix.

The pendulum is in an equilibrium position when the weight hangs directly below the support ($x = 0$) or directly above ($x = \pi$). For example by linearising (3.9) about the stable equilibrium $x = 0$ and writing as a system of first-order equations find;

$$\begin{pmatrix} \dot{v} \\ v \end{pmatrix} = \begin{pmatrix} 0 & -1 \\ 1 & 0 \end{pmatrix} \begin{pmatrix} \dot{x} \\ x \end{pmatrix}. \tag{3.10}$$

In the notation of (3.5), $\mathbf{I} = 1$ and $\mathbf{A} = -1$ is negative definite. Conversely linearising about the equilibrium $x = \pi$ has $\mathbf{A} = 1$ which is obviously positive definite and hence unstable.

2.2 Lyapunov stability analysis

The definitions and theorems in this section are taken from [65], restated to remove unnecessary generality [b]. The full statements can be found there as well as proofs of the theorems.

Definition 3.3 (Dynamical system)**.** A dynamical system is defined by mapping $\mathbf{x} = \mathbf{x}(t, \mathbf{x}_0)$ where $\mathbf{x}_0 \in A \subset \mathbb{R}^n$ is the initial condition drawn from a set of initial conditions A and $t \geq 0$. For a particular initial condition $\mathbf{x}_0$ then $\mathbf{x}(t, \mathbf{x}_0)$ is called a *motion* of the system. The *family of motions* is the set S of all motions produced by all $\mathbf{x}_0 \in A$.

Definition 3.4 (Invariant set)**.** If $\mathbf{x}_0 \in X \subset A$ implies that $\mathbf{x}(t, \mathbf{x}_0) \in X$ for all $t \geq 0$. Then X is an *invariant set*. In particular an *equilibrium point* is an invariant set consisting of the single point $\mathbf{x}_e$.

An important example of an invariant set of a conservative system is $\{\mathbf{x} : H(\mathbf{x}) \leq c\}$, where H is the Hamiltonian and c is some scalar constant.

Definition 3.5 (Stability)**.** An equilibrium point, $\mathbf{x}_e$, of a dynamical system is stable if for all $\epsilon > 0$ there exists a $\delta(\epsilon) > 0$ such that $|\mathbf{x}(t) - \mathbf{x}_e| < \epsilon$ when $|\mathbf{x}(0) - \mathbf{x}_e| < \delta$.

[b] For example here we assume that $t_0 = 0$ and that the state space of the motion is $\mathbb{R}^n$ with the usual Euclidean norm rather than some general metric space.

Below, if something is said to be stable it is to this definition of stability that we refer.

Theorem 3.6 (Lyapunov's Theorem [65])**.** *Assume without loss of generality that* $\mathbf{x}_e = \mathbf{0}$*. Given a function* $v : \Omega_r \to \mathbb{R}$*, where* $\Omega_r = \{\mathbf{x} : |x| < r\}$*. If for all* $\mathbf{x} \in \Omega_r$*, where* r *is arbitrarily small,*

1. $v(\mathbf{0}) = 0$,
2. $v(\mathbf{x}) > 0$ *if* $\mathbf{x} \neq \mathbf{0}$,
3. $\dot{v}(\mathbf{x}) \leq 0$.

Then the equilibrium, $\mathbf{x}_e$*, is stable. The function* $v(\mathbf{x})$ *is called a Lyapunov function.*

Example 3.7 (Conservative System)**.** A second-order ODE of the form

$$\ddot{x}_i = f_i(\mathbf{x}) \tag{3.11}$$

defines a dynamical system. Assume that $f_i(\mathbf{0}) = 0$ so that $\mathbf{x} = \dot{\mathbf{x}} = 0$ is an equilibrium and that there exists a function $U(\mathbf{x})$ such that $f_i = -\frac{\partial U}{\partial x_i}$. For such a system the energy $H = \frac{1}{2}\dot{\mathbf{x}} \cdot \dot{\mathbf{x}} + U(\mathbf{x})$ is conserved by the motion of (3.11), i.e. $\dot{H} = \dot{\mathbf{x}} \cdot \ddot{\mathbf{x}} - \nabla U \cdot \dot{\mathbf{x}} = 0$ because $\ddot{x}_i = -\frac{\partial U}{\partial x_i}$. To investigate the stability of (3.11) it suffices to define a Lyapunov function $V(\mathbf{x}, \dot{\mathbf{x}}) = H|_{\Omega_r} - H_0$ i.e. V is equal to the energy, restricted to a neighbourhood of the origin, minus the energy present in the equilibrium position. Furthermore assume $U(\mathbf{0})$ is a local minimum of the potential so that $U(\mathbf{x}) > U(0)$ for all $\mathbf{x} \in \Omega_r$. Referring to the three conditions in 3.6 it is clear that V satisfies all the criteria and therefore the origin is stable.

This example shows how a common criteria for stability, that the potential energy have a local minimum [64], can be derived from Lyapunov's theorem. The potential energy actually has a local minimum at $\mathbf{x} = \mathbf{0}$ if

1. $\left.\frac{\partial U}{\partial x_i}\right|_{\mathbf{x}=\mathbf{0}} = 0$ for all $i = 1 \ldots N$.
2. $A_{ij} = \left.\frac{\partial U}{\partial x_i x_j}\right|_{\mathbf{x}=\mathbf{0}}$ is positive definite.

Referring back to the previous section; if $f_i = -\frac{\partial U}{\partial x_i}$ then the first item is simply the requirement that $\mathbf{x} = \mathbf{0}$ is actually an equilibrium. Recall that in the previous section it was proved that unless $\frac{\partial f_i}{\partial x_j}^0$ is negative definite the equilibrium will be unstable. As $A_{ij} = \frac{\partial U}{\partial x_i x_j} = -\frac{\partial f_i}{\partial x_j}^0$ it is possible to say that for a conservative system the negative definiteness of $\frac{\partial f_i}{\partial x_j}^0$, or equivalently the positive definiteness of A_{ij}, is a necessary and sufficient condition for stability of the equilibrium point.

Theorem 3.8. *The dynamical system* (3.2) *is conservative if and only if* $\frac{\partial f_i}{\partial x_j} = \frac{\partial f_j}{\partial x_i}$, *where* $f_i(\mathbf{x}) = m\ddot{x}_i$.

Proof. see Appendix 2.2 □

This theorem introduces the so-called integrability condition [52]. We show in the next example that a particular, standard, set of SPH equations, a discretisation of (3.18), are not integrable. Thereby showing that conservation of energy in SPH cannot be assumed.

Example 3.9 (Integrability of SPH equtions)**.** We transform the PDE (3.18) into the ODE:

$$\ddot{u}_i = \frac{1}{\rho} \sum_{j \in N(i)} (\sigma_i + \sigma_j) W'_{ij} \tag{3.12a}$$

$$\sigma_i = E \sum_{j \in N(i)} (u_j - u_i) W'_{ij}. \tag{3.12b}$$

Note the acceleration $\ddot{u}_i = f_i(\mathbf{u})$ is a function of the particle displacements only. By theorem 3.8 equation (3.12) is integrable if, and only if, $\frac{\partial f_i}{\partial u_k} = \frac{\partial f_k}{\partial u_i}$. To proceed, the following formulae are needed: the derivative of the kernel gradient

$$\frac{\partial W_{mj}}{\partial u_p} = W'_{mj} (\delta_{mp} - \delta_{jp}).$$

The stress

$$\begin{aligned} \frac{1}{E} \frac{\partial \sigma_m}{\partial u_p} &= \sum_{j \in N(m)} (\delta_{jp} - \delta_{mp}) W'_{mj} + (u_j - u_m)(\delta_{jp} - \delta_{mp}) W''_{mj} \\ &= W'_{mp} + (u_p - u_m) W''_{mp} - \delta_{mp} \left[\sum_{j \in N(m)} W'_{mj} + (u_j - u_m) W''_{mj}, \right. \end{aligned} \tag{3.13}$$

and finally the acceleration, note that it is assumed that $i \neq p$ as $\frac{\partial f_i}{\partial u_i} = \frac{\partial f_i}{\partial u_i}$.

$$\begin{aligned}\rho\frac{\partial f_i}{\partial u_p} &= \sum_{j\in N(i)}\left(\frac{\partial \sigma_i}{\partial u_p}+\frac{\partial \sigma_j}{\partial u_p}\right)W'_{ij}+\sum_{j\in N(i)}\left(\sigma_i+\sigma_j\right)W''_{ij}\left(\delta_{ip}-\delta_{jp}\right)\\ &= \sum_{j\in N(i)}\left(\frac{\partial \sigma_i}{\partial u_p}+\frac{\partial \sigma_j}{\partial u_p}\right)W'_{ij}-\left(\sigma_i+\sigma_p\right)W''_{ip}. \end{aligned} \tag{3.14}$$

The second term on the RHS of (3.14) is symmetric with respect to i and p due to the symmetry of W''_{ij}. The integrability criterion is therefore satisfied if the first term is also symmetric. Define the anti-symmetric function $G_{ij} = W_{ij} + (u_j - u_i)\, W''_{ij}$ substitute (3.13) into (3.14) rearrange and find,

$$\begin{aligned}\sum_{j\in N(i)}\left(\frac{\partial \sigma_i}{\partial u_p}+\frac{\partial \sigma_j}{\partial u_p}\right)W'_{ij} &= \sum_{j\in N(i)} W'_{ij}\left[W'_{ip}+\left(u_p-u_i\right)W''_{ip}+W'_{jp}+\left(u_p-u_j\right)W''_{jp}\right]\\ &\qquad -\sum_{j\in N(i)} W'_{ij}\delta_{jp}\left[\sum_{m\in N(j)} W'_{jm}+\left(u_m-u_j\right)W''_{jm}\right]\\ &= \sum_{j\in N(i)} W'_{ij}\left(G_{ip}+G_{jp}\right)-\sum_{m\in N(p)} W'_{ip}G_{pm}\\ &= \sum_{j=1}^{N}\left[W'_{ij}\left(G_{ip}+G_{jp}\right)-W'_{ip}G_{pj}\right], \end{aligned} \tag{3.15}$$

in the last line the dummy index m is changed to j and the summation is taken over the whole range. This makes no difference to the value of the sum as the truncated sum over the neighbour particles is designed to exclude particles that give no contribution to the total. To see that (3.15) is not symmetric imagine that a single particle $m \in N(p) \backslash N(i)$ [c] is displaced and all other particles are unmoved. Consequently $G_{ij} = W'_{ij}$ for all $j \neq m$ and $\sum_m W'_{im}(0) = 0$. Therefore (3.15) becomes

$$\sum_{j=1}^{N} W'_{ij}G_{jp} - W'_{ip}\sum_{j=1}^{N} G_{pm} = \sum_{j=1}^{N} W'_{ij}W'_{jp} - W'_{ip}\sum_{j=1}^{N} W'_{pj} - W'_{ip}u_m W''_{pm}. \tag{3.16}$$

In the first sum on the RHS the only non-zero terms are where j is in the neighbourhood of i and p, hence the substitution of W'_{jp} for G_{jp}. The corresponding term from $\frac{\partial f_k}{\partial u_i}$,

[c] m is in the neighbourhood of p but not in the neighbourhood of i.

formed by interchanging i and p in (3.15), is

$$\begin{aligned}\sum_{j=1}^{N}\left[W'_{pj}\left(G_{pi}+G_{ji}\right)+W'_{pi}G_{ij}\right] =& W'_{pi}\sum_{j=1}^{N}W'_{pj}+\sum_{j=1}^{N}W'_{pj}W'_{ji}\\ =& -W'_{ip}\sum_{j=1}^{N}W'_{pj}+\sum_{j=1}^{N}W'_{ij}W'_{jp} \quad \text{(because } W'_{ij}=-W'_{ji}\text{)}.\end{aligned} \tag{3.17}$$

Equations (3.17) and (3.16) are not identical due to the term $-W'_{ip}u_mW''_{pm}$ and therefore (3.12) are not integrable and the system defined does not conserve energy.

3 Equations of motion

3.1 Problem specification

For the propagation of longitudinal waves in an elastic rod the equations of linear elasticity reduce to [53]

$$\begin{aligned}\rho u_{tt} =& \sigma_x\\ \sigma =& Eu_x.\end{aligned} \tag{3.18}$$

Where E is Young's modulus and ρ is the rod's density. Equations (3.18) can be re-stated as a single, second-order PDE,

$$u_{tt}=c^2u_{xx}, \tag{3.19}$$

i.e. the scalar wave equation with wave speed $c=\sqrt{\frac{E}{\rho}}$. We will consider (3.19) on an interval $I=[a,b]$ with boundary condition $u\left(a\right)=u\left(b\right)=u_x\left(a\right)=u_x\left(b\right)=0$.

If we multiply (3.19) by u_t and integrate over I then,

$$\begin{aligned}\frac{1}{c^2}\int_I u_{tt}u_t\mathrm{d}x =& \int_I u_{xx}u_t\mathrm{d}x\\ =& \left[u_xu_t\right]_a^b-\int_I u_xu_{tx}\mathrm{d}x.\end{aligned} \tag{3.20}$$

The second line follows by integration by parts and the boundary conditions dictate that the first term is equal to zero. Equation (3.20) can therefore be rewritten in the form

$$\frac{\mathrm{d}}{\mathrm{d}t}\left[\int_I (u_t)^2 + c^2 (u_x)^2 \,\mathrm{d}x\right] = 0. \tag{3.21}$$

The term within the square brackets is conserved; the first term is the kinetic energy and the second the strain or potential energy. Therefore the PDE (3.19) defines a conservative system. When discretising the equation using SPH if the resulting ODE also defines a conservative system then the total energy is a natural candidate for a Lyapunov function.

3.2 Discretisation

The solution of the PDE is a function $u = u(x,t)$. It exists in two dimensions x and t. The phase space is infinite dimensional; u has a value at each of the infinite points in the interval I. After discretisation the system is an ODE; the solution is a vector-valued function of a single variable $x_i = x_i(t)$ for $i = 1$ to N and its phase space is $2N$-dimensional[d]. Therefore in the ODE these N functions of time play the same role as the $u = u(x,t)$ does in the PDE. Confusion can arise by the change in role of the letter x from an independent variable to denoting (albeit with the addition of an index) the solution. In the ODE the role of x is taken by the the index set $\{1, \ldots N\}$ i.e. space has been discretised.

We discretise (3.19) as follows. The continuous interval $I = [a,b]$ is represented by N evenly-spaced particles labelled left to right from 1 to N. The position of the i^{th} particle is x_i and its displacement is $u_i = x_i - x_i^0$. Each x_i and u_i can be seen as the i^{th} component of vectors $\mathbf{x}$ and $\mathbf{u}$, respectively. Similarly for the velocity $\dot{u}_i$ and $\dot{\mathbf{u}}$. To represent the boundary conditions sufficient particles are assumed to exist outside of the domain so that all particles initially have a complete set of neighbours. These boundary particles are fixed in their initial position for all $t \geq 0$.

[d] $2N$ rather than N because each $\dot{x}_i$ is an element of the phase space.

The different meanings of the operators $\frac{\partial}{\partial x}$ and $\frac{\partial}{\partial x_i}$ should be noted. The former appears in the PDE and is approximated using SPH, this is denoted by angled brackets so that the approximation of the x-derivative of the displacement field at the location of the particle i is $\langle u_x \rangle_i$. The approximation is a function of the particle positions $\{x_i\}_{i=1}^N$ and it is legitimate therefore to calculate $\frac{\partial}{\partial x_i} \langle u_x \rangle_i$, but $\frac{\partial}{\partial x} \langle u_x \rangle_i = 0$ because $\langle u_x \rangle_i$ is not a function of x.

Below we prefer to write the discretised equations in terms of the particles' displacement so that the equilibrium is at $\mathbf{u} = \mathbf{0}$. This simply represents a shift in the origin of the coordinate system. We have $u_i = x_i - x_i^0$ so $\frac{\partial u_i}{\partial x_j} = \delta_{ij}$ and

$$\frac{\partial}{\partial u_i} g(\mathbf{u}) = \frac{\partial}{\partial u_i} g(\mathbf{u}(\mathbf{x})) = \frac{\partial}{\partial x_j} g(\mathbf{x}) \frac{\partial x_j}{\partial u_i} = \frac{\partial}{\partial x_i} g(\mathbf{x}).$$

Therefore $\frac{\partial}{\partial x_i}$ and $\frac{\partial}{\partial u_i}$ are equivalent. Strictly a different symbol should be used for functions of different variables e.g. $W_{ij} = W(x_i, x_j) = M(u_i, u_j)$ but standard notation (i.e. W_{ij} for the kernel function) will be retined below as this is certainly clearer so long as it is remembered that henceforth it is to be taken as a function of $\mathbf{u}$ instead of $\mathbf{x}$.

3.3 Derivation of conservative equations of motion

Example 3.9 demonstrated that SPH is not in general conservative. However it is possible to derive conservative equations by defining a potential energy function U and deriving the forces f_k via the formula $f_k = -\frac{\partial U}{\partial u_k}$. This will by construction conserve energy and, if additionally U is invariant with respect to translation i.e. $U(\mathbf{x}) = U(\mathbf{x} + \mathbf{s})$, linear momentum is conserved by Noether's theorem [4] [e].

By analogy with (3.21) define the function

$$U(\mathbf{u}) = \frac{c^2}{2} \sum_{i=1}^{N} (\langle u_x \rangle_i + T)^2 . \tag{3.22}$$

[e] This is of course only true if there are no external forces. If zero displacement boundary conditions are enforced then, as this in effect introduces an external force, momentum will not actually be conserved.

The function $\langle u_x \rangle_i$ is the approximation of the spatial derivative of the displacement at the position occupied by particle i. The constant T has been added to admit the possibility that the bar is pre-stressed. This is an ad-hoc addition but it can be justified as follows. Comparison with (3.21) would have the whole term $g_i(\mathbf{u}) = \langle u_x \rangle_i + T$ as the "real" approximation of u_x. Assuming that $\langle u_x \rangle|_{\mathbf{u}=\mathbf{0}} = 0$ for all i then $g_i(\mathbf{0}) = T$, i.e. a constant displacement gradient or, equivalently, a uniform expansion of contraction. It is as if before $t = 0$ all particles, including any boundary particles, were displaced by a factor of Tx_i resulting in a certain tension (or compression). Recall that the particle displacement is defined as $u_i = x_i - x_i(0)$, that is with respect to the particle positions at $t = 0$, so the "pre-history" is relevant only as a justification for the addition of a constant in to (3.22).

Given U as given in (3.22) define $f_k = -\frac{\partial U}{\partial u_k}$ then

$$f_k = -c^2 \sum_{i=1}^{N} \left(\langle u_x \rangle_i + T \right) \frac{\partial}{\partial u_k} \langle u_x \rangle_i \,. \tag{3.23}$$

The total energy is

$$H = \frac{1}{2} \sum_{i=1}^{N} \left(v_i^2 + c^2 \left(\langle u_x \rangle_i + T \right)^2 \right). \tag{3.24}$$

This is conserved because

$$\begin{aligned} \dot{H} =& \sum_{i=1}^{N} v_i \dot{v}_i + c^2 \sum_{k=1}^{N} \left[\sum_{i=1}^{N} \left(\langle u_x \rangle_i + T \right) \frac{\partial}{\partial u_k} \langle u_x \rangle_i \right] v_k \\ =& \sum_{k=1}^{N} \left(v_k \dot{v}_k - f_k v_k \right) = 0 \end{aligned} \tag{3.25}$$

as required.

It is not strictly necessary for the stability analysis but we will now calculate the exact form of f_k to compare with conventional formulae. The form of $\langle u_x \rangle_i$ is all important to the final form of the approximation, a choice must be made and we take

$$\langle u_x \rangle_i = \sum_{j \in N(i)} \left(u_i - u_j \right) W'_{ij}. \tag{3.26}$$

The particle volume $V_i = \frac{m_i}{\rho_i}$ is taken to be constant because the mass of each particle is choosen to be equal to m and in line with the assumptions of linear elasticity the density

is also assumed to be a constant $\rho = 1$. Therefore the particle volume term is subsumed within the kernel. Define $W'_{ij} = \frac{\partial W_{ij}}{\partial u_i}$ so that

$$\frac{\partial W_{ij}}{\partial u_k} = W'_{ij}\left(\delta_{ik} - \delta_{jk}\right),$$

this simply expresses the anti-symmetry of the derivative of the kernel and its dependence on u_i and u_j, i.e. W_{ij} is not a function of u_k unless $k = i$ or j. This correctly evaluates the gradient of a constant displacement and is therefore invariant under uniform translation and the equations of motion derived conserve momentum.

Define $\left\langle u_x^T \right\rangle_i = \left\langle u_x \right\rangle_i + T$ then, by equation (3.23),

$$f_k = -c^2 \sum_{i=1}^{N} \left\langle u_x^T \right\rangle_i \sum_{j=1}^{N} \frac{\partial}{\partial u_k} \left[\left(u_j - u_i\right) W'_{ij}\right].$$

Apply the chain rule

$$f_k = -c^2 \sum_{i=1}^{N} \left\langle u_x^T \right\rangle_i \sum_{j=1}^{N} \left[\left(\delta_{jk} - \delta_{ik}\right) W'_{ij} + \left(u_j - u_i\right) W''_{ij}\left(\delta_{ik} - \delta_{jk}\right)\right].$$

By the the property of the Kroneker delta symbol, i.e. $\sum_m \delta_{mp} u_m = u_p$ and changing the order of summation,

$$\begin{aligned}
f_k =& -c^2 \sum_{i=1}^{N} \left\langle u_x^T \right\rangle_i \left[W'_{ik} - \delta_{ik} \sum_{j=1}^{N} W'_{ij} + \delta_{ik} \sum_{j=1}^{N} \left(u_j - u_i\right) W''_{ij} - \left(u_k - u_i\right) W''_{ik}\right], \\
=& -c^2 \left\{ \sum_{i=1}^{N} \left\langle u_x^T \right\rangle_i \left[W'_{ik} - \left(u_k - u_i\right) W''_{ik}\right] + \sum_{i=1}^{N} \sum_{j=1}^{N} \left\langle u_x^T \right\rangle_i \left[-\delta_{ik} W'_{ij} + \delta_{ik}\left(u_j - u_k\right) W''_{ij}\right] \right\}, \\
=& -c^2 \left\{ \sum_{i=1}^{N} \left\langle u_x^T \right\rangle_i \left[-W'_{ki} + \left(u_i - u_k\right) W''_{ki}\right] + \sum_{j=1}^{N} \left\langle u_x^T \right\rangle_k \left[-W'_{kj} + \left(u_j - u_k\right) W''_{kj}\right] \right\}.
\end{aligned}$$

Next using the facts that $W'_{mp} = -W'_{pm}$ and $W''_{mp} = W''_{pm}$,

$$f_k = c^2 \left\{ \sum_{i=1}^{N} \left\langle u_x^T \right\rangle_i \left[W'_{ki} + \left(u_k - u_i\right) W''_{ki}\right] + \sum_{i=1}^{N} \left\langle u_x^T \right\rangle_k \left[W'_{ki} + \left(u_k - u_i\right) W''_{ki}\right] \right\}.$$

If we define the function $G_{ki} = W'_{ki} + \left(u_k - u_i\right) W''_{ki}$ the final formula for f_k is

$$f_k = c^2 \sum_{i \in N(k)} \left[\left\langle u_x^T \right\rangle_k + \left\langle u_x^T \right\rangle_i\right] G_{ki}. \tag{3.27}$$

Note that $G_{ki}\left(0\right) = W'_{ki}\left(0\right)$ and G_{mp} is anti-symmetric so that momentum is conserved locally as in standard SPH.

4 Stability of SPH

For a general system, whether derived from a potential or not, consider the equation for the force on particle i. Take

$$f_i = c^2 \sum_{j \in N(i)} S_{ij}(\alpha) H_{ij}. \tag{3.28}$$

The positive constant c^2 is irrelevent to the analysis and will henceforth be neglected. Define, $S_{ij}(\alpha) = \left\langle u_x^T \right\rangle_j + \alpha \left\langle u_x^T \right\rangle_i$ for various values of alpha this may correspond to,

1. The "plus" form: $S_{ij}(1) = \left\langle u_x^T \right\rangle_j + \left\langle u_x^T \right\rangle_i$,
2. The "minus" form: $S_{ij}(-1) = \left\langle u_x^T \right\rangle_j - \left\langle u_x^T \right\rangle_i$,
3. The uncorrected form: $S_{ij}(0) = \left\langle u_x^T \right\rangle_j$.

The function H_{ij} stands in for the derivative of the kernel function. It may be a basic kernel function, $H_{ij} = W'_{ij}$; or a corrected kernel, for example the Shepard function; or the modified kernel $H_{ij} = G_{ij} = W'_{ij} + (u_i - u_j) W''_{ij}$. Regardless we will assume that $\sum_{i \in N(j)} H^0_{ij} = 0$, because the particles are regularly distributed or the kernel is normalised. We must confirm that $\mathbf{u} = \mathbf{0}$ is an equilibrium by showing that $f_i(0) = 0$. The approximation of the displacement gradient, $\langle u_x \rangle$, is given by (3.31) and therefore $\langle u_x \rangle_i|_{\mathbf{u}=\mathbf{0}}$. For the "minus" form of the momentum equation (3.28) becomes

$$f_i = c^2 \sum_{j \in N(i)} (T - T)(\alpha) H^0_{ij} = 0$$

and for the "plus" and uncorrected forms we have, respectively

$$\begin{aligned} f_i =& c^2 T \sum_{j \in N(i)} (\alpha) H^0_{ij} = 0, \\ f_i =& 2c^2 T \sum_{j \in N(i)} (\alpha) H^0_{ij} = 0. \end{aligned}$$

Because $\sum_{i \in N(j)} H^0_{ij} = 0$.

In example 3.7 it was shown that the gradient $\frac{\partial f_i^0}{\partial u_k}$ characterises the stability of the equilibrium. To summarise, for a non-conservative function if $-\frac{\partial f_i^0}{\partial u_k}$ is not positive definite the system is unstable. In addition if f_i can be derived form a potential, i.e. the system conserves energy, and if $-\frac{\partial f_i^0}{\partial u_k}$ is positive definite the equilibrium is stable.

$$\frac{\partial f_i^0}{\partial u_k} = \sum_{j\in N(i)} \frac{\partial S_{ij}^0}{\partial u_k} H_{ij}^0 + \sum_{j\in N(i)} S_{ij}^0 \frac{\partial H_{ij}^0}{\partial u_m}. \tag{3.29}$$

Taking the first term we find

$$\begin{aligned} \sum_{j\in N(i)} \frac{\partial S_{ij}^0(\alpha)}{\partial u_k} H_{ij}^0 &= \sum_{j\in N(i)} \frac{\partial}{\partial u_k}(\langle u_x\rangle_j + T)\, H_{ij} + \alpha \frac{\partial}{\partial u_k}(\langle u_x\rangle_i + T) \sum_{j\in N(i)} H_{ij}^0 \\ &= \sum_{j\in N(i)} \frac{\partial}{\partial u_k} \langle u_x\rangle_j \, H_{ij}^0. \end{aligned} \tag{3.30}$$

All the other terms ar equal to zero because $\sum_{i\in N(j)} H_{ij}^0 = 0$ and $\frac{\partial T}{\partial u_k} = 0$. Differentiating

$$\langle u_x\rangle_j = \sum_{m\in N(j)} (u_m - u_j) K_{mj}, \tag{3.31}$$

where K_{mj} is the kernel,[f] equation (3.29) becomes,

$$\begin{aligned} \sum_{j\in N(i)} \frac{\partial}{\partial u_k} \langle u_x\rangle_j \, H_{ij}^0 &= \sum_{j\in N(i)} H_{ij}^0 \sum_{m\in N(j)} \frac{\partial}{\partial u_k} \left[(u_m - u_j) K_{jm}\right] \\ &= \sum_{j\in N(i)} H_{ij}^0 \left[\sum_{m\in N(j)} (\delta_{mk} - \delta_{jk}) K_{jm}^0 + \sum_{m\in N(j)} (u_m - u_j) \frac{\partial K_{jm}^0}{\partial u_k} \right] \\ &= \sum_{j\in N(i)} H_{ij}^0 \left[K_{jk}^0 - \delta_{jk} \sum_{m\in N(j)} K_{jm}^0 + 0 \right] = \sum_{j\in N(i)} H_{ij}^0 K_{jk}^0. \end{aligned} \tag{3.32}$$

We assume that $\sum_{i\in N(j)} K_{ij}^0 = 0$ and use $\frac{\partial u_i}{\partial u_j} = \delta_{ij}$.

If, as is usually be the case, $H_{ij}^0 = K_{ij}^0 = -H_{ji}^0$ then $\sum_{j\in N(i)} H_{ij}^0 H_{kj}^0$ is negative definite:

Proof.

$$u_i H_{ij}^0 H_{jk}^0 u_k = -H_{ji}^0 u_i H_{jk}^0 u_k = z_j z_j > 0 \qquad \text{(where } z_j = H_{jk}^0 u_k\text{)}.$$

Where summation over repeated indicies is implied. □

[f] Usually $K_{ij} = H_{ij}$ but, as in the conservative equations derived above where $K_{ij} = W'_{ij}$ and $H_{ij} = W'_{ij} + (u_i - u_j)\, W''_{ij}$, for the sake of generality we consider that they may differ. Note however that $W'_{ij} + (u_i - u_j)\, W''_{ij}\big|_{\mathbf{u}=\mathbf{0}} = W'_{ij}\big|_{\mathbf{u}=\mathbf{0}}$ so that at the equilibrium the different kernel functions coincide.

Unlike the first term, the second term in equation (3.29) depends on α:

$$\sum_{j\in N(i)} S^0_{ij}(\alpha)\frac{\partial H^0_{ij}}{\partial u_k} = S^0_{ij}(\alpha)\frac{\partial}{\partial u_k}\sum_{j\in N(i)} H_{ij}\bigg|_{\mathbf{u=0}}. \tag{3.33}$$

If $\alpha = -1$, the "minus" form, $S^0_{ij}(-1) = T - T = 0$ then (3.33) is equal to zero. Equally if the kernel is normalised, for example the Shepard function, then $\sum_{i\in N(j)} H_{ij} \equiv 0$ and (3.33) will again be equal to zero. This result should be expected because by using $S^0(-1)$ or a normalised kernel the approximation of the divergence of a constant stress field is exactly correct so that the addition of a constant tension T to the approximation has no effect. In contrast if $\alpha = 0$ or 1 then equation (3.33) is

$$\sum_{j\in N(i)} S^0_{ij}(0)\frac{\partial H^0_{ij}}{\partial u_k} = T\sum_{j\in N(i)}\frac{\partial H^0_{ij}}{\partial u_k} \tag{3.34a}$$

or

$$\sum_{j\in N(i)} S^0_{ij}(-1)\frac{\partial H^0_{ij}}{\partial u_k} = 2T\sum_{j\in N(i)}\frac{\partial H^0_{ij}}{\partial u_k} \tag{3.34b}$$

respectively.

When (3.33) is not identically zero it is always possible to choose a value of T such that $-\frac{\partial f_i}{\partial u_k}$ is not positive definite.

Proof. The diagonal entries of a positive definite matrix must be positive (see Appendix A § 2.1 page 148). In particular the origin will be unstable if for any $i = 1 \dots N$

$$-\frac{\partial f_i}{\partial u_i} = B_{ii} + TC_{ii} < 0.$$

Therefore if $C_{ii} > 0$ choose $T > B_{ii}/C_{ii}$ or if $C_{ii} < 0$ choose $T < B_{ii}/C_{ii}$. □

First we consider the case when $H_{ij} = W'_{ij}$, we have

$$\frac{\partial W'_{ij}}{\partial u_k} = W''_{ij}\left(\delta_{ik} - \delta_{jk}\right). \tag{3.35}$$

Therefore

$$\sum_{j\in N(i)} \frac{\partial W'_{ij}}{\partial u_k}\bigg|_{\mathbf{u=0}} = \sum_{j\in N(i)} W''_{ij}(0)\left(\delta_{ik} - \delta_{jk}\right) = -W''^0_{ik} + \delta_{ik}\sum_{j\in N(i)} W''^0_{ij}. \tag{3.36}$$

For the conservative version of SPH derived above $H_{ij} = W'_{ij} + (u_i - u_j)\, W''_{ij}$, and

$$\sum_{j\in N(i)} \frac{\partial}{\partial u_k} \left(W'_{ij} + (u_i - u_j)\, W''_{ij}\right)\Big|_{\mathbf{u}=\mathbf{0}} = -\, W''^0_{ik} + \delta_{ik} \sum_{j\in N(i)} W''^0_{ij} + \sum_{j\in N(i)} (\delta_{ik} - \delta_{jk})\, W'''^0_{ij}$$
$$= -\, 2W''^0_{ik} + 2\delta_{ik} \sum_{j\in N(i)} W''^0_{ij}. \tag{3.37}$$

Define $A_{ik} = -\frac{\partial f_i}{\partial u_k}$, combining the results from above we find:

The "minus" form: $\alpha = -1$. If the derivative of the kernel is anti-symmetric at the equilibrium i.e. if $H^0_{ik} = -H^0_{ki}$, then

$$A_{ik} = H^0_{ij} H^0_{kj} \tag{3.38}$$

is positive definite. Unfortunately, one cannot conclude that the system is stable based on the positive definiteness of A_{ik}, just that no necessary condition for stability has been found by linearisation.

Normalised kernel. Similar to the last case, if $H^0_{ik} = -H^0_{ki}$ then A_{ik} will be positive definite. Taking the Shepard function as an example, in general the anti-symmetry of the derivative does not hold, i.e.

$$\tilde{W}_{ij} = \frac{W_{ij}}{\sum_l W_{il}} \neq \frac{W_{ji}}{\sum_l W_{jl}} = \tilde{W}_{ji}. \tag{3.39}$$

But on a regular grid at $\mathbf{u} = \mathbf{0}$ then $\tilde{W}^0_{ik} = -\tilde{W}^0_{ki}$, and A_{ik} is positive definite. As above no conclusion can be reached as to the stability or otherwise of the equilibrium in this case, but the particular instability identified by Swegle does not appear.

The three remaining cases - the "plus" form, $\alpha = 1$; the uncorrected form, $\alpha = 0$; and the conservative form from equation (3.27) - can be treated together. In each case

$$A_{ik} = \sum_{j\in N(i)} W'^0_{ij} W'^0_{kj} - nT\delta_{ik} \sum_{j\in N(i)} W''^0_{ij} + nTW''^0_{ik} \tag{3.40}$$

where $n = 1, 2$ or 4 if the uncorrected, "plus", or conservative version, respectively, is considered.

It is possible to derive conditions for the kernel, dependent on T, to ensure that (3.40) is positive definite. For the energy conserving version of SPH derived above this proves that the equilibrium is stable. It is a fact of linear algebra that a linear combination of positive definite matrices $\sum_i a_i \mathbf{A}_i$ is positive definite if $a_i > 0$ for all i. A_{ik} is a linear combination of matrices. The first is positive definite as proved above. The second matrix in (3.40) is of the form $a\mathbf{I}$ where $\mathbf{I}$ is the identity matix and is therefore positive definite if $T \sum_{j \in N(i)} W''^0_{ij} > 0$. Finally for a particular kernel W''_{km} may be positive definite, negative definite or indeed neither. Using the following theorem for certain special cases however it can be shown that W''_{km} is negative definite.

Theorem 3.10 (Bochner [15])**.** *Given a real valued function $F(\mathbf{x})$ and a matrix $\mathbf{A}$ with components $A_{ij} = F(\mathbf{x}_i - \mathbf{x}_j)$, where for $k = 1 \ldots n$ each $\mathbf{x}_k \in X \subset \mathbb{R}^N$ is distinct. Then $\mathbf{A}$ is positive definite if the Fourier transform of F is positive.*

If the Fourier transform of a kernel function $W(r)$, where $r = \|\mathbf{r}\|_2$ has a positive Fourier transform $\tilde{W}(s)$, then the Fourier transform of $W''(r)$ is $-s^2\tilde{W}(s)$ which is negative definite by the original assumption. Therefore by theorem 3.10, the matrix with components $A_{ij} = W''(\|\mathbf{x}_i - \mathbf{x}_j\|)$ is negative definite. As stated in the introduction one class of kernel functions which have positive Fourier transforms are Wendland functions, see [15] and also appendix A § 1.

Taking all of the above (3.40) will definitely be positive definite if (but not only if) all of the following hold:

1. W_{km} is a Wendland function or another function with a positive Fourier transform (such as a Gaussian).

2. $T < 0$ so that $TW''_{km}(0)$ is positive definite.

3. $T \sum_m W''_{km}(0) < 0$ as $T < 0$ this means that $\sum_m W''_{km}(0) > 0$.

This result supports the idea that Wendland kernels, or kernels with positive definite fourier transforms, are inherently more stable in compression. If an energy conserving

form of SPH is being considered then the above list constitutes a sufficient condition for the origin to be stable. Another possibility is using a piecewise linear kernel (a "hat" funtion) then all second derivatives (except for W''_{ii}) are equal to zero, and only the first, positive definite, matrix in (3.40) remains. However this kernel is not generally used as derivatives are not approximated accurately.

It is now possible to derive necessary conditions for the stability of the equilibrium analagous to the classic Swegle [85] condition; $TW'' > 0$. By examining the principal minors (definition A.2) of (3.40) we can derive necessary conditions for stability. First we examine the diagonal elements, if any are negative then A_{ik} cannot be positive definite and the system must be unstable, note all functions should be understood to be taken at $\mathbf{u} = \mathbf{0}$. Therefore if

$$0 > A_{ii} = \sum_{j \in N(i)} W'_{ij} W'_{ij} - nT \sum_{j \in N(i)} W''_{ij} + nTW''_{ii} = \sum_{j \in N(i)} W'_{ij} W'_{ji} - nT \sum_{j \in N(i) \setminus \{i\}} W''_{ij}, \quad (3.41)$$

or

$$nT \sum_{j \in N(i) \setminus \{i\}} W''_{ij} > \sum_{j \in N(i)} W'_{ij} W'_{ij}, \quad (3.42)$$

the system is unstable. If we assume that the particles only interact with their nearest neighbours then (3.42) will be

$$nTW''_{i,i+1} > (W'_{i,i+1})^2. \quad (3.43)$$

Swegle criterion. Compare equation (3.43) with that derived by Swegle which in the notation of this chapter is $TW''_{i,i+1} > 0$. If we assume that $W''_{i,i+1} > 0$ then it may be seen that the new condition (3.43) admtis the possibilty that the equilibrium may remain stable under some degree of tension. The difference in the two conditions arises because in [85] the approximation of the displacement gradient is different, specifically

$$\left\langle u_x^T \right\rangle_i = T + \frac{K}{2} \left(u_{i+1} - u_{i-1} \right), \quad (3.44)$$

where K is the bulk modulus. Equation (3.44) is not how the displacement gradient is calculated in SPH and it may not be extended to higher dimensions as the more realistic

approximation used above. Nevertheless, if (3.44) is used in equation (3.29) with $\alpha = 0$ then we find

$$\begin{aligned}\frac{\partial f_i}{\partial u_k} =& \frac{K}{2}\sum_{j\in N(i)}\left(\delta_{j+1,k}-\delta_{j-1,k}\right)W'^0_{ij} + T\sum_{j\in N(i)}\frac{\partial W'^0_{ij}}{\partial u_k}\\ =& \frac{K}{2}\left(W^0_{i,k-1}-W'^0_{i,k+1}\right) + T\sum_{j\in N(i)}\frac{\partial W'^0_{ij}}{\partial u_k}.\end{aligned} \tag{3.45}$$

If the above is not negative definite the equilibrium will be unstable, in particular if a diagonal element is positive then instability is proved,

$$\frac{K}{2}\left(W'^0_{i,i-1}-W'^0_{i,i+1}\right) + 2T\sum_{j\in N(i)}W''^0_{i,i+1} = KW'_{i,i-1} + TW''_{i,i+1}. \tag{3.46}$$

The first term is always positive because the kernel, W_{ij}, is symmetric and positive, therefore if $TW''_{ik} > 0$ the equilibrium is unstable.

The condition (3.42) maybe refined somewhat by considering the determinant of the second principal minors. Recall that the second principal minor is a matrix extracted form a larger matrix by removing all but two rows and *their corresponding* columns i.e. if row i is removed so is column i. A second principal minor of A_{ik} is

$$A_{ii}A_{i+1,i+1} - A_{i,i+1}A_{i+1.i} = A^2_{ii} - A^2_{i,i+1} = (A_{ii}+A_{i,i+1})(A_{ii}-A_{i,i+1}). \tag{3.47}$$

Because A_{ij} is symmetric so $A_{i,i+1} = A_{i+1.i}$ and also because of the regular arrangement of particles all of the components on the same diagonal are equal - $A_{i,j} = A_{i+1,j+1}$ for all i and j. If one or other (not both) of the factors in (3.47) are negative then A_{ij} is not positive definite and the system is unstable. We can assume that $A_{ii} > 0$ lest the system be unstable by (3.42). If $A_{i,i+1} > 0$ then $A_{ii} + A_{i,i+1} > 0$ and if $A_{ii} - A_{i,i+1} = A_{ii} - |A_{i,i+1}| < 0$ the system is unstable. Similarly if $A_{i,i+1} < 0$ then $A_{ii} - A_{i,i+1} > 0$ and if $A_{ii} + A_{i,i+1} = A_{ii} - |A_{i,i+1}| < 0$ and the system is unstable. Therefore a more restrictive necessary condition for stability is;

$$\sum_{j\in N(i)} W'_{ij}W'_{ij} - nT\sum_{j\in N(i)\setminus\{i\}}W''_{ij} - \left|\sum_{j\in N(i)} W_{ij}W_{i+1,j} + nTW''_{i,i+1}\right| < 0 \tag{3.48}$$

or

$$nT\sum_{j\in N(i)\setminus\{i\}} W''_{ij} > \sum_{j\in N(i)} (W'_{ij})^2 - \left|\sum_{j\in N(i)} W_{ij}W_{i+1,j} + nTW''_{i,i+1}\right|. \tag{3.49}$$

It can be seen therefore that a system where (3.42) does not hold may still be unstable by (3.49). If the particles only interact will their nearest neighbours then (3.47) becomes

$$(2(W'_{i,i+1})^2 - 3nTW''_{i,i+1})(2(W'_{i,i+1})^2 - nTW''_{i,i+1}) < 0. \tag{3.50}$$

Because $\sum_{j\in N(i)} W_{ij}W_{i+1,j} = 0$ in this case as one or other of the factors in each sum is equal to zero. We may assume that the second bracket is positive because otherwise instability is established by the first condition. Therefore for the nearest neighbour case we have;

$$nTW''_{i,i+1} > \frac{2}{3}W'^2_{i,i+1}. \tag{3.51}$$

This is only a small improvement on (3.43). It is possible to continue looking at further principal minors to seek possible further refinement on the stability criterion (3.49) but a different approach is to investigate the positive definiteness of A_{ij} numerically. We do this by checking the positive definiteness[g] of (3.40) for increasing values of T for a range of smoothing lengths h. Figures 3.2c - d (page 110) plot the smallest value of T for a given h that the matrix in equation (3.40) stops being positive definite and consequently the equilibrium becomes unstable. For comparison in figures 3.2a - b give the value of T such that the first criterion derived above (3.42) implies instability of the system. Note that all of the plots in 3.2 were generated from equation (3.40) with $n = 4$, i.e. for the energy conserving form and the vertical axis should be scaled appropriately for other values of n. For example, if $n = 2$ then all values on the vertical axis should be multiplied by two. This also implies that the energy conserving version is less stable than the "plus" form which is in turn less stable than the uncorrected form. The conclusions to be drawn from the plots are:

- The analytically derived stability criterion (3.42) is an overestimate of the tension required to destabilise the system by a factor of approximately 100.

[g]This can be done by attempting a Cholesky factorisation of the matirix. If, and only if, it succeeds the matrix is positive definite [37].

- For context the magnitude of T required to induce instability is (recall from page 90 that T can be considered as an expansion factor) equal to that induced by the stretching of a bar with an initial length of 1.0000 unit to less than 1.0005 units.
- For the various kernel functions a more stable "sweet spot" exists when the smoothing length is between 1.2 to 2 times the minimum interparticle spacing, Δx. (A.20).
- The performance of the various kernel functions do not differ markedly.

4.1 Conservative SPH

We now consider the special case of the conservative equations. In particular we wish to derive conditions for the kernel function which lead to a stable equilibrium. The potential energy is

$$U(\mathbf{u}) = \frac{1}{2}\sum_{j=1}^{N}\left(\langle u_x\rangle_j + T\right)^2. \tag{3.22}$$

then $f_i = -\frac{\partial U}{\partial x_i}$ is

$$f_i = -\sum_{j=1}^{N}\left(\langle u_x\rangle_j + T\right)\frac{\partial}{\partial u_i}\langle u_x\rangle_j. \tag{3.52}$$

And for the Hessian $\frac{\partial^2 U}{\partial u_i \partial u_k} = -\frac{\partial f_i}{\partial u_k}$ we have

$$\frac{\partial^2 U}{\partial u_p \partial u_k} = \sum_{i=1}^{N}\frac{\partial}{\partial u_p}\langle u_x\rangle_i \frac{\partial}{\partial u_k}\langle u_x\rangle_i + \sum_{i=1}^{N}\left(\langle u_x\rangle_i + T\right)\frac{\partial^2}{\partial u_p \partial u_k}\langle u_x\rangle_i. \tag{3.53}$$

At $\mathbf{u} = \mathbf{0}$ (3.53) reduces to

$$\frac{\partial^2 U}{\partial u_p \partial u_k} = \sum_{i=1}^{N}\frac{\partial}{\partial u_p}\langle u_x\rangle_i^0 \frac{\partial}{\partial u_k}\langle u_x\rangle_i^0 + T\sum_{i=1}^{N}\frac{\partial^2}{\partial u_p \partial u_k}\langle u_x\rangle_i^0. \tag{3.54}$$

The first matrix on the RHS of (3.54) is positive definite because it is the product of a matrix with its transpose. Once again if the second matrix is not equal to zero then some value of T can always be found to make the system unstable. The previous section derived necessary conditions for stability for the case when this matrix is equal to zero, we now proceed to derive conditions on the kernel W_{ij} such the system will be stable regardless of T.

4.1.1 Stable kernel functions

Define a general form for $\langle u_x \rangle_i$;

$$\langle u_x \rangle_i = \sum_{j=1}^{N} (u_j - \alpha u_i) \tilde{W}'_{ij}. \tag{3.55}$$

The constant α is present for convenient exposition only and is either equal to 1 or 0 depending on whether the correction $(-u_i \sum_{j=1}^{N} \tilde{W}'_{ij})$ is appled or not. The tilde over the kernel $(\tilde{W})$ is there to indicate that the kernel function may have been modified or corrected in some as yet unspecified way. For example the Shepard function kernel;

$$\tilde{W}_{ij} = \frac{W_{ij}}{\sum\limits_{m \in N(i)} W_{im}}. \tag{3.56}$$

For $\mathbf{u} = \mathbf{0}$ to be an equilibrium (3.52) must hold;

$$f_k(\mathbf{0}) = -c^2 T \sum_{i=1}^{N} \frac{\partial}{\partial u_k} \langle u_x \rangle_i \Big|_{\mathbf{u}=\mathbf{0}} = 0. \tag{3.52}$$

To check this first calculate

$$\begin{aligned} \sum_{i=1}^{N} \frac{\partial}{\partial u_k} \langle u_x \rangle_i &= \sum_{i=1}^{N} \sum_{j=1}^{N} \frac{\partial}{\partial u_k} \left[(u_j - \alpha u_i) \tilde{W}'_{ij} \right] \\ &= \sum_{i=1}^{N} \sum_{j=1}^{N} (\delta_{jk} - \alpha \delta_{ik}) \tilde{W}'_{ij} + \sum_{i=1}^{N} \sum_{j=1}^{N} (u_j - \alpha u_i) \frac{\partial \tilde{W}'_{ij}}{\partial u_k}. \end{aligned} \tag{3.57}$$

At $\mathbf{u} = \mathbf{0}$ the second term is equal to zero and

$$\sum_{i=1}^{N} \frac{\partial}{\partial u_k} \langle u_x \rangle_i \Big|_{\mathbf{u}=\mathbf{0}} = \sum_{i=1}^{N} \tilde{W}'_{ik}(0) - \alpha \sum_{j=1}^{N} \tilde{W}'_{kj}(0) = \sum_{i=1}^{N} \left(\tilde{W}'_{ik}(0) - \alpha \tilde{W}'_{ki}(0) \right). \tag{3.58}$$

If $\tilde{W}'_{ij}(0) = \tilde{W}'_{ji}(0)$ and $\alpha = 1$ then (3.58) will clearly be equal to 0. Or, if $\tilde{W}_{ij}(0) = -\tilde{W}_{ji}(0)$ and the particles are arranged requlary[h] so that $\sum_{j=1}^{N} \tilde{W}'_{ij}(0) = 0$. For a normal, uncorrected, kernel the later case pertains. A symmetric kernel, and the consequent anti-symmetry of its derivative, is almost a rule of SPH. This symmetry may be broken however by the act of correcting. For example, in general

$$\frac{W_{ij}}{\sum_l W_{il}} \neq \frac{W_{ji}}{\sum_l W_{jl}}.$$

[h] A regular grid can be defined to be an arrangement of particles such that for all particles i and for all particles $j \in N(i)$ there exists a particle $k \in N(i)$ such that $(x_i - x_k) = -(x_i - x_j)$.

But given an initially regular arrangement of particles then, for some constant c, $\sum_{j=1}^{N} W_{ij}(0) = c$ for all i. Therefore

$$\frac{W_{ij}(0)}{\sum_l W_{il}(0)} = \frac{W_{ji}(0)}{\sum_l W_{jl}(0)}.$$

Assuming that an equilibrium exists calculate $\sum_{i=1}^{N} \frac{\partial}{\partial u_m \partial u_k} \langle u_x \rangle_i^0$. By differentiating (3.57) with respect to $\frac{\partial}{\partial u_m}$ find;

$$\sum_{i=1}^{N} \frac{\partial}{\partial u_m \partial u_k} \langle u_x \rangle_i = \sum_{i=1}^{N} \left(\frac{\partial \tilde{W}'_{ik}}{\partial u_m} - \alpha \frac{\partial \tilde{W}'_{ki}}{\partial u_m} \right) + \sum_{i=1}^{N} \sum_{j=1}^{N} (\delta_{jm} - \alpha \delta_{im}) \frac{\partial \tilde{W}'_{ij}}{\partial u_k} + \sum_{i=1}^{N} \sum_{j=1}^{N} (u_j - \alpha u_i) \frac{\partial \tilde{W}'_{ij}}{\partial u_k \partial u_m}$$

The last term is zero. Rearrange the first two terms to find

$$\sum_{i=1}^{N} \left. \frac{\partial \langle u_x \rangle_i}{\partial u_m \partial u_k} \right|_{\mathbf{u}=\mathbf{0}} = \sum_{i=1}^{N} \left(\frac{\partial \tilde{W}'_{ik}}{\partial u_m} - \alpha \frac{\partial \tilde{W}'_{ki}}{\partial u_m} \right) \Bigg|_{\mathbf{u}=\mathbf{0}} + \sum_{i=1}^{N} \left(\frac{\partial \tilde{W}'_{im}}{\partial u_k} - \alpha \frac{\partial \tilde{W}'_{mi}}{\partial u_k} \right) \Bigg|_{\mathbf{u}=\mathbf{0}}. \quad (3.59)$$

If a practical kernel function $\tilde{W}$ can be found such that (3.59) expression is zero then it is proved above that the system thus defined would be stable.

A candidate is the Shepard function (3.56), but this does not work. It is evident that $\sum_{j=1}^{N} \hat{W}_{ij} \equiv 1$ and therefore $\frac{\partial}{\partial u_k} \sum_{j=1}^{N} \hat{W}_{ij} \equiv 0$ for all k and similarly for any higher derivatives. Specifically $\frac{\partial}{\partial u_i} \sum_{j=1}^{N} \hat{W}_{ij} = \sum_{j=1}^{N} \hat{W}'_{ij} \equiv 0$. Consequently if $\tilde{W}$ is the Shepard function then (3.59) is

$$\sum_{i=1}^{N} \left(\frac{\partial \tilde{W}'_{ik}}{\partial u_m} \right) \Bigg|_{\mathbf{u}=\mathbf{0}} + \sum_{i=1}^{N} \left(\frac{\partial \tilde{W}'_{im}}{\partial u_k} \right) \Bigg|_{\mathbf{u}=\mathbf{0}}.$$

Unfortunately, this is not identically zero because the sum is over the opposite index $\sum_i \hat{W}'_{ij}$ rather than $\sum_j \hat{W}'_{ij}$. Note that in this case the additional $-\alpha u_i$ term in the original approximation is superfluous because using the Shepard function gives the exact derivative for a constant displacement field. We now suggest some alternatives that *are* stable for all T. This is not presented as a fully comprehensive list and each option has disadvantages that may make it less useful.

1. Perhaps the simplest option is to use a kernel such that the second derivative is

equal to zero then (3.58) will be equal to zero. For example a hat function

$$W(r,h) = \frac{1}{2h}\begin{cases} 1+\frac{r}{2h} & -2h < r < 0 \\ 1-\frac{r}{2h} & 0 < r < 2h \\ 0 & \text{otherwise} \end{cases}. \tag{3.60}$$

This function does not posses many of the properties thought desirable; the derivative is discontinuous and when using it to approximate a derivative all particles within the neighbourhood contribute equally. The result is smoothed particle hydrodynamics absent smoothing.

2. The derivative of the Shepard function is

$$\tilde{W}'_{ij} = \frac{W'_{ij}\sum_l W_{il} - W_{ij}\sum_l W'_{il}}{\left(\sum_l W_{il}\right)^2}. \tag{3.61}$$

By summing (3.61) over j it is seen that $\sum_{j=1}^{N} \tilde{W}'_{ij} = 0$ as expected. Equation (3.61) can be modified so that

$$\tilde{W}'_{ij} = \frac{W'_{ij}\sum_l W_{lj} - W_{ij}\sum_l W'_{lj}}{\left(\sum_l W_{jl}\right)^2}. \tag{3.62}$$

Then summing over i find

$$\begin{aligned}\sum_{i=1}^{N} \tilde{W}'_{ij} =& \frac{\sum_i \left(W'_{ij}\sum_l W_{lj} - W_{ij}\sum_l W'_{lj}\right)}{\left(\sum_l W_{jl}\right)^2} \\ =& \frac{\sum_i W'_{ij}\sum_l W_{lj} - \sum_i W_{ij}\sum_l W'_{lj}}{\left(\sum_l W_{jl}\right)^2} = 0.\end{aligned}$$

Therefore with $\tilde{W}$ defined as in (3.62) and $\alpha = 0$ the system will be stable because then (3.59) is

$$\sum_{i=1}^{N} \frac{\partial \tilde{W}'_{ik}}{\partial u_m}\bigg|_{\mathbf{u}=\mathbf{0}} + \sum_{i=1}^{N} \frac{\partial \tilde{W}'_{im}}{\partial u_k}\bigg|_{\mathbf{u}=\mathbf{0}} = \frac{\partial}{\partial u_m}\sum_{i=1}^{N} \tilde{W}'_{ik}\bigg|_{\mathbf{u}=\mathbf{0}} + \frac{\partial}{\partial u_k}\sum_{i=1}^{N} \tilde{W}'_{im}\bigg|_{\mathbf{u}=\mathbf{0}} = 0,$$

because the sums are identically zero.

This has a flaw however; it does not conserve momentum. To see this, recall that linear momentum is conserved if the potential energy is invariant with respect to

translation (see §3.3) . The potential energy is given by (3.22) and this is invariant if, for all i, $\langle u_x \rangle_i$ is. For the kernel function in question $\sum_{j \in N(i)} \tilde{W}'_{ij} \not\equiv 0$ so

$$\sum_{j \in N(i)} (u_j + s)\, \tilde{W}'_{ij} \neq \sum_{j \in N(i)} u_j \tilde{W}'_{ij}$$

and therefore momentum is not conserved.

3. If $\tilde{W}_{ij}$ is the ij element of a matrix then if it is the Shepard function the rows of the matrix sum to zero. The consequence of this is that the approximation for the displacement gradient (3.55) will be exact for a constant displacement/rigid translation of the body and that momentum is conserved. If $\tilde{W}_{ij}$ is described by equation (3.62) then each column sums to zero and we have shown above that the system will be stable. Therefore if both the rows and columns of $\tilde{W}_{ij}$ sum to zero the resulting system will be stable and conserve momentum.

   It is possible to generate a matrix from W'_{ij} with row and column sums equal to zero by the following method (taken from [76]). Given an $N \times N$ matrix A_{ij}, define $\bar{A}_{i:} = \frac{1}{N} \sum_{j=1}^{N} A_{ij}$ i.e. the mean of the entries in the i^{th} row. Analagously define $\bar{A}_{:j}$ as the mean of the j^{th} column. The first step is to modify each each row of A_{ij} by subtracting the row means from each row, in [76] this is referred to as a "row mean polish". Then the second step is to perform a "column mean polish" by subtracting the column means, of the new matrix generated from the previous step, from each column - see algorithm 3.1. After the whole procedure has been applied the rows and columns will sum to zero. This is obviously the case for the columns as the column mean polish is applied last. That the rows still sum to zero can be verified. Define A^1_{ij} as the result of "row polishing" A_{ij} and A^2_{ij} as the result of "column polishing" A^1_{ij} in terms of the original matrix A^2_{ij} is

$$A^2_{ij} = A^1_{ij} - \bar{A}^1_{:j} = A_{ij} - \bar{A}_{i:} - \frac{1}{N} \sum_l \left(A_{lj} - \bar{A}_{l:} \right). \tag{3.63}$$

   If (3.63) is summed over j then

$$\sum_j A^2_{ij} = \sum_j A_{ij} - \sum_j \bar{A}_{i:} - \sum_j \left(\frac{1}{N} \sum_l \left(A_{lj} - \bar{A}_{l:} \right) \right)$$

Algorithm 3.1 Row and column mean polishing of matrix

for $i = 1$ **to** N **do** ▷ Calculate row sums

  for $j = 1$ **to** N **do**

    $\bar{A}_{i:} \leftarrow \bar{A}_{i:} + A_{ij}$

  end for

end for

$\bar{A}_{i:} \leftarrow \frac{1}{N}\bar{A}_{i:}$

for $i = 1$ **to** N **do** ▷ Row mean polish

  $A_{ij} \leftarrow A_{ij} - \bar{A}_{i:}$

end for

for $j = 1$ **to** N **do** ▷ Calculate columns sums

  for $i = 1$ **to** N **do**

    $\bar{A}_{:j} \leftarrow \bar{A}_{:j} + A_{ij}$

  end for

end for

$\bar{A}_{:j} \leftarrow \frac{1}{N}\bar{A}_{:j}$

for $j = 1$ **to** N **do** ▷ Column mean polish

  $A_{ij} \leftarrow A_{ij} - \bar{A}_{:j}$

end for

$$
\begin{aligned}
=& N\bar{A}_{i:} - N\bar{A}_{i:} - \frac{1}{N}\sum_{l}\left(\sum_{j} A_{lj} - \sum_{j}\bar{A}_{l:}\right) \\
=& 0 - \frac{1}{N}\sum_{l}\left(N\bar{A}_{l:} - N\bar{A}_{l:}\right) = 0.
\end{aligned}
$$

Applied to the derivative of the kernel W'_{ij}, the modified/corrected kernel is

$$
\begin{aligned}
\tilde{W}'_{ij} =& W'_{ij} - \frac{1}{N}\sum_{p=1}^{N} W'_{ip} - \frac{1}{N}\sum_{l}\left(W'_{lj} - \frac{1}{N}\sum_{m=1}^{N} W'_{lm}\right) \\
=& W'_{ij} - \bar{R}'_i - \bar{C}'_j + \frac{1}{N}\sum_{l=1}^{N}\bar{R}'_l.
\end{aligned}
\tag{3.64}
$$

$\bar{R}'_i$ is the average of the i^{th} row of W'_{ij} and $\bar{C}'_j$ is the average of the j^{th} column. Using this kernel the system will be stable and conserve momentum. There is a major

disadvantage however; the matrix W'_{ij} is banded due to the compact support of the kernel, reflecting the fact that particles only influence their neighbours. Equation (3.64) potentially defines a fully populated matrix so it is possible $\tilde{W}'_{ij} \neq 0$ for $j \notin N(i)$. Apart from the consequent inefficiency in the computation the "action at a distance" of a particle on another which is not close is unphysical.

4. Finally we show that a combination of a Shepard function and a column mean polish also has the desired property - zero column and row means. First note that if

$$\tilde{W}_{ij} = \frac{W_{ij}}{\sum_k W_{ik}}$$

then

$$\tilde{W}'_{ij} = \frac{W'_{ij} \sum_k W_{ik} - W_{ij} \sum_k W'_{ik}}{\left(\sum_k W_{ik}\right)^2}$$

and therefore

$$\sum_j \tilde{W}'_{ij} = \frac{1}{\left(\sum_k W_{ik}\right)^2} \left(\sum_j W'_{ij} \sum_k W_{ik} - \sum_j W_{ij} \sum_k W'_{ik} \right) = 0.$$

The matrix with components $\tilde{W}'_{ij}$ has rows that sum to zero. Now apply a column mean polish as described above

$$\hat{W}'_{ij} = \tilde{W}'_{ij} - \frac{1}{N} \sum_k W'_{kj}.$$

The column mean polish guarantees that $\sum_i \hat{W}'_{ij} = 0$, but summing over the rows give

$$\begin{aligned} \sum_j \hat{W}'_{ij} =& \sum_j \tilde{W}'_{ij} - \frac{1}{N} \sum_j \sum_k \tilde{W}'_{kj} \\ =& 0 - \frac{1}{N} \sum_k \sum_j \tilde{W}'_{kj} = 0. \end{aligned}$$

Therefore the matrix has columns and rows that sum to zero. The same objection raised above - that the kernel no longer has a compact support - applies here equally.

A stability analysis of SPH has been performed using semi-discrete equations, this isolates the effect of the special feature of SPH; the spatial discretisation. The analysis

was performed on standard versions of the SPH equations for linear elasticity in 1D by linearisation. If the SPH equations are,

$$\ddot{u}_i = f_i(\mathbf{u}), \tag{3.65}$$

then it was found that the critical matrix with respect to stability is

$$A_{ik} = -\frac{\partial f_i^0}{\partial u_k}. \tag{3.66}$$

In particular if A_{ik} is not positive definite then the system is unstable. For standard, non-conservative, SPH if A_{ik} is positive definite then no conclusion with regards to stability should be drawn. It was found that if the momentum equation is 0^{th}-order complete, the divergence of a constant stress field is evaluated exactly, then A_{ik} is positive definite and hence a linear stabilty analysis does not indicate that tensile instability exists. This may explain the greater stability observed in practice for corrected formulations e.g. NCSPH, MLS or RKPM - although in chapter 4 it will be shown that in practice instability can still occur.

For non-0^{th}-order complete versions of the momentum equation a stability criterion,

$$nT \sum_{j \in N(i)} W''_{ij} > \sum_{j \in N(i)} W'^2_{ij},$$

was derived based on the first principal minor of (3.66). In contrast to the classic Swegle result we found that instability could only be proven when the tension goes above a certain critical value (assuming that $\sum_{i \in N(j)} W''_{ij} > 0$). We calculated this value for varying values of the smoothing length and a range of different kernel functions. By comparison, with the critical values of T found by checking numerically whether (3.66) is positive definite, it was found that the simple stability criterion overestimated the tension required to induce instability. Furthermore, it was found that the level of tension required to induce instability was quite small - equivalent to an expansion of the bar of around 0.05%.

Leaving aside the treatment of time as a continuous or discrete variable, fundamentally the linear stability analysis performed above and the von Neumann analyses are equivalent. Linear analysis can only provide necessary conditions for stability. In order to

try to produce a sufficient condition for stablity we turned to Lyapunov's method. The disadvantge of this approach is the need to find a Lyapunov function for which there is no general method. However a natural candidate for a Lyapunov function is the total energy of a system, indeed the Lyapunov function can be thought of as a generalised energy function. It was found that SPH as typically formulated is not integrable; the force function cannot be integrated to find the potential energy. As such for normal SPH the total energy is not available as a Lyapunov function. However a conservative version of SPH was derived and it was shown by Lyapunov's method that the equilibrium is stable if (3.66) is positive definite. Further, that it would be positive definite for all T if the kernel function $W\left(\left|\mathbf{x}_i - \mathbf{x}_j\right|, h\right)$ is chosen such that, for all i and j and for all $\mathbf{u}$; $\sum_{j=1}^{N} W'_{ij} = \sum_{i=1}^{N} W'_{ij} = 0$. Suggestions are given for methods to construct such functions though each has distinct disadvantages.

Although the stability results are only strictly applicable to conservative SPH, the linear stability analysis showed that conservative SPH is less stable in tension than non-conservative SPH, requiring exactly half the tension to become unstable. This suggests that conditions that imply stablity in conservative SPH may help stabilise ordinary SPH. This is explored experimentally in chapter 4.

Finally a link between the positive definiteness of the Fourier transform of a kernel and the absence of an instability in compression is made. The same link was derived, by a different method, in [19] to explain the superior stability of Wendland kernels in fluid simulation. No evidence has been found here to suggest that Wendland kernels are more stable in tension than spline functions. In fact inspection of figure 3.2 suggests that they may be slightly inferior, though this is not conclusive.

All of the stability results derived here and, to the author's knowledge, elsewhere, apply only to the stability of an equilibrium that has been perturbed by some arbitrarily small amount. This limits the confidence one can have that the sufficient conditions derived here guarantee stability in practice. This is especially pertinent for SPH where large deformations of an initial configuration can be expected. Lyapunov's method can be

applied to more general invariant sets [65]. In particular for a conservative system, the set $\{\mathbf{u} : H(\mathbf{u}) < c\}$ where H is the total energy is invariant. Future work may concentrate on proving that an invariant set of this form is stable, thereby proving that, for example, if the system is confined to a particular region of phase space, it will be stable.

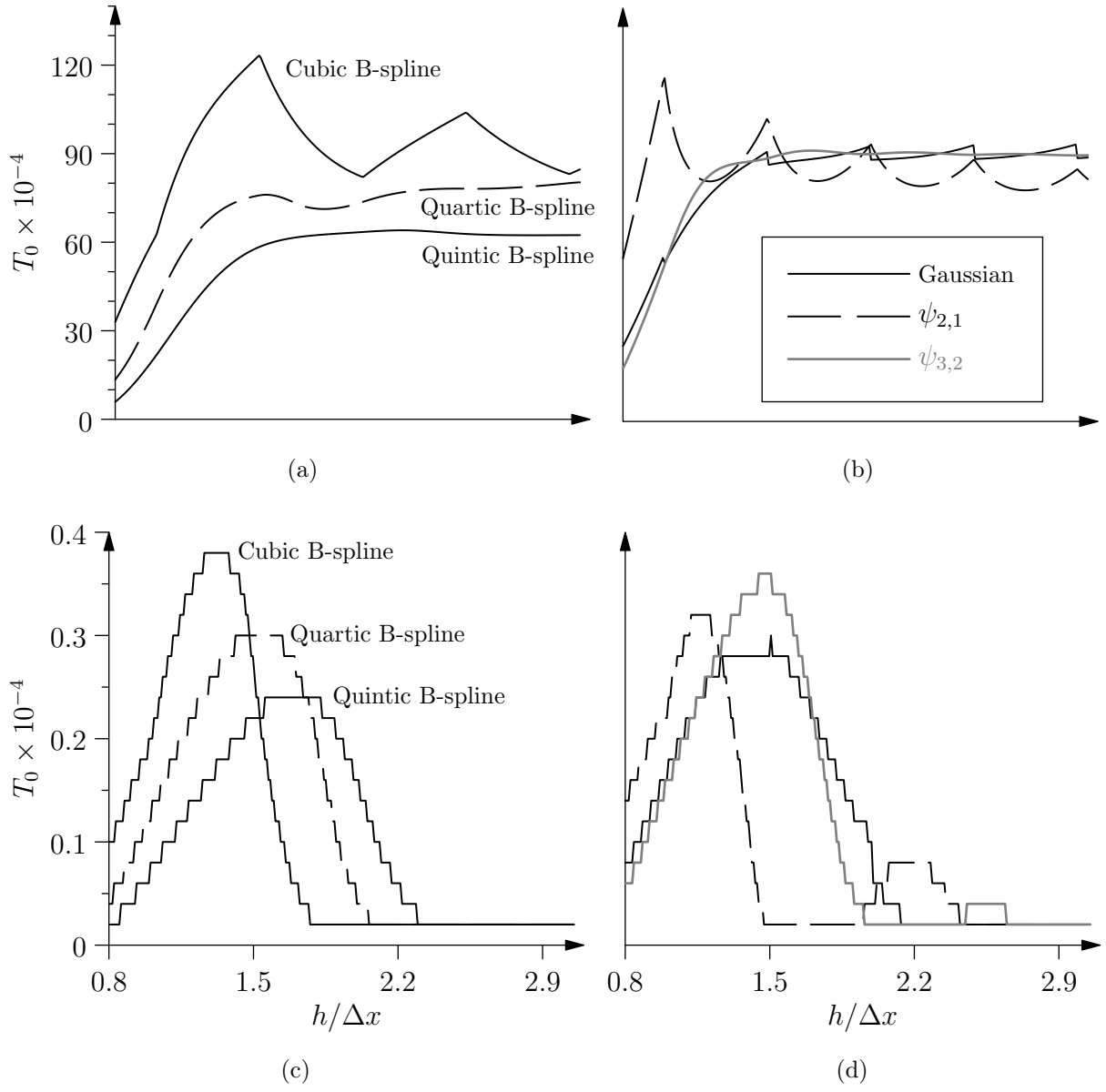

Figure 3.2: Plots generated using a system of 30 particles. The expressions for the different kernel functions are given in appendix A § 1 with the proviso that here the compact support for each kernel of equal size is $\Omega_i = x_i, x_j \, |x_i - x_j|$. The rows share a vertical axis, and the columns a horizontal axis. The plots on the right share the legend. Further details in main text on page 99.

Chapter 4

Stabilised SPH

1 Introduction

Chapter 3 introduced the problem of tensile instability and derived energy-conserving equations of motion, it was shown that a sufficient condition for the stability of these equations is

$$\sum_{j \in N(i)} W'_{ij} = \sum_{i \in N(j)} W'_{ij} = 0. \tag{4.1}$$

This condition is equivalent to asking that a matrix $A_{ij} = W'_{ij}$ has rows and columns that sum to zero. In chapter 3§4.1.1 three suggestions were given for kernel functions that obey the condition (4.1). Unfortunately each has distinct disadvantages that make it unsuitable for practical application. The method described below is inspired by the third item on that list (page 104) where the derivative of the kernel function is modified as follows;

$$\tilde{W}'_{ij} = W'_{ij} - \frac{1}{N}\sum_{p=1}^{N} W'_{ip} - \frac{1}{N}\sum_{l}\left(W'_{lj} - \frac{1}{N}\sum_{m=1}^{N} W'_{lm}\right). \tag{4.2}$$

It was shown that modified in this way the kernel passes the stability criterion (4.1). The criterion strictly only applies in the specific context of equations derived from a potential energy i.e. where the force on particle k is $f_k = \frac{\partial U}{\partial x_k}$. For example, using the modified

kernel (4.2), we have

$$\langle u_x \rangle_i = \sum_{j \in N(i)} u_j \tilde{W}_{ij}, \tag{4.3}$$

and the potential energy is defined to be

$$U = \frac{c^2}{2} \sum_{i=1}^{N} \left(\langle u_x \rangle_i + T \right)^2 . \tag{4.4}$$

We now derive the expression for the force on particle k:

$$\begin{aligned} f_k =& c^2 \sum_{i=1}^{N} \langle u_x \rangle_i \frac{\partial}{\partial u_k} \langle u_x \rangle_i \\ =& c^2 \sum_{i=1}^{N} \left(\langle u_x \rangle_i \tilde{W}'_{ik} + \sum_{j=1}^{N} u_j \frac{\partial \tilde{W}'_{ij}}{\partial u_k} \right) \qquad (4.5) \\ =& c^2 \sum_{i=1}^{N} \langle u_x \rangle_i \tilde{W}'_{ik} + c^2 \sum_{i=1}^{N} \langle u_x \rangle_i \sum_{j=1}^{N} u_j \frac{\partial \tilde{W}'_{ij}}{\partial u_k}. \qquad (4.6) \end{aligned}$$

First we calculate

$$\begin{aligned} \frac{\partial \tilde{W}_{ij}}{\partial u_k} =& W''_{ij}(\delta_{ik} - \delta_{jk}) - \frac{1}{N} \sum_{p=1}^{N} W''_{ip}(\delta_{ik} - \delta_{pk}) \\ & - \frac{1}{N} \sum_{l} \left(W''_{lj}(\delta_{lk} - \delta_{jk}) - \frac{1}{N} \sum_{m} W''_{lm}(\delta_{lk} - \delta_{mk}) \right) \\ =& W''_{ij}(\delta_{ik} - \delta_{jk}) - \frac{1}{N} \delta_{ik} \sum_{p=1}^{N} W''_{ip} + \frac{1}{N} W''_{ik} \\ & - \frac{1}{N} W''_{kj} + \frac{1}{N} \delta_{jk} \sum_{l} W''_{lj} - \frac{1}{N^2} \sum_{m} W''_{km} + \frac{1}{N^2} \sum_{l} W''_{lk} \\ =& W''_{ij}(\delta_{ik} - \delta_{jk}) - \delta_{ik} \bar{A}''_i + \frac{1}{N} W''_{ik} - \frac{1}{N} W''_{kj} + \delta_{jk} \bar{A}''_j. \end{aligned}$$

The last two terms on the penultimate line cancel and we define $\bar{A}''_i = \frac{1}{N}\sum_p W''_{ip}$. Next multiply the above by u_j sum over j

$$\begin{aligned}\sum_j u_j \frac{\partial \tilde{W}_{ij}}{\partial u_k} &= \delta_{ik}\sum_j u_j W''_{ij} - u_k W''_{ik} \\ &\quad - \frac{1}{N}\delta_{ik}\sum_j u_j \bar{A}''_i + \frac{1}{N}\sum_j u_j W''_{ik} \\ &\quad - \frac{1}{N}\sum_j u_j W''_{kj} + \frac{1}{N}u_k \bar{A}''_k \\ &= \delta_{ik}\sum_j u_j W''_{ij} - u_k W''_{ik} - \delta_{ik}\bar{u}\bar{A}''_i + \bar{u}W''_{ik} \\ &\quad - \frac{1}{N}\sum_j u_j W''_{kj} + \frac{1}{N}u_k \bar{A}''_k.\end{aligned}$$

Where $\bar{u} = \frac{1}{N}\sum_k u_k$. Then multiply by $\langle u_x\rangle_i$ and sum over i;

$$\begin{aligned}\sum_i \langle u_x\rangle_i \sum_j u_j \frac{\partial \tilde{W}_{ij}}{\partial u_k} &= \langle u_x\rangle_k \sum_j u_j W''_{kj} - u_k \sum_i \langle u_x\rangle_i W''_{ik} - \bar{u}\bar{A}''_k \langle u_x\rangle_k \\ &\quad + \bar{u}\sum_i \langle u_x\rangle_i W''_{ik} - \frac{1}{N}\sum_j u_j W''_{kj}\sum_i \langle u_x\rangle_i + \frac{1}{N}u_k \bar{A}''_k \sum_i \langle u_x\rangle_i \\ &= \langle u_x\rangle_k \sum_j u_j W''_{kj} - u_k \sum_i \langle u_x\rangle_i W''_{ik} - \bar{u}\bar{A}''_k \langle u_x\rangle_k \\ &\quad + \bar{u}\sum_i \langle u_x\rangle_i W''_{ik} - \overline{\langle u_x\rangle}\sum_j u_j W''_{kj} + u_k \bar{A}''_k \overline{\langle u_x\rangle}.\end{aligned}$$

Where $\overline{\langle u_x\rangle} = \frac{1}{N}\sum_i \langle u_x\rangle_i$. Gathering terms and changing all the dummy varibles to i, find

$$\begin{aligned}\sum_i \langle u_x\rangle_i \sum_j u_j \frac{\partial \tilde{W}_{ij}}{\partial u_k} &= \sum_i \left(u_i \langle u_x\rangle_k - u_k \langle u_x\rangle_i\right) W''_{ik} \\ &\quad + \sum_i \left(\bar{u}\langle u_x\rangle_i - \overline{\langle u_x\rangle}u_i\right) W''_{ik} + \bar{A}''_k \left(u_k \overline{\langle u_x\rangle} - \bar{u}\langle u_x\rangle_k\right).\end{aligned} \tag{4.7}$$

Therefore f_k is

$$\begin{aligned}f_k = c^2 \Bigg[&\sum_{i=1}^N \langle u_x\rangle_i \tilde{W}'_{ik} + \sum_{i=1}^N \left(u_i \langle u_x\rangle_k - u_k \langle u_x\rangle_i\right) W''_{ik} \\ &+ \sum_{i=1}^N \left(\bar{u}\langle u_x\rangle_i - \overline{\langle u_x\rangle}u_i\right) W''_{ik} + \bar{A}''_k \left(u_k \overline{\langle u_x\rangle} - \bar{u}\langle u_x\rangle_k\right)\Bigg].\end{aligned} \tag{4.8}$$

Equation (4.8) is very unwieldy, and is likely to be extremly inefficient, not least because every particle will contribute to f_k. This non-locality is also incompatible with the finite propagation of information in elasticity in particular and hyperbolic PDE in general. The corrected kernel (4.2) was however the inspiration for the corrected momentum equation presented in this chapter.

2 Corrected SPH momentum equation

It is not acceptable on physical principal for the momentum equation to acquire information from distant particles instantly. Therefore we define the following local version of the kernel,

$$\mathbf{C}_{ij} = \nabla W_{ij} V_j - \frac{1}{n_i} \sum_{k \in N(i)} \nabla W_{ik} V_k - \frac{1}{n_j} \sum_{k \in N(j)} \nabla W_{kj} V_k + \frac{1}{n_i} \sum_{j \in N(i)} \frac{1}{n_j} \sum_{k \in N(j)} \nabla W_{jk} V_k. \quad (4.9)$$

Where n_i is the number of neighbours of the particle i and $V_k = \frac{m_k}{\rho_k}$ is the particle volume. Note the similarity to (4.2). The corrected momentum equation uses this function as a kernel;

$$\mathbf{f}_i = m\mathbf{a}_i = \sum_{j \in N(i)} \frac{\sigma_j}{\rho_j} \cdot \mathbf{C}_{ij}. \quad (4.10)$$

$\mathbf{C}_{ij}$ has non-compact support, for any j the third sum in (4.9) may be non-zero. The sum $\sum_{j \in N(i)}$, rather than $\sum_{j=1}^{N}$, in (4.10) is important to ensure the approximation is local.

2.1 Stability

First note that $\mathbf{C}_{ij}$ has the following properties:

1. Discounting particles near the boundary, if the initial configuration is regular then $\mathbf{C}_{ij}(0) = \nabla W_{ij}(0)$.

2. $\sum_{j \in N(i)} \mathbf{C}_{ij} \equiv \mathbf{0}$

Proof. Define $S(i) = \sum_{j \in N(i)} \nabla W_{ij} V_j = -\sum_{j \in N(i)} \nabla W_{ji} V_j$ then

$$\begin{aligned}\sum_{j \in N(i)} \mathbf{C}_{ij} &= \sum_{j \in N(i)} \left(\nabla W_{ij} - \frac{1}{n_i} \sum_{k \in N(i)} \nabla W_{ik} - \frac{1}{n_j} \sum_{k \in N(j)} \nabla W_{kj} + \frac{1}{n_i} \sum_{j \in N(i)} \frac{1}{n_j} \sum_{k \in N(j)} \nabla W_{jk} \right) \\ &= \underbrace{S(i) - \sum_{j \in N(i)} \frac{1}{n_i} S(i)}_{=0} + \underbrace{\sum_{j \in N(i)} \frac{1}{n_j} S(j) - \sum_{j \in N(i)} \frac{1}{n_i} \sum_{j \in N(i)} \frac{1}{n_j} S(j)}_{=0} = 0.\end{aligned}$$

where the particle volumes are included implicitly. □

In the stability analysis of the previous chapter we considered the 1D wave equation. Under the assumptions made there equation (4.10) becomes

$$f_i = c^2 \sum_{j \in N(i)} \Big(\langle u_x \rangle_j + T \Big) C_{ij}, \tag{4.11}$$

where we use

$$\langle u_x \rangle_j = \sum_{m \in N(j)} (u_m - u_j) W'_{jm}. \tag{4.12}$$

It was shown in chapter 3 § 2.1 that if the matrix with components $\frac{\partial f_i}{\partial u_k}$ is not negative definite then the system will be unstable. For equation (4.11) we find

$$\begin{aligned}\frac{1}{c^2} \frac{\partial f_i}{\partial u_k} &= \sum_{j \in N(i)} C_{ij}(0) \frac{\partial}{\partial u_k} \langle u_x \rangle_j + T \frac{\partial}{\partial u_k} \sum_{j \in N(i)} C_{ij} \\ &= \sum_{j \in N(i)} W'_{ij}(0) \left. \frac{\partial}{\partial u_k} \langle u_x \rangle_j \right|_{\mathbf{u}=\mathbf{0}} + T \left. \frac{\partial}{\partial u_k} \sum_{j \in N(i)} C_{ij} \right|_{\mathbf{u}=\mathbf{0}} \\ &= \sum_{j \in N(i)} W'_{ij}(0) \left. \frac{\partial}{\partial u_k} \langle u_x \rangle_j \right|_{\mathbf{u}=\mathbf{0}} + 0.\end{aligned}$$

Where we have used the fact that $\mathbf{C}_{ij}(0) = \nabla W_{ij}(0)$ on a regular grid, and that $\sum_{j \in N(i)} \mathbf{C}_{ij} \equiv \mathbf{0}$. That the remaining term is in fact negative definite was established in chapter 3 §4. Emphasising once again, unless the system is conservative, if $\frac{\partial f_i}{\partial u_k}$ is negative definite then no conclusion can be reach in regards to stability. However if it is not negative definite the system is *guaranteed* to be unstable for some T. The next section will investigate numerically the stability of the method

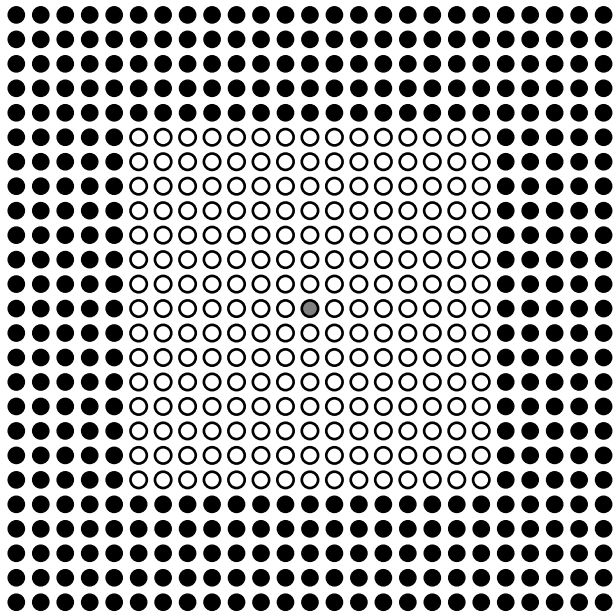

Figure 4.1: Swegle stability test. The solid black particles are fixed and all of the other particles are free to move. The center, grey, particle is given a small initial velocity. The material is held under a uniform pressure, either positive or negative.

2.2 Swegle test

Swegle *et al.* [85] introduced a simple numerical stability test to demonstrate the phenomenon of tensile instability. This problem will be used here as a simple numerical stability test for modified or corrected SPH formulations. In particular we compare the basic, normalised-corrected and, total Lagrangian forms of SPH with the new method proposed above.

The problem is set up as in figure 4.1. The material is subject to a uniform volume strain $\xi = \frac{V}{V_0}$, so that V_o is the volume where the stress would be zero. Figure 4.2 shows how given an inital velocity perturbation of $v_0 = 10^{-10}\text{cm}\mu\text{s}^{-1}$ (the initial minimum particle spacing is 0.01cm) the kinetic energy can grow exponentially.

In particular SPH and NCSPH are seen to be unstable in tension, $\xi > 1.0$, which can be somewhat mitigated by smoothing the velocity. For NCSPH this is particularly interesting as the stability analysis of the previous chapter showed that the stability matrix, $-\frac{\partial f_i}{\partial u_k}$, is positive definite. This highlights the limitations of the linear stabiltity analysis.

In contrast the new method proposed here is seen to be stable in tension. Unfortunately we seem to have exchanged one mode of instability for another. The instability reappears under compression. The author cannot offer an explanation for this effect. We showed

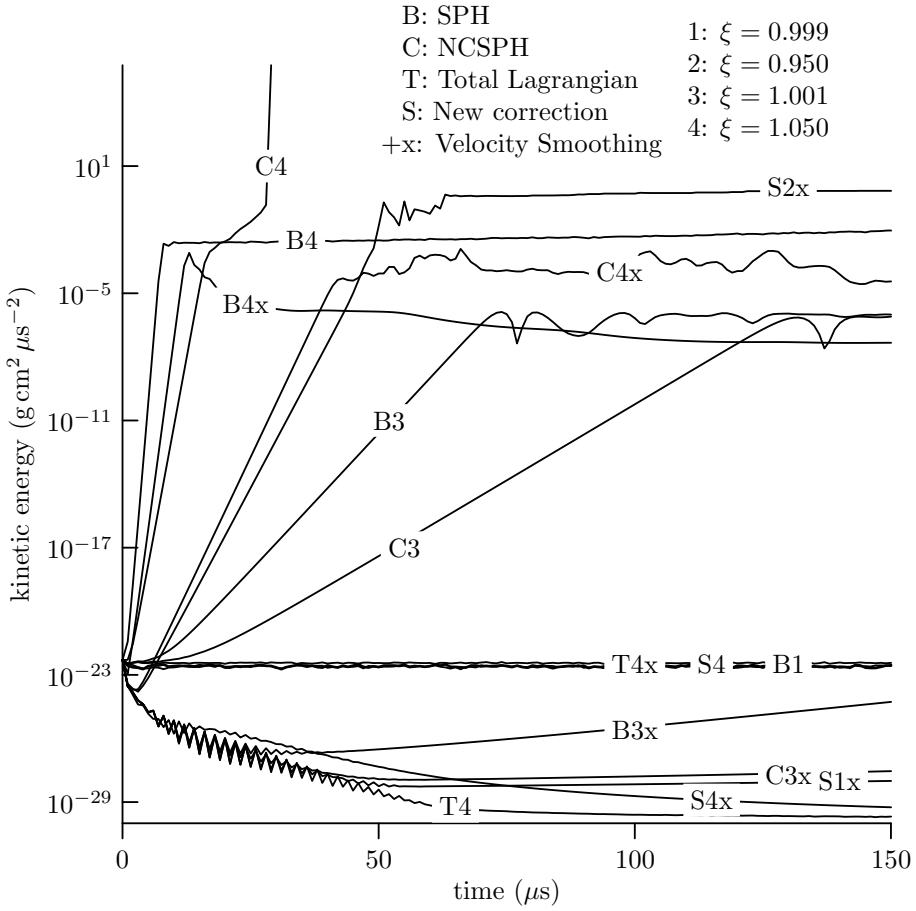

Figure 4.2: Evolution of the kinetic energy for indicated SPH formulations, $\xi = V/V_0$ is the volume strain. The initial kinetic energy is in the graph's units 5×10^{-23}.

above be a linear analysis (in 1D) that just as for NCSPH the stability matrix is positive definite. But, just as for NCSPH, in practice the stability of the linearised system does not carry over to the non-linear system.

2.3 Stabilised SPH

Given two methods, one stable in tension and the other in compression, the obvious solution is to switch between the two. For the purposes of this chapter the scheme described below will be called stabilised SPH (S-SPH). The following explanation will assume a 2D problem.

The ordinary SPH momentum equation is,

$$\mathbf{a}_i = \sum_{j \in N(i)} \left(\frac{\sigma_i}{\rho_i} + \frac{\sigma_j}{\rho_j} \right) \nabla W_{ij}. \tag{4.13}$$

Define a correction term,

$$\mathbf{g}_i = - \sum_{j \in N(i)} \left(\frac{\sigma_i}{\rho_i} + \frac{\sigma_j}{\rho_j} \right) \left(\frac{1}{n_i} \sum_{k \in N(i)} \nabla W_{ik} + \frac{1}{n_j} \sum_{k \in N(j)} \nabla W_{kj} - \frac{1}{n_i} \sum_{j \in N(i)} \frac{1}{n_j} \sum_{k \in N(j)} \nabla W_{jk} \right). \tag{4.14}$$

This has the form of the basic SPH momentum equation but with the kernel replaced by the last three terms of (4.9). The symmetry term $\frac{\sigma_i}{\rho_i}$ has been added for consistency with the ordinary SPH momentum equation.

In stabilised SPH then, the acceleration is,

$$\hat{\mathbf{a}}_i = \begin{cases} \mathbf{a}_i & : \text{In compression} \\ \mathbf{a}_i + \mathbf{g}_i & : \text{In tension} \end{cases}. \tag{4.15}$$

It remains only to provide a criterion for what is meant by "in compression" and "in tension". The most obvious choice is

$$\hat{\mathbf{a}}_i = \begin{cases} \mathbf{a}_i & : \text{if } p_i \geq 0 \\ \mathbf{a}_i + \mathbf{g}_i & : \text{if } p_i < 0 \end{cases}. \tag{4.16}$$

Where p_i is the calculated pressure at the i particle. But this is found not to work in general, though it does for the Swegel test above. Instead, denoting the components of vectors with greek letters, we have

$$\hat{a}_{i,\alpha} = \begin{cases} a_{i,\alpha} & : \text{if } \sum_{j \in N(i)} \sigma_{j,\alpha\alpha} \leq 0 \\ a_{i,\alpha} + g_{i,\alpha} & : \text{if } \sum_{j \in N(i)} \sigma_{j,\beta\beta} > 0 \end{cases}. \tag{4.17}$$

Conservation of momentum There is no guarantee that the method described will conserve linear momentum. The fact that the momentum equation at each particle can change independently suggests that we should not expect conservation of momentum due

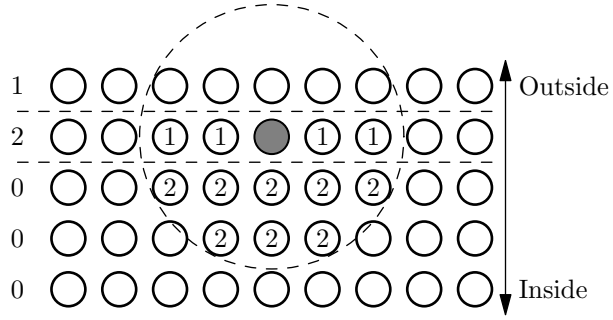

Figure 4.3: To give boundary particles the "correct" number of neighbours. Particles to the interior are counted twice, and particles on the same boundary level are counted once. Particles towards the exterior are not counted. Numbers on the far left refer to the boundary level see chapter 2.

to the anti-symmetry of the inter-particle forces, as is seen with basic SPH. Therefore we symmetrise the particle-particle interactions as the algorithm proceeds (see algorithm 4.2).

3 Implementation

The proposed method requires little modification to the basic integration algorithm. One is only required to calculate the row and column means at each time step, calculate the correction criteria (4.17) and apply if necessary.

We calculate the row and column means, $\frac{1}{n_i}\sum_{j\in N(i)} W_{ij}V_j$ and $\frac{1}{n_j}\sum_{i\in N(j)} W_{ij}V_i$, respectively, once for each time step before solving the momentum equation, see algorithm 4.1. An extra wrinkle in the implementation is that care must be taken with particles near the boundary. To see why note that in (4.9) the extra terms are approximately equal to zero; $\sum_{j\in N(i)} \nabla W_{ij} \approx 0$. However near a boundary, particle deficiency means that this correction term will become very large, which will lead to large errors in the approximation. For this reason the kernel is normalised *on the first time-step* in the manner of a Shepard function. The following expression is substituted into (4.9)

$$\nabla \tilde{W}_{ij} = \frac{\nabla W_{ij} \sum_{k\in N(i)} W^0_{ik} - W_{ij} \sum_{k\in N(i)} \nabla W^0_{ik}}{\left(\sum_{k\in N(i)} W^0_{ik}\right)^2}. \tag{4.18}$$

Algorithm 4.1 Calculate row and column means

for $i = 1$ to Number of Particles **do**

$V_i = m_i/\rho_i$

for $j \in N(i)$ **do**

$V_j = m_j/rho_j$

$row\_mean[i] \leftarrow row\_mean[i] + V_j \nabla W_{ij}$ ▷ Using (4.18) for the kernel

$column\_mean[i] \leftarrow column\_mean[i] + V_i \nabla W_{ji}$

end for

end for

$row\_mean[i] \leftarrow row\_mean[i]/n_i$ ▷ n_i and n_j calculated as in figure 4.3

$column\_mean[i] \leftarrow column\_mean[i]/n_i$

$mean\_mean[i] = \sum_{j \in N(i)} column\_mean[j])/n_i$

The $\sum_{k \in N(i)} W^0_{ik}$ and $\sum_{k \in N(i)} \nabla W^0_{ik}$ are stored for use on all subsequent time steps. This has the effect of simulating a full neighbourhood for the boundary particles. With this modification we have now that $\mathbf{C}_{ij}(0) = \nabla W_{ij}(0)$ for all i and j. One further point in regard to the boundary particles is that when calculating the mean $\frac{1}{n_i} \sum_{k \in N(i)} \nabla \tilde{W}_{ik}$ when i is near to the boundary the number of neighbours should be amended to once again simulate a full neighbourhood. Figure 4.3 should make the procedure clear; the concept of boundary levels is explained in chapter 2 when discussing the implementation of NRBCs. The complete stabilised SPH alogorithm for the momentum equation can now be given (algorithm 4.2). Note in algorithm 4.2 that regardless of the state of tension the correction is not applied to particles on the very outer layer. Not excluding these particles causes the outer particles to become disordered. One final point is that velocity smoothing (XSPH) must be used to maintain stability. Without velocity smoothing the particles on the boundary become disordered and this disorder spreads through the domain, figure 4.4.

The extra computational effort required above that for a basic SPH simulation can be split into two parts. The extra initialisation cost due to needing to identify boundary

Algorithm 4.2 Stabilised SPH

▷ $\mathbf{S}_{ij} = \frac{\sigma_i}{\rho_i} + \frac{\sigma_j}{\rho_j}$.

▷ Here BP is the set of particles on the outermost layer of the material.

Call algorithm 4.1

for $i = 1$ to Number of Particles **do**

Calculate $sum[1] = \sum_{j \in N(i)} \sigma_{j,11}$, and $sum[2] = \sum_{j \in N(i)} \sigma_{j,22}$

for $j \in N(i)$ **do**

$\mathbf{g}_{ij} = -\mathbf{S}_{ij} \cdot (row\_mean[i] + column\_mean[j] - mean\_mean[i])$

$\mathbf{f}_{ij} = \mathbf{S}_{ij} \cdot \nabla W_{ij} V_j$

if $sum[\alpha] > 0$ **or** $i \in BP$ **then**

$g_{ij,\alpha} = 0$

end if

$\mathbf{a}_i \leftarrow \mathbf{a}_i + 0.5(\mathbf{f}_{ij} + \mathbf{g}_{ij})$

$\mathbf{a}_j \leftarrow \mathbf{a}_j - 0.5(\mathbf{f}_{ij} + \mathbf{g}_{ij})$ ▷ Symmetrise particle-particle interaction

end for

end for

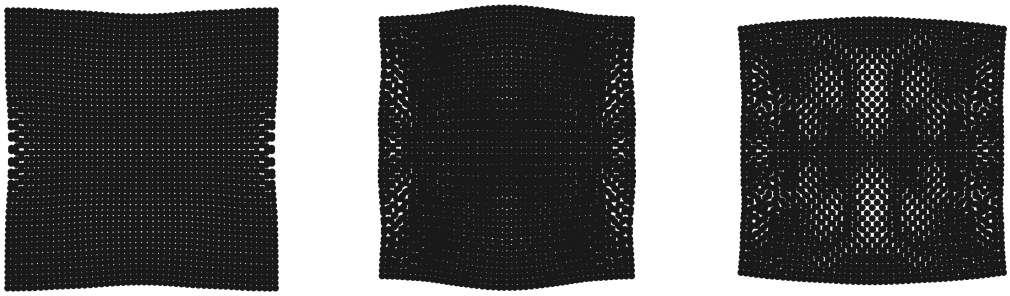

(a) $t = 2.25$ (b) $t = 3.75$ (c) $t = 4.21$

Figure 4.4: Stabilised SPH without velocity smoothing - for problem described in §4.1.1.

particles and initalise the normalisation constants in equation (4.18). Done only once, neither of these is particularly time-consuming. During the main loop of MCM the only extra routine is essentially algorithm 4.1, called before the momentum equation is solved. A crude timing experiment where the cpu time required to call the basic and the modified momentum equation routine 100 times, estimate the modified routine at roughly 1.8 times the computational cost. Solving the momentum equation of course consumes only a fraction of the whole time taken by the integration loop.

4 Numerical examples

4.1 Symmetrical impact

To assess the accuracy as well as the stability of the method we consider two impact problems. In this section we consider a symmetrical impact, 4.5, and compare the results obtained to the LS-DYNA 3D FE package. The problem is set up as in figure 4.5. The material is treated as a single piece rather than, the perhaps more practical case of, separate impacting plates because we do not wish for the comparison with the FE results to be influenced by differences in the contact algorithm.

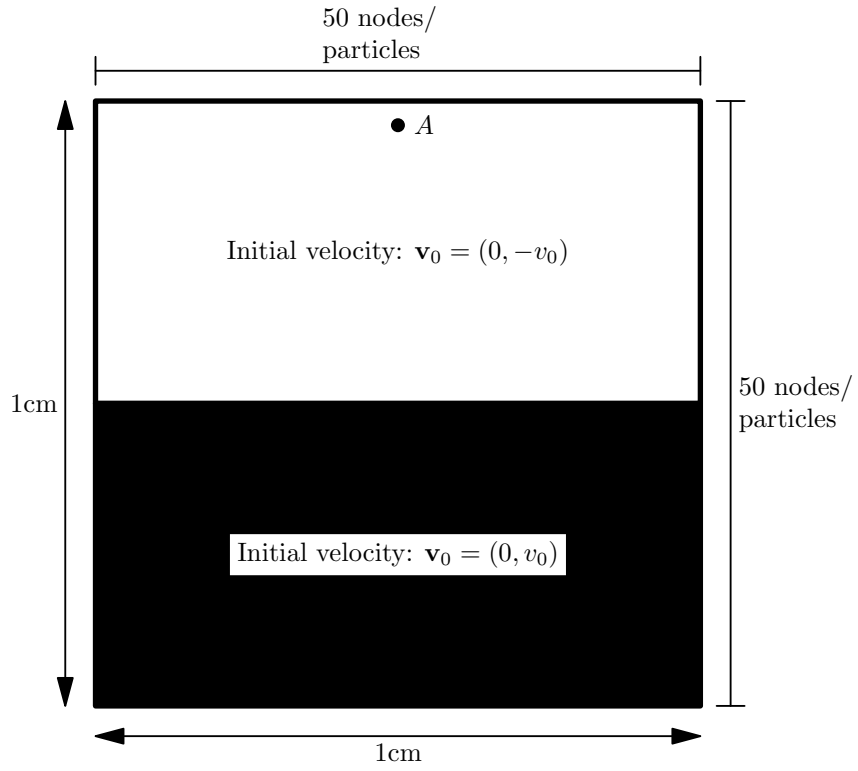

Figure 4.5: A single material given an initial velocity distribution as indicated, $v_0 = \pm\ 0.06\text{cm}\mu\text{s}^{-1}$ i.e. we test two cases. The base units for the problem are grams, centimetres, and microseconds. We use a linear elastic material model with initial density, $\rho_o = 7.8$; Young's modulus, $E = 2.1$; and Poisson's ratio, $\nu = 0.3$. Unless otherwise indicated the smoothing length is $1.3\Delta x$, where Δx is initial minimum particle separation. Particle A, is that for the plots in figures 4.7 and 4.9.

4.1.1 Initial compression

For the impacting plates, figure 4.7 shows that TL-SPH and S-SPH are very similar. Both are more closely aligned with the FE solution than basic SPH or NCSPH. Basic SPH in particular shows an extreme divergence from the FE solution. This is due to particles clumping and the beginnings of numerical fracture, as can be seen in figure 4.8(b). To a lesser degree, the NCSPH also shows the beginnings of numerical fracture, figure 4.8(c). S-SPH on the other hand remains stable, figure 4.8(a).

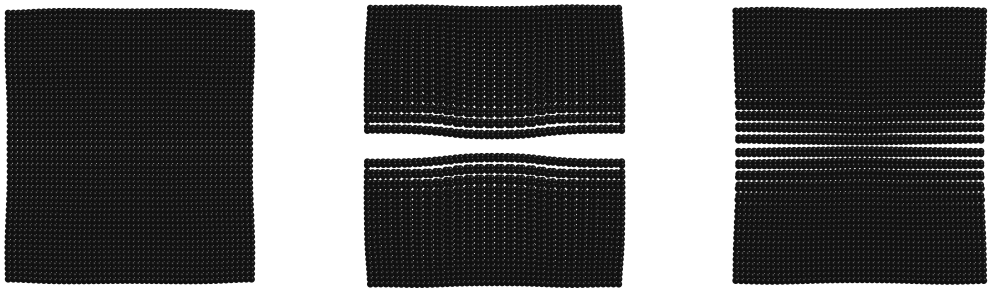

(a) Stabilised (b) Basic (c) Normalised-corrected

Figure 4.6: Particle positions for symmetric impact at time $t = 3.05\mu$s. Time only approximately equal as instability/particle clumping causes the stable time step to reduce.

4.1.2 Initial expansion

If the initial velocities are reversed from the previous test, so the material is expanding at the beginning, consequently this is an even more severe test of stability under tension. Basic SPH and NCSPH both fail completely in this case as can be seen from figure 4.9, in particular the kinetic energy for both formulations reach a relatively steady state as the two halves separate, seen in 4.8. The FE, TL-SPH and S-SPH solutions all continue to oscillate. Figure once again shows the close correspondance between TL-SPH and S-SPH and their agreement, in outline, with the FE solution. That the FE solution seems to run slightly ahead of SPH can be accounted for, at least partly, by the collocation of nodes and particles in their initial configurations. This was done for easy comparison but if the "real" boundary in SPH is taken to be located some small distance from the outer layer of particles, then the SPH simulations are arguably of slightly larger blocks.

4.2 Asymmetrical impact

In this section we consider a test desgined to highlight the problem of numerical fracture in SPH. In most respects save the dimensions, this test is identical to the previous case, though only the case of an initial impact is considered. A characteristic of this problem is the strain the bar is subjected to as the displacement wave propagates and reflects from

the two free ends. The total length of the bar over time is shown in 4.11. We can see that both SPH and NCSPH fail and continue to expand. Figures 4.12a and 4.12b show the numerical fracturing of the bar. S-SPH however remains stable, with only a slight deviation from the TL-SPH solution, showing up after 20μs. This may be related to the particle re-organisation which develops slowly from around that time. The end result may be seen in figures 4.12c and 4.12d. The exact cause of this clumping is unknown at present, it may be a zero energy mode exited by the oscillation near the impact site.

4.3 Transient surface load on clamped beam

We now consider an impact-like problem where a rectangular block of particles is fixed at both ends. A section of particles half way between the two ends is prescribed an initial velocity in the negative y-direction of $0.3\text{cm}\mu\text{s}^{-1}$. Figure 4.14, shows that the displacement of the beam as calculated by S-SPH, TL-SPH and FE are in close agreement wheras the basic SPH has failed due to tensile instability, figure 4.15. NCSPH is close to failure, 4.16. S-SPH in figure 4.17 and 4.18 show close agreement.

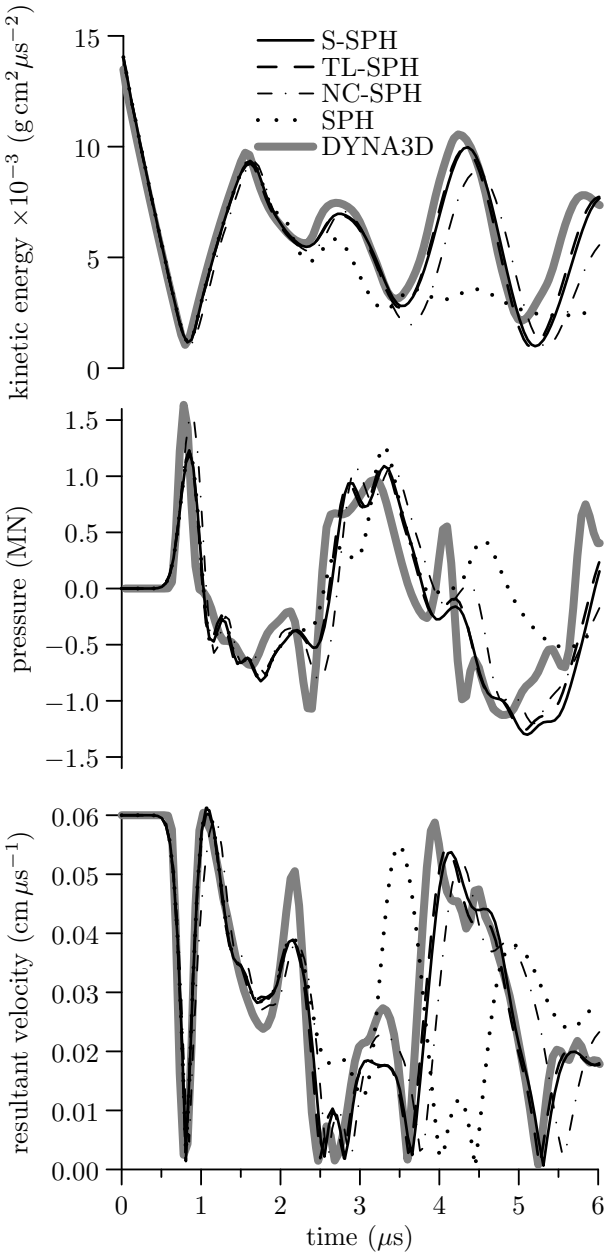

Figure 4.7: For $v_o > 0$ - the top and bottom half are initially moving together. Plot of global kinetic energy, pressure and resultant velocity at particle/node A indicated in figure 4.5. Legend and x-axis are shared by all three plots.

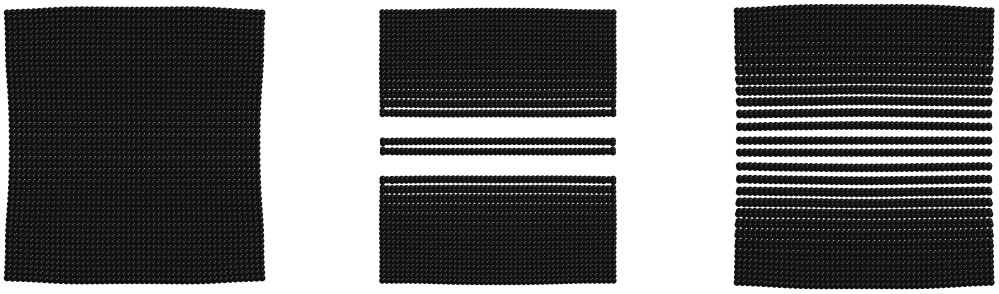

(a) Stabilised (b) Basic (c) Normalised-corrected

Figure 4.8: Particle positions for at time $t = 1.6\mu$s where the top and bottom half of the plate are initially moving apart. Time only approximately equal as the stable time-step varies between the different simulations.

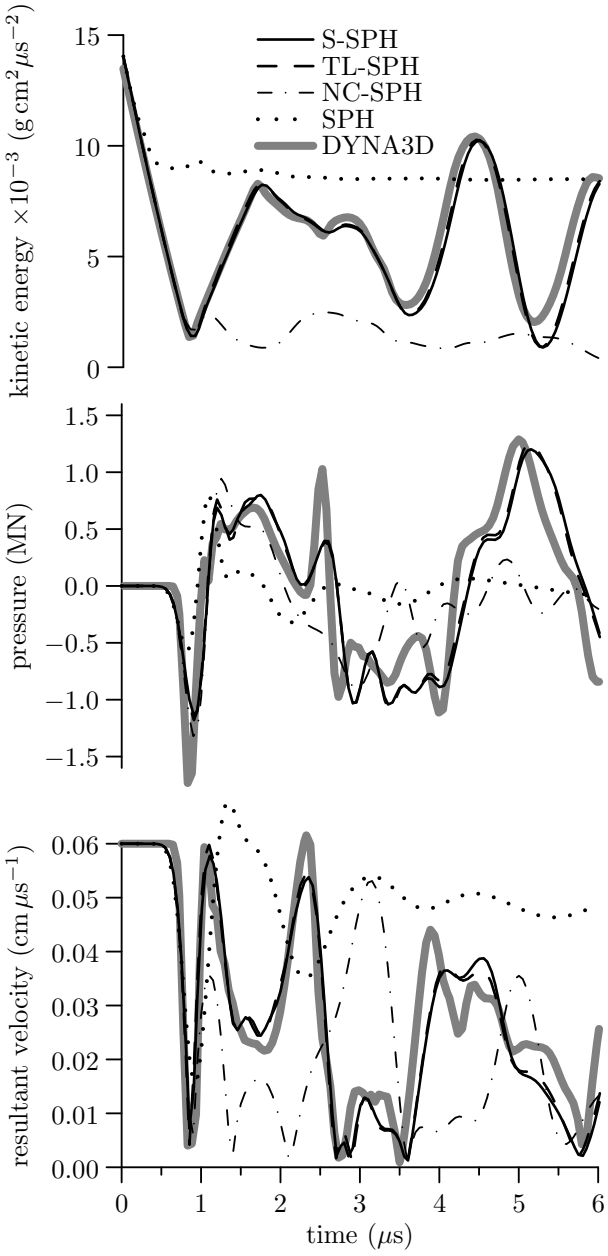

Figure 4.9: For $v_o < 0$ - the top and bottom half are initially moving apart. Plot of global kinetic energy, pressure and resultant velocity at particle/node A indicated in figure 4.5.

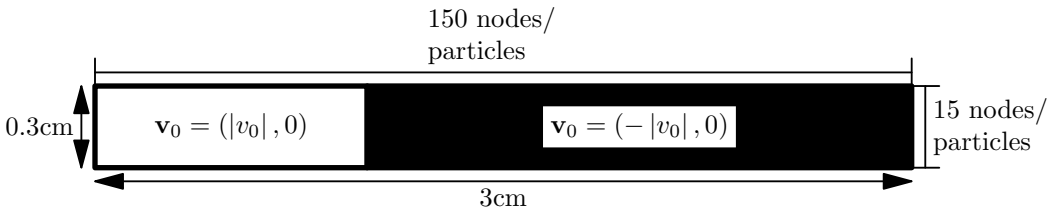

Figure 4.10: Asymetrical impact. The physical properties of the material are identical to that in figure 4.5.

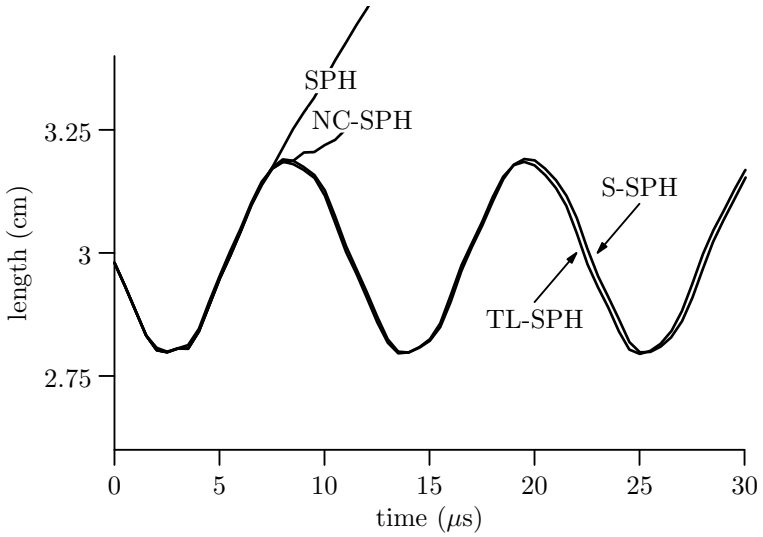

Figure 4.11: Length of bar in asymmetrical bar impact.

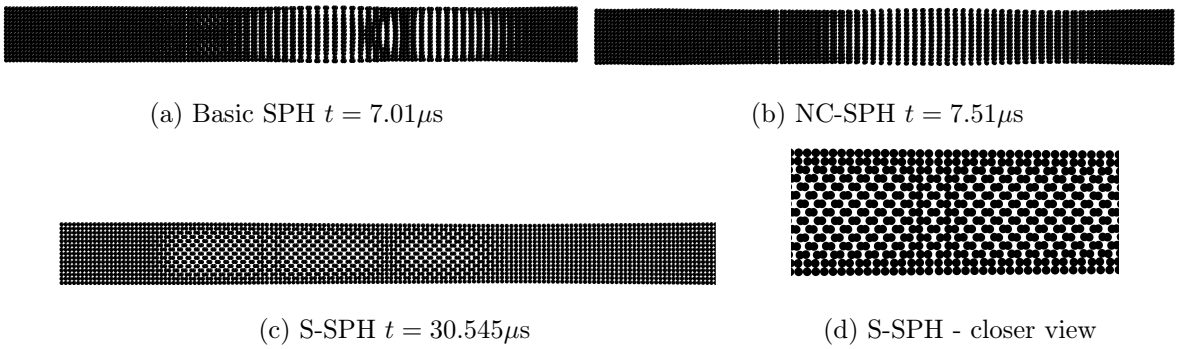

(a) Basic SPH $t = 7.01\mu$s

(b) NC-SPH $t = 7.51\mu$s

(c) S-SPH $t = 30.545\mu$s

(d) S-SPH - closer view

Figure 4.12: Particle configuration after impact. Figure (d) is a closer view of figure (c), showing some particle clumping. Note that the particles in (c) and (d) where made to appear smaller then those in the other figures to make the clumping clearer.

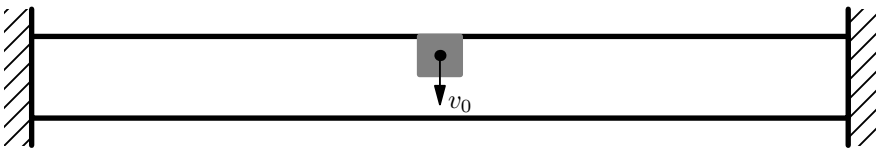

Figure 4.13: The physical dimensions and discretisation are as in figure 4.10. The ends are fixed by applying a zero displacement condition to the first and last five, vertical, layers of particles, next to the boundaries.

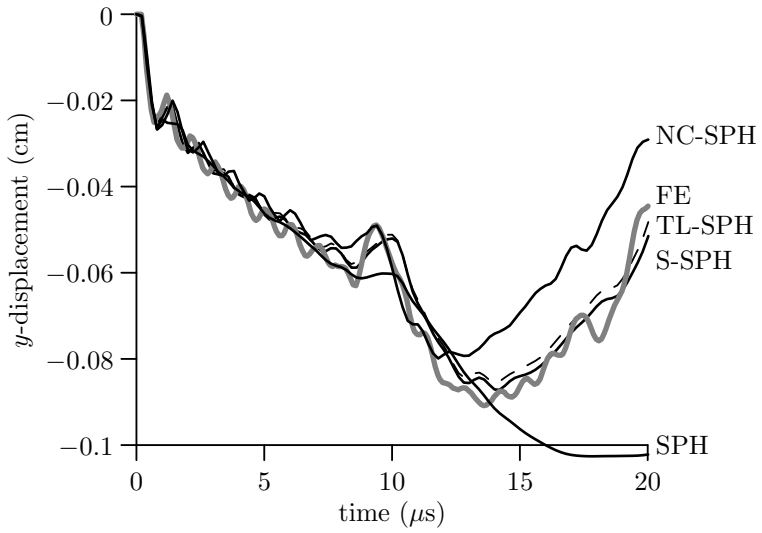

Figure 4.14: y-displacement of the bottom surface of the midline of the beam in 4.13 The physical properties of the material are identical to that in figure 4.5.

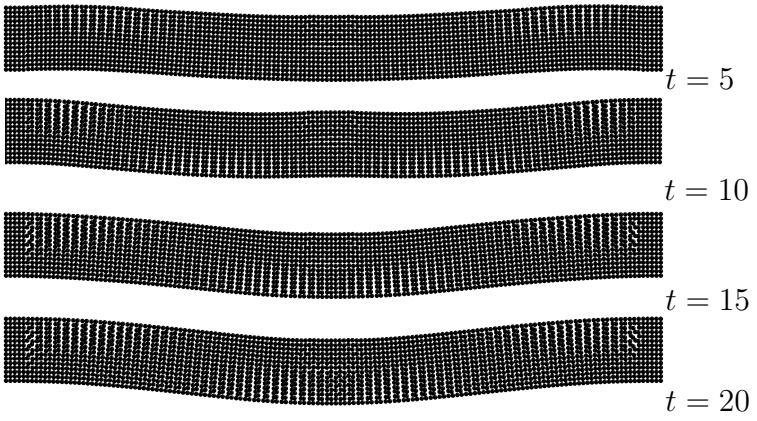

Figure 4.15: Basic SPH. Particle displacements after transient load on a clamped beam.

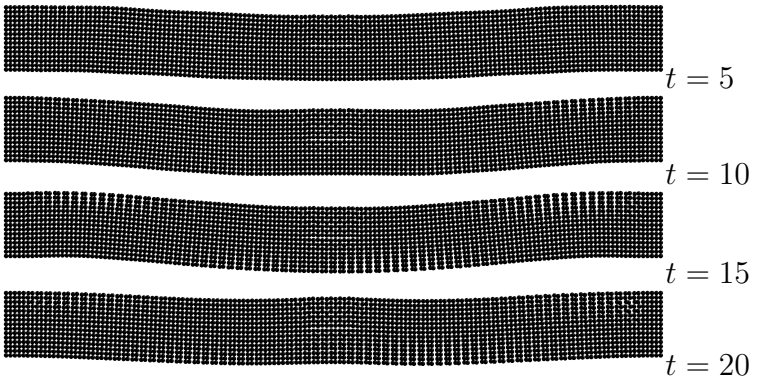

Figure 4.16: NC-SPH. Particle distribution after transient load on a clamped beam.

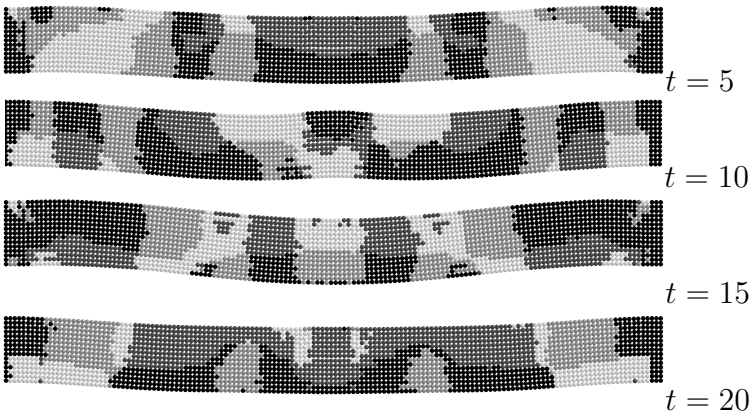

Figure 4.17: S-SPH. Particle distribution after transient load on a clamped beam. Shades indicate whether the correction has been applied; The shades form darkest to lightest respectievly that the correction is active in the x and y-direction, just the y-direction, just the x-direction, or finally not at all.

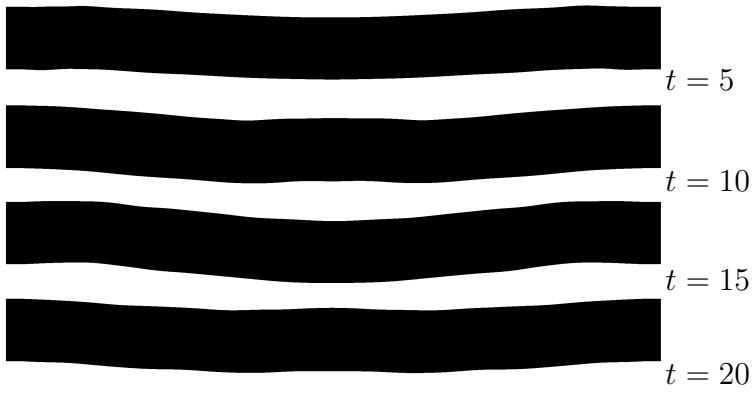

Figure 4.18: FE. Particle distribution after transient load on a clamped beam.

Conclusion

Two weaknesses of SPH are that it is computationally expensive compared to, for example, FE and it is unstable. This thesis has addressed both of these problems, albeit for the former, indirectly.

A well established NRBC used in finite differences for elastic waves has been applied to SPH and its performance assessed. The primary method used was the compression of an elastic square. Variations on first-order conditions where tested. The E-M condition was found to perform remarkably well considering its simplicity and negligible computational overhead. The problem of a transient surface load was considered, and it was found that body waves, generated from the surface can be absorbed well by a NRBC applied to the underside of a domain. This may have applications in simulating, for example, impact on "deep" bodies. Surface waves however are absorbed less well, though depending on the application the level of error is not excessive and may be acceptable. SPH lags behind other computational methods in this area, the E-M boundary conditions were first described in the 1970s, and future work in this area may follow the historical development of NRBC in other fields by introducing better absorbing layers, perhaps based on the perfectly matched layer. Alternatively if the problems with particle deficiency leading to poor approximation of derivatives can be overcome, then the arbitrarily high-order boundary conditions, descibed for example in [34], may be implemented.

Tensile instability is a hinderance to wider exploitation of SPH in solid mechnincs. A stability analysis of SPH has been performed using the semi-discrete equations. This isolates the effect of the special feature of SPH; the spatial discretisation. A linear analysis

was performed in 1D on standard versions of the SPH equations for linear elasticity. Necessary conditions for stability were derived that differ from the Swegle criteria by allowing for the possibility of some tension before instability is bound to appear. It was found that if the momentum equation is 0^{th}-order complete i.e. the divergence of a constant stress field is evaluated exactly, then the *lnearised* system is stable. This may explain the greater stability observed in practice for corrected formulations e.g. NCSPH, MLS or RKPM - although it was shown in the following chapter that instability can still occur, in particular NCSPH whilst certainly more stable that basic SPH definitely exhibits tensile instability. This highlights the limitations of a linear analysis, which can produce only necessary conditions for stability.

Leaving aside the treatment of time as a continuous or discrete variable, fundamentally the linear stability analysis performed above and the von Neumann analyses performed by others are equivalent. In order to try to produce a sufficient condition for stablity we turned to Lyapunov's method. The disadvantge of this approach is the need to find a Lyapunov function for which there is no general method. However a natural candidate for a Lyapunov function is the total energy of a system; indeed the Lyapunov function can be thought of as a generalised energy function. It was found that SPH as typically formulated is not integrable; the force function cannot be integrated to find the potential energy. As such for normal SPH the total energy is not available as a ready made Lyapunov function candidate. However a conservative version of SPH was derived and it was shown by Lyapunov's method that the equilibrium is stable when the kernel function $W\left(\left|\mathbf{x}_i - \mathbf{x}_j\right|, h\right)$ is chosen such that, for all i and j and for all $\mathbf{u}$; $\sum_{j=1}^{N} W'_{ij} = \sum_{i=1}^{N} W'_{ij} = 0$. This constitutes a sufficient condition for the stabilty of SPH, or at least a conservative version of it.

Although the stability results are only strictly applicable to conservative SPH, the linear stability analysis showed that a conservative version of SPH is less stable than non-conservative SPH, requiring exactly half the tension to become unstable. This suggests that conditions that imply stablity in conservative SPH may help stabilise ordinary SPH.

All of the stability results derived here and, to the author's knowledge, elsewhere, apply only to the stability of an equilibrium that has been perturbed by some arbitrarily small amount. This limits the confidence one can have that the sufficient conditions derived here guarantee stability in practice. This is especially pertinent for SPH where large deformations of an initial configuration can be expected. Lyapunov's method can be applied to more general invariant sets [65]. In particular for a conservative system, the set $\{\mathbf{u} : H(\mathbf{u}) < c\}$ where H is the total energy is invariant. Future work may concentrate on proving that an invariant set of this form is stable. The geometry of the potential energy/Lyapunov function is all important, exploring this analytically or numerically may provide further insight into the stability of SPH.

Finally a new way to stabilise SPH was described; S-SPH. By switching between two formulations, two unstable methods combine to become one stable method. The results of varous validation tests show its stability and accuracy is comparable to TL-SPH. The advantage of the present method is that it is Eulerian and is potentially of wider applicability than TL-SPH where the particle neighbourhoods are fixed, limiting the possibilties for modelling extreme deformations without "re-meshing". Further work to extend the method to be first-order consistent and to conserve angular momentum would be of interest. We only considered elastic solids but it may also be of use in fluids and other materials and this should also be investigated.

References

[1] M Antuono, A Colagrossi, S Marrone, and D Molteni. Free surface flows solved by means of SPH schemes with numerical diffusive terms. *Computer Physics Communications*, 181(3), 2009.

[2] D Appelo and G Kreiss. A new absorbing layer for elastic waves. *Journal of Computational Physics*, 215, 2006.

[3] V Arnold. *Ordinary Differential Equations*. Springer, third edition, 1991.

[4] V I Arnold. *Mathematical Methods of Applied Mechanics*. Springer, second edition, 1989.

[5] D S Balsara. Von Neumann stability analysis of smoothed particle hydrodynamics - suggestions for optimal algorithms. *Journal of Computational Physics*, 121, 1995.

[6] A Bamberger, P Joly, J E Roberts, and J L Teron. Absorbing boundary conditions for Rayleigh waves. Technical report, Institut National de Recherche en Information et en Automatique, 1985.

[7] T Belytschko, Y Guo, W K Liu, and S P Xiao. A unified stability analysis of meshless particle methods. *International Journal for Numerical Methods in Engineering*, 48, 2000.

[8] T Belytschko, Y Krongauz, J Dolobow, and C Gerlach. On the completness of meshfree particle methods. *International Journal for Numerical Methods in Engineering*, 43, 1998.

[9] T Belytschko, Y Krongauz, D Organ, M Fleming, and P Krysl. Meshless methods: An overview and recent developments. *Computer Methods in Applied Maechanics and Engineering*, 139, 1996.

[10] Carl M Bender and Steven A Orszag. *Advanced Mathematical Methods for Scientists Engineers*, chapter 7. McGraw-Hill, 1978.

[11] W Benz and R Buchler. Smooth particle hydrodynamics - a review. In *Numerical Modeling of Non-linear Steller Pulsation: Problems and Prospects*. Kluwer Academic Publishers, 1990.

[12] J Berenger. A perfectly matched layer for the absorption of electromagnetic waves. *Journal of Computational Physics*, 114, 1994.

[13] J Bonet and T-S L Lok. Variational and momentum preservation aspects of smooth particle hydrodynamic formulations. *Computer Method in Applied Mechanics and Engineering*, 180, 1999.

[14] J Bonet and M X Rodriguez-Paz. Hamiltonian formulation of the variable-h SPH equations. *Journal of Computational Physics*, 209, 2005.

[15] M D Buhmann. *Radial Basis Functions: Theory and Implimentations*. Cambridge University Press, 2003.

[16] Robert Clayton and B Engquist. Absorbing boundary conditions for acoustic and elastic wave equations. *Bulletin of the Seismological Society of America*, 1977.

[17] F Collino and C Tsogka. Application of the perfectly matched layer model to the linear elastodynamic problem in anisotropic heterogeneous media. *Geophysics*, 66(1), 2001.

[18] T De Vuyest. *Hydrocode modelling of water impact*. PhD thesis, Cranfield University, 2003.

[19] W Dehnen and H Aly. Improving convergence in smoothed particle hydrodynamics simulations without pairing instability. *Monthly Notices of the Royal Astronomical Society*, 425:1068–1082, 2012.

[20] G A Dilts. Moving-least squares - particle hydrodynamics i, consistancy and stability. *International Journal for Numerical Methods in Engineering*, 44, 1997.

[21] A Ditowski and D Gottlieb. On the Engquist Majda absorbing boundary conditions for hyperbolic systems. *Contemporary Mathematics*, 2000.

[22] C T Dyka and R P Ingel. An approach for tension instability in smoothed particle hydrodynamics (SPH). *Computers and Structures*, 57(4), 1995.

[23] Jeff D Eldredge, Tim Colonius, and Anthony Leonard. A vortex particle method for two-dimensional compressible flow. *Journal of Computational Physics*, 179, 2002.

[24] B Engquist and A Majda. Absorbing boundary conditions for the numerical simulation of waves. *Math. Comp.*, 31, 1977.

[25] August E Evrard. Beyond n-body: 3d cosmological gas dynamicsh. *Monthly Notices Royal Astronomical Society*, 235, 1988.

[26] I Federico, S Marrone, A Calagrossi, F Aristodemo, and P Veltri. Simulation of hydraulic jump through sph model. In *XXXII Convegno Nazionale di Idraulica e Costruzioni Idrauliche*, Palermo, September 2010.

[27] G Festa and S Nielsen. Pml absorbing boundaries. *Bulletin of the Seismological Society of America*, 93(2), 2003.

[28] H Flanders. *Differential forms with applications to the physical sciences*. Dover, 1989. Republication of origional published in 1963 by Academic Press, Inc.

[29] D A Fulk and D W Quinn. An analysis of 1-d smoothed particle hydrodynamics kernels. *Journal of Computational Physics*, 126, 1996.

[30] R A Gingold and J J Monaghan. Smoothed particle hydrodynamics: theory and application to non-spherical stars. *Monthly Notices Royal Astronomical Society*, 181, 1977.

[31] R A Gingold and J J Monaghan. A numerical study of the roche and darwin problems for polytropic stars. *Monthly Notices Royal Astronomical Society*, 188, 1979.

[32] R A Gingold and J J Monaghan. Kernel estimates as a basis for general particle methods in hydrodynamics. *Journal of Computational Physics*, 46, 1982.

[33] D Givoli. Non-reflecting boundary conditions. *Journal of Computational Physics*, 94, 1991.

[34] D Givoli. High-order local non-reflecting boundary conditions: A review. *Wave Motion*, 39, 2004.

[35] D Givoli and I Patlashenko. Optimal local non-reflecting boundary conditions. *Applied Numerical Mathematics*, 27, 1998.

[36] Dan Givoli and Joseph B Keller. Non-reflecting boundary conditions for elastic waves. *Wave Motion*, 12, 1990.

[37] G H Golub and C F Van Loan. *Matrix Computations*. The Johns Hopkins University Press, 1996.

[38] K E Graff. *Wave Motion in Elastic Solids*. Dover, 1991.

[39] Murthy N Guddati and Joh L Tassoulas. Continued-fraction absorbing boundary conditions for the wave equation. *Journal of Computational Acoustics*, 8, 2000.

[40] Thomas Hagstrom. Radiation boundary condition for the numerical simulation of waves. *Acta Numerica*, 1999.

[41] Isaac Harari and Zio Shohet. On non-reflecting boundary conditions in unbounded elastic solids. *Computer Methods in Applied Mechanics and Engineering*, 163, 1998.

[42] L Hernquist. Some cautionary remarks about smoothed particle hydrodynamics. *Astrophysical Journal*, 404, 1993.

[43] L Hernquist and N Katz. Treesph: A unification of SPH with the hierarchical tree method. *The Astrophysical Jouranl Supplement Series*, 70, 1989.

[44] Robert L Higdon. Absorbing boundary conditions for difference approximations to the multi-dimensional wave equation. *Mathematics of Computation*, 47(176), 1986.

[45] Robert L Higdon. Radiation boundary conditions for elastic wave propagation. *SIAM Journal on Numerical Analysis*, 27(4), 1990.

[46] R A Horn and C R Johnson. *Matrix Analysis*. Cambridge University Press, 1985.

[47] P Howell, G Kozyreff, and J Ockendon. *Applied Solid Mechanics*. Cambridge University Press, 2009.

[48] Joseph B Keller and D Givoli. Exact non-reflecting boundary conditions. *Journal of Computational Physics*, 82, 1989.

[49] H K Khalil. *Nonlinear Systems*. Prentice - Hall, second edition, 1996.

[50] S Kitsionas and A P Whitworth. Smoothed particle hydrodynamics with particle splitting, applied to self-gravitating collapse. *Monthly Notices Royal Astronomical Society*, 330, 2002.

[51] K Lancaster P, Åăalkauskas. *Curve and Surface Fitting: An Introduction*. Academic Press, Harcourt Brace Jovanovich, 1986.

[52] C Lanczos. *The Variational Principles of Mechanics*. University of Toronto Press, 4^{th} edition, 1970.

[53] L D Landau and E M Lifshitz. *Theory of Elasticity*. Elsevier, 1986.

[54] L D Landau and E M Lifshitz. *Fluid Mechanics*. Pergamon Press, 1987.

[55] Martin Lastiwka, Mihai Basa, and Nath J Quinlan. Permeable and non-reflecting boundary conditions in SPH. *International Journal for Numerical Methods in Fluids*, 61, 2009.

[56] L D Libersky and Petschek A G. Smoothed particle hydrodynamics with strength of materials. *Advances in the Free Lagrange Method, Lecture Notes in Physics*, 395, 1991.

[57] G R Liu and M B Liu. *Smoothed Particle Hydrodynamics - a meshfree particle method*. World Scientific Publishing, 2003.

[58] W K Liu, L S Jun, J Adee, and T Belytschko. Reproducing kernel particle methods for structural dynamics. *International Journal for Numerical Methods in Engineering*, 38, 1995.

[59] W K Liu, S Jun, and Y F Zhang. Reproducing kernel particle methods. *International Journal for Numerical Methods in Engineering*, 20, 1995.

[60] Livermore Software Technology Corporation. *LS-DYNA Theory Manual*, 2006.

[61] L B Lucy. A numerical approach to the testing of fusion process. *Astronomical journal*, 88, 1977.

[62] F Macia, M Antuono, A Colagrossi, T Rung, and C Ulrich. Benefits of using a Wendland kernel for free-surface flows. In 6^{th} *International SPHERIC Workshop*, 2011.

[63] Lawrence E Malvern. *Introduction to the Mechanics of a Continuous Medium*. Prentice-Hall, 1969.

[64] K R Meyer, G R Hall, and D Offin. *Introduction to Hamiltonian dynamical systems and the N-body problem*, volume 90 of *Applied mathematical sciences*. Springer, second edition, 2009.

[65] A N Michel, L Hou, and D Liu. *Stability of dynamical systems*. Systems and Control: Foundations and Applications. Birkhauser, 2008.

[66] J J Monaghan. Why particle methods work. *Siam Journal for Scientific and Statistical Computing*, 3(4), 1982.

[67] J J Monaghan. Particle methods for hydrodynamics. *Computer Physics Reports*, 3, 1985.

[68] J J Monaghan. An introduction to SPH. *Computer Physics Communications*, 48, 1988.

[69] J J Monaghan. Simulating free surface flow with sph. *Journal of Computational Physics*, 110, 1994.

[70] J J Monaghan. SPH without a tensile instability. *Journal of Computational Physics*, 159, 2000.

[71] J J Monaghan. Smoothed particle hydrodynamics. *Reports on Progress in Physics*, 68, 2005.

[72] J J Monaghan and A Kocharyan. SPH simulation of multi-phase flow. *Computer Physics Communications*, 87, 1995.

[73] K W Morton and D F Mayers. *Numerical Solution of Partial Differential Equations*. Cambridge University Press, 2005.

[74] R P Nelson and J C B Papaloizou. Variable smoothing lengths and energy conservation in smoothed particle hydrodynamics. *Monthly Notices of the Royal Astronomical Society*, 270, 1994.

[75] Richar P Nelson and Joh C B Papaloizou. Three-dimensional hydrodynamic simulation of collapsing prolate clouds. *Monthly Notices Royal Astronomical Society*, 265, 1993.

[76] Richard A Olshen and Bala Rajaratnam. Successive normalisation of rectangular arrays. Technical report, Stanford University, Division of Bio-statistics, 2009.

[77] J Michael Owen, Jens V Villumsen, Paul R Shapiro, and Hugo Martel. Adaptive smoothed particle hydrodynamics: Methodology ii. *The Astrophysical Journal Supplement Series*, 116, 1998.

[78] M H Patel, R Vignjevic, and J C Campbell. An SPH technique for evaluating the behaviour of ships in extreme oceean waves. *International Journal of Maritime Engineering*, 151, 2009.

[79] D J Price and J J Monaghan. Smoothed particle magnetohydrodynamics ii. variational principles and variable smoothing length terms. *Monthly Notices of the Royal Astronomical Society*, 348, 2003.

[80] T Rabczuk, T Belytschok, and S P Xiao. Stable particle methods based on langrangian kernels. *Computer Methods in Applied Mechanics and Engineering*, 193, 2004.

[81] P W Randles and L D Libersky. Smoothed particles hydrodynamics: Some recent improvments and applications. *Computer Methods in Applied Mechanics and Engineering*, 139, 1996.

[82] P W Randles and L D Libersky. Normalised SPH with stress points. *International Journal for Numerical Methods in Engineering*, 48, 2000.

[83] Paul R Shapiro, Hugo Martel, Jens V Villumsen, and J Michael Owen. Adaptive smoothed particle hydrodynamics with application to cosmology: Methodology. *The Astrophysical Journal Supplement Series*, 103, 1996.

[84] J Sochaki. Absorbing boundary conditions foe elastic wave equations. *Applied Mathematics and Computation*, 28, 1988.

[85] J W Swegle, D L Hicks, and S W Attaway. Smoothed particle hydrodynamics stability analysis. *Journal of Computational Physics*, 116, 1995.

[86] Semyo V Tsynkov. Numerical solution of problems on unbounded domains. a review. *Applied Numerical Mathematics*, 27, 1998.

[87] R Vacondio. *Shallow Water and Navier-Stokes SPH-like numerical modelling of rapidly varying free-surface flows.* PhD thesis, Universitá degli Studi di Parma, Facoltá di Ingegneria, 2010.

[88] R Vignjevic, J Campbell, J Jaric, and S Powell. Derivation of SPH equations in a moving referential coordinate system. *Computer Methods in Applied Mechanics and Engineering*, 198, 2009.

[89] R Vignjevic, J Campbell, and L Libersky. A treatment of zero energy modes in the smoothed particle hydrodynamics method. *Computer Methods in Applied Mechanics and Engineering*, 184(1), 2000.

[90] C A Wingate, R F Stellingwerf, R F Davidson, and M W Burkett. Models of high velocity impact phenomena. *International Journal of Impcat Engineering*, 14, 1993.

Appendix A

Additional mathematics

1 SPH kernel functions

For reference we give some alternative kernel functions where $r = |x - y| / h$ and c is a normalisation constant. First B-spline functions of increasing order [57]:

Cubic B-Spline.

$$W(r,h) = \frac{c}{h} \begin{cases} 1 - \frac{3}{2}r^2 + \frac{3}{4}r^3 & : r < 1 \\ \frac{1}{4}(2-r)^3 & : 1 \leq r < 2 \\ 0 & : r \geq 2, \end{cases} \tag{A.1}$$

Quartic B-Spline.

$$W(r,h) = \frac{c}{h} \begin{cases} \left(r + \frac{5}{2}\right)^4 - 5\left(r + \frac{3}{2}\right)^4 + 10\left(r + \frac{1}{2}\right)^4 & : r < \frac{1}{2} \\ \left(\frac{5}{2} - r\right)^4 - 5\left(\frac{3}{2} - r\right)^4 & : \frac{1}{2} \leq r < \frac{3}{2} \\ \left(\frac{5}{2} - r\right)^4 & : \frac{3}{2} \leq r < \frac{5}{2} \\ 0 & : r \geq \frac{5}{2}, \end{cases} \tag{A.2}$$

Quintic B-Spline.

$$W(r,h) = \frac{c}{h}\begin{cases} (3-r)^5 - 6(2-r)^5 + 15(1-r)^5 & : r < 1 \\ (3-r)^5 - 6(2-r)^5 & : 1 \le r < 2 \\ (3-r)^5 & : 2 \le r < 3 \\ 0 & : r \ge 3, \end{cases} \tag{A.3}$$

If we introduce the notation $(a)_+ = \min\{0, a\}$ then the above can be written more concisely

$$W(r,h) = \frac{c}{h}\left[(3-r)_+^5 - 6(2-r)_+^5 + 15(1-r)_+^5\right]. \tag{A.4}$$

Gaussian. Many variations on a Gaussian kernel exist (see [29]). For example,

$$W(r,h) = ce^{-(r/h)^2}. \tag{A.5}$$

This has infinte support but may be truncated, i.e. assumed to be zero for all $r > \alpha$, for some constant α.

Wendland Kernels. The Wendland functions form a heirarchy of compactly supported "bell-shaped" functions. They are distinguished by the fact that their Fourier transform is always positive definite. See [15] and [19] for details. Two, of many, examples given in [19] are

$$\psi(r)_{2,1} = c(1-r)_+^3(1+3r), \tag{A.6}$$

$$\psi(r)_{3,2} = c(1-r)_+^5(1+5r+8r^2). \tag{A.7}$$

2 Theorems and definitions for stability analysis

2.1 Miscellaneous matrix definitions and theorems [46]

The following definitions will assume all matrices and vectors have only real entries but this is sufficient for our needs.

Definition A.1 (Positive/negative definite matrix)**.** A positive definite matrix is any matrix $\mathbf{A}$ such that $\mathbf{x} \cdot \mathbf{Ax} > 0$ for all non-zero vectors $\mathbf{x}$. If strict inequality is not obtained i.e. $\mathbf{x}^T \cdot \mathbf{Ax} \geq 0$, then $\mathbf{A}$ is positive semi-definite. If $-\mathbf{A}$ is positive (semi-) definite then $\mathbf{A}$ is negative (semi-)definite.

Definition A.2 (Principal sub-matrix and principal minors)**.** A principal sub matrix of a square matrix $\mathbf{A}$ is a matrix formed by deleting a proper subset of the rows and corresponding columns of $\mathbf{A}$ i.e. if the i^{th} row is deleted so must the i^{th} column. The principal minors are the determinants of the principal sub-matrices.

The following well known facts are pertinent to the following stability analysis:

1. The eigenvalues of a symmetric matrix are all real.
2. A symmetric $n \times n$ matrix $\mathbf{A}$ is positive (semi-)definite if and only if $\lambda_i > 0$ ($\lambda_i \geq 0$) $\forall \lambda_i \in \sigma(\mathbf{A})$.
3. A symmetric $n \times n$ matrix $\mathbf{A}$ is negative (semi-)definite if and only if $\lambda_i < 0$ ($\lambda_i \leq 0$) $\forall \lambda_i \in \sigma(\mathbf{A})$.
4. Every principal sub-matrix of a positive definite matrix is positive definite.
5. All of the principal minors of $\mathbf{A}$ are positive if, and only if, $\mathbf{A}$ is positive definite.
6. The principal minors of a negative definite matrix are negative if the corresponding sub-matrix has an odd number of rows and positive otherwise.

2.2 Proof of theorem 3.8

Note that if $f_i = -\frac{\partial U}{\partial x_i}$ then $\dot{H} = 0$, i.e. the system is conservative. If $f_i = -\frac{\partial U}{\partial x_i}$ then, because partial differentiation commutes (Poincaré Lemma),

$$\begin{aligned}\frac{\partial f_i}{\partial x_j} =& \frac{\partial^2 U}{\partial x_j \partial x_i} \\ =& \frac{\partial^2 U}{\partial x_i \partial x_j} = \frac{\partial f_j}{\partial x_i}.\end{aligned}$$

Conversely, conservation of energy requires that the force $\mathbf{F}$ does no net work if the point $\mathbf{x}(t)$ moves around a closed countour; the system should not gain or lose energy if it returns to its initial state. That is, $\int_{\partial D} \sum_{i=1}^{N} f_i \mathrm{d}x_i \equiv 0$. If $\frac{\partial f_i}{\partial x_j} = \frac{\partial f_j}{\partial x_i}$ then,

$$\begin{aligned}\int_{\partial D} \sum_{i=1}^{N} f_i \mathrm{d}x_i &= \int_D \sum_{i=1}^{N} \left(\sum_{j=1}^{N} \frac{\partial f_i}{\partial x_j} \mathrm{d}x_j \right) \mathrm{d}x_i \\ &= \int_D \sum_{i<j} \left[\left(\frac{\partial f_i}{\partial x_j} - \frac{\partial f_j}{\partial x_i} \right) \mathrm{d}x_j \mathrm{d}x_i \right] = 0.\end{aligned}$$

The sum $\left(\sum_{i<j}\right)$ is taken over all pairs (i, j) such that $1 \leq i < j \leq n$. The first line follows from Stokes' formula, $\int_{\partial D} \omega = \int_D \mathrm{d}\omega$ [28], and the definition of exterior differentiation; $\mathrm{d}f = \sum_{i=1}^{N} \frac{\partial f}{\partial x_i} \mathrm{d}x_i$. The second line uses the skew-symmetry of the exterior product $\mathrm{d}x_i \mathrm{d}x_j = -\mathrm{d}x_j \mathrm{d}x_i$ and the inital assumption that $\frac{\partial f_i}{\partial x_j} = \frac{\partial f_j}{\partial x_i}$.

3 Elastic waves

This section is a brief overview of elastic waves in infinite and semi-infinite isotropic media, specifically pressure waves, shear waves, and surface (Rayleigh) waves the main references used are [53, 47, 38]. The assumption throughout is that the displacement $\mathbf{u}$ does not vary in the z-direction so that we are, in effect, considering two dimensions (x and y) only. We will first consider the scalar wave equation to introduce plane harmonic waves. It is by considering the behaviour of these waves, incident to a boundary, that the NRBC will be introduced (following [21]).

3.1 The wave equation

3.1.1 1D wave equation

First consider the 1D wave equation

$$\begin{gathered}\frac{\partial^2 u}{\partial t^2} = c^2 \frac{\partial^2 u}{\partial x^2} \\ u(x, 0) = f(x) \quad \text{and} \quad \dot{u}(x, 0) = 0.\end{gathered} \tag{A.8}$$

The solution to (A.8) is [38]

$$u(x,t) = \frac{1}{2}f(x-ct) + \frac{1}{2}f(x+ct). \tag{A.9}$$

Therefore the initial displacement is propagated, without distortion, to the right ($f(x-ct)$) and to the left ($f(x+ct)$) at *phase speed* c. A *harmonic wave* is a solution of (A.8) that is a wave of a single frequency;

$$u(x,t) = Ae^{ik(x-ct)} = Ae^{i(kx-\omega t)}. \tag{A.10}$$

A is the amplitude, $k = \frac{2\pi}{\lambda}$ is the wave number, λ is the wavelength, $c = \frac{\omega}{k}$ is the phase velocity, and ω is the angular frequency. Harmonic waves are often used to analyse wave phenomena because they can make the problem easier and more general solutions can be constructed by superpostion [38].

3.1.2 2D wave equation

In higher dimensions the wave equation is

$$\frac{\partial u}{\partial t} = c^2 \Delta u. \tag{A.11}$$

The higher dimensional analog of harmonic waves are *plane* harmonic waves. A plane wave is a wave where all points on a plane normal to the direction of propagation have the same motion, see figure A.1. A plane harmonic wave has the functional form

$$u = Ae^{ik(\mathbf{n}\cdot\mathbf{r}-ct)}. \tag{A.12}$$

It is easy to verify that this is indeed a solution of (A.11):

$$\begin{aligned}
\frac{\partial^2 u}{\partial x^2} &= -n_1^2 k^2 u \\
\frac{\partial^2 u}{\partial y^2} &= -n_2^2 k^2 u \\
\frac{\partial^2 u}{\partial t^2} &= -k^2 c^2 u,
\end{aligned}$$

therefore by substitution of the above into (A.11) find

$$-k^2c^2u + k^2c^2\left(n_1^2 + n_2^2\right)u = k^2c^2u \times (-1 + (1)) = 0,$$

as required.

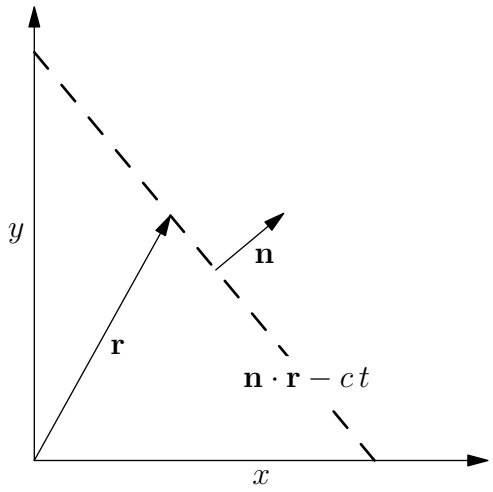

Figure A.1: Plane wave: All points along the plane $\mathbf{n}\cdot\mathbf{r} - ct$ =constant undergo the same motion. The wave propagates with *phase velocity* $\mathbf{c} = c\,\mathbf{n}$, i.e. in the direction $\mathbf{n}$ with speed c.

3.2 Pressure and shear waves

The equations of linear elasticity are [47]

$$\rho\frac{\partial^2\mathbf{u}}{\partial t^2} = \mu\Delta\mathbf{u} + (\lambda+\mu)\,\nabla(\nabla\cdot\mathbf{u}), \tag{A.13}$$

where λ and μ are the Lamé constants.

Helmholtz representation. The Helmholtz representation [63] of a vector field is

$$\mathbf{u} = \nabla\phi + \nabla\times\mathbf{G} \qquad \text{where} \qquad \nabla\cdot\mathbf{G} = 0. \tag{A.14}$$

The vector is split into the sum of the gradient of a scalar potential ϕ and the curl of a vector potential $\mathbf{G}$. The additional condition on the vector potential $\nabla\cdot\mathbf{G} = 0$ makes the representation unique. Note that in (A.14) the vector $\mathbf{u}$ is split into a divergence-free (solenoidal) part, $\nabla\times\mathbf{G}$, and an irrotational part, $\nabla\phi$. Therefore $\mathbf{u}$ can also be written

$$\mathbf{u} = \mathbf{u}_l + \mathbf{u}_t \tag{A.15}$$

where $\mathbf{u}_t = \nabla\times\mathbf{G}$ and $\nabla\cdot\mathbf{u}_t = 0$; and $\nabla\phi = \mathbf{u}_l$ and $\nabla\times\mathbf{u}_l = 0$.

The fact that two distinct types of elastic waves exist can be derived using the Helmholtz representation of a vector. First substitute (A.14) into (A.13);

$$\rho\frac{\partial^2\left(\nabla\phi+\nabla\times\mathbf{G}\right)}{\partial t^2} = \mu\Delta\left(\nabla\phi+\nabla\times\mathbf{G}\right) + (\lambda+\mu)\,\nabla(\nabla\cdot(\nabla\phi+\nabla\times\mathbf{G})).$$

By interchanging the order of differentiation and using the identity $\nabla \cdot \nabla = \Delta$ and the fact that $\nabla \cdot \nabla \times \mathbf{G} = 0$ the above equation becomes

$$\rho \nabla \frac{\partial^2 \phi}{\partial t^2} + \rho \nabla \times \frac{\partial^2 \mathbf{G}}{\partial t^2} = \mu \nabla \Delta \phi + \mu \nabla \times \Delta \mathbf{G} + (\lambda + \mu) \nabla \Delta \phi.$$

Finally by grouping terms we find

$$\nabla \left(\rho \frac{\partial^2 \phi}{\partial t^2} - (\lambda + 2\mu) \Delta \phi \right) + \nabla \times \left(\rho \frac{\partial^2 \mathbf{G}}{\partial t^2} - \mu \Delta \mathbf{G} \right) = 0. \tag{A.16}$$

This equation will be satisfied if both bracketed terms vanish i.e.

$$\frac{\partial^2 \phi}{\partial t^2} - \frac{(\lambda + 2\mu)}{\rho} \Delta \phi = 0, \tag{A.17a}$$

$$\frac{\partial^2 \mathbf{G}}{\partial t^2} - \frac{\mu}{\rho} \Delta \mathbf{G} = 0. \tag{A.17b}$$

Equations (A.17) are both wave equations but with different phase speeds. For equation (A.17a) the phase speed is $c_p = \sqrt{(\lambda + 2\mu)/\rho}$, this type of elastic wave is called a pressure or longitudinal wave, abbreviated to P-wave. For equation (A.17b) the phase speed is $c_s = \sqrt{\mu/\rho}$, this is a shear or transverse wave (S-wave). Note that as $\mu > 0$ it is always true that $c_p > c_s$, P-waves are faster than S-waves. Note that neither c_p nor c_s depend on k; the P- and S-waves are non-dispersive - all waves, regardless of frequency, propagate at the same speed. Equation (A.13) can be rewritten in terms of c_p and c_s;

$$\frac{\partial^2 \mathbf{u}}{\partial t^2} = c_s^2 \Delta \mathbf{u} + \left(c_p^2 - c_s^2 \right) \nabla (\nabla \cdot \mathbf{u}). \tag{A.18}$$

Plane elastic waves [53]. Suppose that a plane wave is travelling along the x axis so that the $\mathbf{u}(x,t) = (u_1, u_2)$ is a function of x and t only. With this assumption all the spatial derivatives in (A.18) bar $\frac{\partial}{\partial x}$ are equal to zero. Equation (A.18) then reduces to

$$\frac{\partial^2 u_1}{\partial t^2} = c_p^2 \frac{\partial^2 u_1}{\partial x^2}, \tag{A.19a}$$

$$\frac{\partial^2 u_2}{\partial t^2} = c_s^2 \frac{\partial^2 u_2}{\partial x^2}. \tag{A.19b}$$

Therefore the displacement in a P-wave (A.19a) is parallel to the phase velocity and for an S-wave, equation (A.19b), the displacement is perpendicular to the phase velocity.

3.3 Surface waves

The last type of elastic wave to be considered is the Rayleigh wave. These propagate along the free surface of an elastic material but are damped towards the interior so that their action is essentially confined to the surface. The derivation below is a combination of that given in [53] and [38]. Consider a semi-inifinite body existing in the region $y < 0$, so that the free surface is on the x-axis. The solution is the sum of a divergence-free ($\mathbf{u}_l = \nabla\times\mathbf{G}$) and curl-free vector $\mathbf{u}_t = \nabla\phi$. We assume they are plane waves propagating along the x-axis in the positive x direction and have the form,

$$\mathbf{u}_t = \nabla\phi = \nabla\left(f(y)e^{i(kx-\omega t)}\right) \tag{A.20a}$$

$$\mathbf{u}_l = \nabla\times G_3 = \nabla\times\left(g(y)e^{i(kx-\omega t)}\right). \tag{A.20b}$$

From §3.2 we know that ϕ and $\mathbf{G}$ are solutions of the wave equations (A.17). Note that because we assume a plane wave only the z component of the vector potential (G_3) contributes to the total displacement

Proof.

$$\nabla\times\mathbf{G} = \left(\frac{\partial G_3}{\partial y} - \frac{\partial G_2}{\partial z}, \frac{\partial G_1}{\partial z} - \frac{\partial G_3}{\partial x}, \frac{\partial G_1}{\partial y} - \frac{\partial G_2}{\partial x}\right). \tag{A.21}$$

We assume that $\mathbf{u}$ is not a function of z so that $\frac{\partial G_i}{\partial z} = 0$ for all i and the third component of (A.21) can be ignored. Therefore

$$\mathbf{u} = \left(\frac{\partial\phi}{\partial x} + \frac{\partial G_3}{\partial y}, \frac{\partial\phi}{\partial y} - \frac{\partial G_3}{\partial x}\right), \tag{A.22}$$

and only G_3 contributes. □

The first step is to substitute $\phi = f(y)e^{i(kx-\omega t)}$ into (A.17a) to obtain an equation for $f(y)$;

$$\begin{aligned}\frac{\partial^2\phi}{\partial t^2} - c_p^2\Delta\phi &= \frac{\partial^2 f(y)e^{i(kx-\omega t)}}{\partial t^2} - c_p^2\Delta f(y)e^{i(kx-\omega t)} \\ &= \left(-f(y)(-i\omega)^2 - c_p^2 f(y)(ik)^2 - c_p^2\frac{\partial^2 f}{\partial y^2}\right)e^{i(kx-\omega t)} \\ &= \left(f\left(k^2 - \frac{\omega^2}{c_p^2}\right) - \frac{\partial^2 f}{\partial y^2}\right)e^{i(kx-\omega t)} = 0.\end{aligned}$$

This equation is satisfied if $f(y)$ is the solution of the differential equation

$$\frac{\partial^2 f}{\partial y^2} = \left(k^2 - \frac{\omega}{c_p^2}\right) f = \alpha^2 f. \tag{A.23}$$

Therefore

$$f = Ae^{\pm \alpha y} \tag{A.24}$$

where A is a constant. Bearing in mind that a surface wave is sought, the possibilities for the behaviour of $f(y)$ are:

1. If $\alpha^2 < 0$ then the roots would be imaginary and the solution would be periodic.

2. If $f = Ae^{-\alpha y}$ then f would *increase* exponentially towards the interior.

3. If $f = Ae^{\alpha y}$ then f would *decrease* exponentially towards the interior.

Clearly only the last option is acceptable so that

$$\phi = Ae^{\alpha y} e^{i(kx - \omega t)}. \tag{A.25}$$

Exactly the same argument as above can be made after substituting (A.20b) into (A.17b) to show that

$$G_3 = Be^{\beta y} e^{i(kx - \omega t)}, \tag{A.26}$$

where $\beta^2 = k^2 - \frac{\omega^2}{c_s^2}$. The displacement, $\mathbf{u}$, is therefore

$$\mathbf{u} = \nabla\phi + \nabla \times \mathbf{G} = \left(iAke^{\alpha y} + B\beta e^{\beta y}\,,\, A\alpha e^{\alpha y} - iBke^{\beta y}\right) e^{i(kx - \omega t)}. \tag{A.27}$$

It remains to calculate the phase speed $c_r = \frac{\omega}{k}$ and the amplitude ratio A/B. These can be found from the zero-traction boundary condition on $y = 0$. The stress (σ) and displacement are related via the following equations, in index notation,

$$\sigma_{ij} = \lambda \epsilon_{kk} \delta_{ij} + 2\mu \epsilon_{ij} \tag{A.28}$$

$$\epsilon_{ij} = \frac{1}{2}\left(\frac{\partial u_i}{\partial x_j} + \frac{\partial u_j}{\partial x_i}\right), \tag{A.29}$$

where summation is implied over repeated indicies. The zero-traction condition requires that $\sigma_{ij}n_j = 0$, in this case $n_j = \delta_{j2}$ i.e. it is the unit vector parallel to the y-axis. Therefore, as $\sigma_{ij}\delta_{j2} = \sigma_{i2}$, the boundary conditions require that,

$$\begin{aligned}\sigma_{12} &= 2\mu\epsilon_{12} = 0 \\ \sigma_{22} &= \lambda\epsilon_{kk} + 2\mu\epsilon_{22} = 0.\end{aligned} \tag{A.30}$$

We substitute (A.27) into the boundary conditions (A.30) and find, first for σ_{12},

$$\sigma_{12}|_{y=0} = 2ikA\alpha + B(\beta^2 + k^2) = 0, \tag{A.31}$$

where the common factors μ and $e^{i(kx-\omega t)}$ have been divided out. By definition $c_r = \omega k$, so

$$\begin{aligned}\alpha^2 = k^2 - \frac{\omega^2}{c_p^2} &= k^2\left(1 - \frac{c_r^2}{c_p^2}\right), \\ \beta^2 = k^2 - \frac{\omega^2}{c_s^2} &= k^2\left(1 - \frac{c_r^2}{c_s^2}\right), \\ \beta^2 + k^2 &= k^2\left(2 - \frac{c_r^2}{c_p^2}\right).\end{aligned}$$

And (A.31) can be rewritten

$$\sigma_{12}|_{y=0} = 2iA\sqrt{1 - \frac{c_r^2}{c_p^2}} + B\left(2 - \frac{c_r^2}{c_s^2}\right) = 0. \tag{A.32}$$

For σ_{22} the boundary condition is

$$\sigma_{22}|_{y=0} = \lambda A(\alpha^2 - k^2) + 2\mu\left(A\alpha^2 - ikB\beta\right) = 0. \tag{A.33}$$

We use the identities,

$$\begin{aligned}\alpha^2 - k^2 &= -k^2\frac{c_r^2}{c_p^2} \\ \lambda &= -\mu\left(2 - \frac{c_p^2}{c_s^2}\right),\end{aligned}$$

rearrange (A.33), and cancel any common factors. Then

$$\begin{aligned}\sigma_{22}|_{y=0} &= Ak^2\left(\left(2 - \frac{c_p^2}{c_s^2}\right)\left(\frac{c_r^2}{c_p^2}\right) + 2\left(1 - \frac{c_r^2}{c_p^2}\right)\right) - ik^2 2B\sqrt{1 - \frac{c_r^2}{c_s^2}} \\ &= A\left(2 - \frac{c_r^2}{c_s^2}\right) - i2B\sqrt{1 - \frac{c_r^2}{c_s^2}} = 0.\end{aligned} \tag{A.34}$$

Equation (A.32) and (A.34) form a system of homogeneous equations. For a non-zero solution to exist the determinant of the matrix of coefficients must have zero a determinant i.e.

$$\det \begin{pmatrix} 2i\sqrt{1-\frac{c_r^2}{c_p^2}} & 2-\frac{c_r^2}{c_s^2} \\ 2-\frac{c_r^2}{c_s^2} & -i2\sqrt{1-\frac{c_r^2}{c_s^2}} \end{pmatrix} = 4\sqrt{1-\frac{c_r^2}{c_p^2}}\sqrt{1-\frac{c_r^2}{c_s^2}} - \left(2-\frac{c_r^2}{c_s^2}\right)^2 = 0. \tag{A.35}$$

This is the frequency equation and can be written as a cubic equation in $\left(\frac{c_r}{c_s}\right)^2$ [38]. Note that, as with the P- and S-waves, the Rayleigh wave's phase speed is independent of frequency and is non-dispersive. Of the six roots obtained, five can be always be rejected [38]. Obviously half will be negative, one of $\pm\left(\frac{c_r}{c_s}\right)$, of the remaining three, either only one will be real or, of the three real roots, only one will be small enough to satisfy the condition that $\beta > 0$ and be real. Incidentally, this condition also implies that $c_r < c_s$ because

$$\beta = +k\sqrt{1-\frac{c_r}{c_s}} \in \mathbb{R} \qquad \Rightarrow \qquad c_r < c_s.$$

The surface waves are slower that S- and P-waves. In practice solving the cubic equation may be complex but an approximation is given in [38];

$$c_r \approx c_s \frac{0.87+1.12\nu}{1+\nu}, \tag{A.36}$$

where ν is the Poisson ratio.

Finally the amplitude ratio A/B can be found from (A.34) (or (A.32));

$$\frac{A}{B} = \frac{i2\sqrt{1-\frac{c_r^2}{c_s^2}}}{2-\frac{c_r^2}{c_s^2}}. \tag{A.37}$$

Introduce the notation $\psi = 2-\frac{c_r^2}{c_s^2}$ then

$$\frac{A}{B} = 2i\frac{\beta}{k\psi}. \tag{A.38}$$

The displacement can now be written in terms of a single constant A

$$\mathbf{u}|_{y=0} = A\left(ik + 2i\frac{\beta^2}{k\psi}, \alpha + 2\frac{\beta}{\psi}\right)e^{ik(x-c_r t)}. \tag{A.39}$$

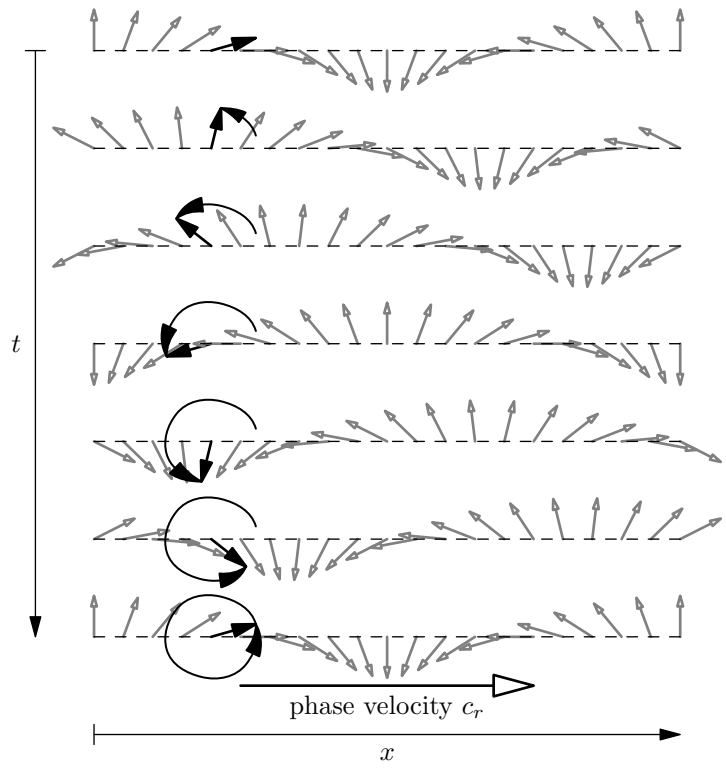

Figure A.2: Displacement of points on a free surface under the action of a Rayleigh wave. A point describes an ellipse as the wave propagates. *Not to scale - illustrative only.*

Define $a(k) = Ai\left(k + 2i\frac{\beta^2}{k\psi}\right)$ and $b(k) = A\left(\alpha + 2\frac{\beta}{\psi}\right)$ and take the real part of (A.39);

$$\mathbf{u}|_{y=0} = \left(a(k)\sin\left(k(x - c_r t)\right),\ b(k)\cos\left(k(x - c_r t)\right)\right). \tag{A.40}$$

For fixed x a point on the free surface $y = 0$ will describe an ellipse - counter-clockwise if the wave is propagating in the positive x direction. This is seen clearly in figure A.2.

Appendix B

Input files

There follows two representative input files for MCM and for DYNA. Note that the initial velocities and the definition of the boundary conditions were hard-wired into the code as needed.

```
**
**    PROBLEM TITLE (MAX = 78 CHARACTERS)                              INPUT VERSION
**                                                                          Âň Âň
Narrow domain for NRBC test                                               2
**********************************************************************************
**
**   CONTROL CARDS
**
**********************************************************************************
**
** CARD 1 - PROBLEM DEFINITION
*AXIS  TYP      MATS STRTPARTS  MAXPARTS
**  Âň    Âň         Âň         Âň         Âň
    2    1         1      5000      5000
**  ------------------------------------------------------------------------------
```

```
** CARD 2 - TIME CONTROL
**  ENDTIM    TSSFAC    DTINIT      DRSF
**       Âň         Âň         Âň         Âň
       4.0       0.8
**  ------------------------------------------------------------------------
** CARD 3 - OUTPUT FILE CONTROL
** DTSTATE PLOT    DTHIST  HISPARTS TRNS      PROB RSRT  RUN
**       Âň    Âň         Âň         Âň    Âň         Âň    Âň    Âň
      0.05    3 5.000E-02         0    0       100    0    0
**  ------------------------------------------------------------------------
** CARD 4 - INPUT AND INITIALIZATION OPTIONS
*FLES VELS MASS    H RO&E
**  Âň    Âň    Âň    Âň    Âň
    1    1    0    0
**  ------------------------------------------------------------------------
** CARD 5 - ANALYSIS OPTIONS
*CTYP  CTS  VUD  SYM NLCR  NPX  NPY  NPZ NSRC NDET L/NL
**  Âň    Âň    Âň    Âň    Âň    Âň    Âň    Âň    Âň    Âň    Âň
    0    0    1    1    0    0    0    0    0    0    0
**  ------------------------------------------------------------------------
** CARD 6 - INTERPOLATION OPTIONS
*SMOL KERN NEIG
**  Âň    Âň    Âň
    0    1   40
**  ------------------------------------------------------------------------
** CARD 7 - OPTIONS (BLANK AT THIS TIME)
**
**  Âň    Âň    Âň    Âň
```

```
**
**********************************************************************************
**
**   MATERIAL CARDS
**
**********************************************************************************
**
**   ################################################################################
**
**    MATERIAL 1
**
**   ################################################################################
**
** CARD 1 - MATERIAL CONTROL CARD
**MID MTYP        RO  EOS                AVIS      QBVC      LBVC
**  Âň    Âň         Âň    Âň    Âň         Âň    Âň         Âň         Âň
    1    1       7.8                                 1.5      0.06
**  --------------------------------------------------------------------------------
** CARD 1a - MCM MATERIAL OPTIONS
** TOTMASS  INITIALH  MINROLIM  MAXROLIM
**       Âň         Âň         Âň         Âň
      15.6    0.0260       0.0       0.0
**  --------------------------------------------------------------------------------
** CARD 2
**-------------Material Identification (72 Characters MAX)--------------
**                                                                      Âň
block 1
**  --------------------------------------------------------------------------------
** CARD 3 - YOUNG'S MODULUS
```

```
**       Âň
       2.1
**  ------------------------------------------------------------------------
** CARD 4 - POSSION'S RATIO
**       Âň
       0.3
**  ------------------------------------------------------------------------
** CARD 5 - YIELD STRESS
**       Âň

**  ------------------------------------------------------------------------
** CARD 6 - TANGENT MODULUS
**       Âň

**  ------------------------------------------------------------------------
** CARD 7 - HARDENING PARAMETER
**       Âň

**  ------------------------------------------------------------------------
** CARD 8 - BLANK

**
**   ##########################################################################
**************************************************************************
**
**   PARTICLE COORDINATES & PARTICLE INFORMATION
**
**************************************************************************
**
```

```
** PARTICLES: 2D CARTESIAN (axis option = 2)
**   NID   BC                  X                   Y    MID
**     Âň    Âň                  Âň                  Âň     Âň
       1    0          1.000e-002          1.990e+000      1
       2    0          3.000e-002          1.990e+000      1
       3    0          5.000e-002          1.990e+000      1
       4    0          7.000e-002          1.990e+000      1
       5    0          9.000e-002          1.990e+000      1
       6    0          1.100e-001          1.990e+000      1
       7    0          1.300e-001          1.990e+000      1
       8    0          1.500e-001          1.990e+000      1
       9    0          1.700e-001          1.990e+000      1
      10    0          1.900e-001          1.990e+000      1
.....................................CONT.........................
    4986    0          7.100e-001          1.000e-002      1
    4987    0          7.300e-001          1.000e-002      1
    4988    0          7.500e-001          1.000e-002      1
    4989    0          7.700e-001          1.000e-002      1
    4990    0          7.900e-001          1.000e-002      1
    4991    0          8.100e-001          1.000e-002      1
    4992    0          8.300e-001          1.000e-002      1
    4993    0          8.500e-001          1.000e-002      1
    4994    0          8.700e-001          1.000e-002      1
    4995    0          8.900e-001          1.000e-002      1
    4996    0          9.100e-001          1.000e-002      1
    4997    0          9.300e-001          1.000e-002      1
    4998    0          9.500e-001          1.000e-002      1
    4999    0          9.700e-001          1.000e-002      1
    5000    0          9.900e-001          1.000e-002      1
```

```
**
**********************************************************************************
**
**   INITIAL PARTICLE VELOCITIES (Impact Velocity of 200 m/s)
**
**********************************************************************************
**
**   NID         VX         VY
**     Âň          Âň          Âň
       1        0.0       .5
    5000        0.0       .5
**
**********************************************************************************
**
**   SYMMETRY PLANES
**
**********************************************************************************
**
** CARD 1
**    XMIN       XMAX       YMIN       YMAX       ZMIN       ZMAX
**       Âň          Âň          Âň          Âň          Âň          Âň
         1          0          0          0          0          0
**  ----------------------------------------------------------------------------
** CARD 2
** XMINPOS   XMAXPOS   YMINPOS   YMAXPOS   ZMINPOS   ZMAXPOS
**       Âň          Âň          Âň          Âň          Âň          Âň
       0.0
**
**********************************************************************************
```

**   ---END---

****

This is the keyword file for the FE NRBC test.

```
*KEYWORD memory=75m
*TITLE
$# title
test
*CONTROL_BULK_VISCOSITY
$#      q1        q2      type     btype
  1.500000  0.060000         0         0
*CONTROL_TERMINATION
$#  endtim    endcyc     dtmin    endeng    endmas
  4.000000         0     0.000     0.000     0.000
*DATABASE_BINARY_D3PLOT
$#      dt      lcdt      beam     npltc    psetid
  0.100000         0         0         0         0
$#   ioopt
         0
*BOUNDARY_NON_REFLECTING
         1     0.000     0.000
*PART
$# title
block
$#     pid     secid       mid     eosid      hgid      grav    adpopt      tmid
         1         1         1         0         0         0         0         0
*SECTION_SOLID
$#   secid    elform       aet
         1         0         0
*MAT_ELASTIC
$#     mid        ro         e        pr        da        db  not used
```

```
         1  7.800000  2.100000  0.300000     0.000     0.000         0
*INITIAL_VELOCITY_NODE
$#     nid        vx        vy        vz       vxr       vyr       vzr
         1     0.000     0.000     0.000     0.000     0.000     0.000
         2     0.000     0.000     0.000     0.000     0.000     0.000
         3     0.000     0.000     0.000     0.000     0.000     0.000
         4     0.000     0.000     0.000     0.000     0.000     0.000
         5     0.000     0.000     0.000     0.000     0.000     0.000
         6     0.000     0.000     0.000     0.000     0.000     0.000
         7     0.000     0.000     0.000     0.000     0.000     0.000
         8     0.000     0.000     0.000     0.000     0.000     0.000
         9     0.000     0.000     0.000     0.000     0.000     0.000
        10     0.000     0.000     0.000     0.000     0.000     0.000
.............................CONT.........................................
       667     0.000     0.000     0.000     0.000     0.000     0.000
       668     0.000     0.000     0.000     0.000     0.000     0.000
       669     0.000     0.000     0.000     0.000     0.000     0.000
       670     0.000     0.000     0.000     0.000     0.000     0.000
       671  0.018220 -0.046560     0.000     0.000     0.000     0.000
       672  0.014560 -0.047830     0.000     0.000     0.000     0.000
       673  0.010620 -0.048860     0.000     0.000     0.000     0.000
       674  0.006467 -0.049580     0.000     0.000     0.000     0.000
       675  0.002172 -0.049950     0.000     0.000     0.000     0.000
       676 -0.002172 -0.049950     0.000     0.000     0.000     0.000
       677 -0.006467 -0.049580     0.000     0.000     0.000     0.000
       678 -0.010620 -0.048860     0.000     0.000     0.000     0.000
       679 -0.014560 -0.047830     0.000     0.000     0.000     0.000
       680 -0.018220 -0.046560     0.000     0.000     0.000     0.000
       681     0.000     0.000     0.000     0.000     0.000     0.000
```

682	0.000	0.000	0.000	0.000	0.000	0.000

.....CONT.....

713	0.000	0.000	0.000	0.000	0.000	0.000
714	0.000	0.000	0.000	0.000	0.000	0.000
715	0.000	0.000	0.000	0.000	0.000	0.000
716	0.000	0.000	0.000	0.000	0.000	0.000
717	0.000	0.000	0.000	0.000	0.000	0.000
718	0.000	0.000	0.000	0.000	0.000	0.000
719	0.026320	-0.042510	0.000	0.000	0.000	0.000
720	0.023200	-0.044290	0.000	0.000	0.000	0.000
721	0.019700	-0.045960	0.000	0.000	0.000	0.000
722	0.015810	-0.047430	0.000	0.000	0.000	0.000
723	0.011580	-0.048640	0.000	0.000	0.000	0.000
724	0.007071	-0.049500	0.000	0.000	0.000	0.000
725	0.002378	-0.049940	0.000	0.000	0.000	0.000
726	-0.002378	-0.049940	0.000	0.000	0.000	0.000
727	-0.007071	-0.049500	0.000	0.000	0.000	0.000
728	-0.011580	-0.048640	0.000	0.000	0.000	0.000
729	-0.015810	-0.047430	0.000	0.000	0.000	0.000
730	-0.019700	-0.045960	0.000	0.000	0.000	0.000
731	-0.023200	-0.044290	0.000	0.000	0.000	0.000
732	-0.026320	-0.042510	0.000	0.000	0.000	0.000
733	0.000	0.000	0.000	0.000	0.000	0.000

-----CONT-----

4994	0.000	0.000	0.000	0.000	0.000	0.000
4995	0.000	0.000	0.000	0.000	0.000	0.000
4996	0.000	0.000	0.000	0.000	0.000	0.000
4997	0.000	0.000	0.000	0.000	0.000	0.000
4998	0.000	0.000	0.000	0.000	0.000	0.000

```
      4999     0.000     0.000     0.000     0.000     0.000     0.000
      5000     0.000     0.000     0.000     0.000     0.000     0.000
*SET_SEGMENT
$#     sid       da1       da2       da3       da4    solver
         1     0.000     0.000     0.000     0.000
$#      n1        n2        n3        n4        a1        a2        a3        a4
         1         2      2502      2501     0.000     0.000     0.000     0.000
         2         3      2503      2502     0.000     0.000     0.000     0.000
         3         4      2504      2503     0.000     0.000     0.000     0.000
         4         5      2505      2504     0.000     0.000     0.000     0.000
         5         6      2506      2505     0.000     0.000     0.000     0.000
         6         7      2507      2506     0.000     0.000     0.000     0.000
         7         8      2508      2507     0.000     0.000     0.000     0.000
--------------------------------CONT----------------------------------------
      2000      2050      4550      4500     0.000     0.000     0.000     0.000
      2050      2100      4600      4550     0.000     0.000     0.000     0.000
      2100      2150      4650      4600     0.000     0.000     0.000     0.000
      2150      2200      4700      4650     0.000     0.000     0.000     0.000
      2200      2250      4750      4700     0.000     0.000     0.000     0.000
      2250      2300      4800      4750     0.000     0.000     0.000     0.000
      2300      2350      4850      4800     0.000     0.000     0.000     0.000
      2350      2400      4900      4850     0.000     0.000     0.000     0.000
      2400      2450      4950      4900     0.000     0.000     0.000     0.000
      2450      2500      5000      4950     0.000     0.000     0.000     0.000
*ELEMENT_SOLID
$#    eid       pid        n1        n2        n3        n4        n5        n6        n7        n8
         1         1        51        52         2         1      2551      2552      2502      2501
         2         1        52        53         3         2      2552      2553      2503      2502
         3         1        53        54         4         3      2553      2554      2504      2503
```

```
       4       1      54      55       5       4    2554    2555    2505    2504
       5       1      55      56       6       5    2555    2556    2506    2505
       6       1      56      57       7       6    2556    2557    2507    2506
       7       1      57      58       8       7    2557    2558    2508    2507
       8       1      58      59       9       8    2558    2559    2509    2508
       9       1      59      60      10       9    2559    2560    2510    2509
      10       1      60      61      11      10    2560    2561    2511    2510
      11       1      61      62      12      11    2561    2562    2512    2511
      12       1      62      63      13      12    2562    2563    2513    2512
----------------------------------------CONT-----------------------------------
    2396       1    2494    2495    2445    2444    4994    4995    4945    4944
    2397       1    2495    2496    2446    2445    4995    4996    4946    4945
    2398       1    2496    2497    2447    2446    4996    4997    4947    4946
    2399       1    2497    2498    2448    2447    4997    4998    4948    4947
    2400       1    2498    2499    2449    2448    4998    4999    4949    4948
    2401       1    2499    2500    2450    2449    4999    5000    4950    4949
*NODE
$#   nid               x               y               z      tc      rc
       1       0.0100000       0.9900000       0.0100000       3       7
       2       0.0300000       0.9900000       0.0100000       3       7
       3       0.0500000       0.9900000       0.0100000       3       7
       4       0.0700000       0.9900000       0.0100000       3       7
       5       0.0900000       0.9900000       0.0100000       3       7
       6       0.1100000       0.9900000       0.0100000       3       7
       7       0.1300000       0.9900000       0.0100000       3       7
       8       0.1500000       0.9900000       0.0100000       3       7
       9       0.1700000       0.9900000       0.0100000       3       7
      10       0.1900000       0.9900000       0.0100000       3       7
 -------------------------CONT-------------------------------------------------
```

```
    4987        0.7300000        0.0100000        0.0300000        3        7
    4988        0.7500000        0.0100000        0.0300000        3        7
    4989        0.7700000        0.0100000        0.0300000        3        7
    4990        0.7900000        0.0100000        0.0300000        3        7
    4991        0.8100000        0.0100000        0.0300000        3        7
    4992        0.8300000        0.0100000        0.0300000        3        7
    4993        0.8500000        0.0100000        0.0300000        3        7
    4994        0.8700000        0.0100000        0.0300000        3        7
    4995        0.8900000        0.0100000        0.0300000        3        7
    4996        0.9100000        0.0100000        0.0300000        3        7
    4997        0.9300000        0.0100000        0.0300000        3        7
    4998        0.9500000        0.0100000        0.0300000        3        7
    4999        0.9700000        0.0100000        0.0300000        3        7
    5000        0.9900000        0.0100000        0.0300000        3        7
*END
*COMPONENT
         1  0.769000  0.004000  0.110000     0.000         0         0         0
Part 1
*COMPONENT_PART
         1         1
*COMPONENT_END
```